POLITECNICO DI TORINO
Repository ISTITUZIONALE

mixed modulation format for future optical transmission systems

(Article begins on next page)

04 August 2020

POLITECNICO DI TORINO

SCUOLA DI DOTTORATO

Dottorato in Ingeneria Elettronica e delle Communicazione – XXVIII ciclo

Tesi di Dottorato

Mixed Modulation Format For Future Optical Transmission Systems

Li Rixin

Tutore	**Coordinatore del corso di dottorato**
Prof. Vittorio Curri	
Prof. Andrea Carena	Prof. Ivo Montrosset

March 2016

To the memory of my beloved grandma, may there is no pain in the heaven.

Summary

Developing a flexible network to fully utilize the existing spectral resource is a hot topic in the novel paradigm of optical transmission systems. In this thesis, I analysed hybrid modulation formats as an effective technique for the implementation of flexible transponders that are capable of trading-off the delivered data rate by the light path quality of transmission with a finer granularity. The flexible transponder is an enabling technology to introduce the elastic paradigm in the state-of-the-art networks, while maintaining compatibility with the installed equipment, including fibers, mux-demux and ROADMs, as required by telecommunication operators willing to exploit fixed grid WDM transmission.

Time division hybrid modulation format (TDHMF) is presented as the first solution. Through combining two modulation formats in the time division, TDHMF can achieve arbitrary bit-per-symbol, and provide a huge amount of flexibilities to the network. A comprehensive theoretical assessment of the back-to-back performances is also introduced. In particular, four different transmitter operation strategies are proposed and evaluated. They are the constant power strategy, the same Euclidean distance strategy, the same BER strategy and the minimum BER strategy. Through the back-to-back performance comparison, the same BER strategy is chosen as the most promising strategy, mainly due to its comparable sensitivity performance and the potential of transponder simplification.

This thesis also prepared another solution, which is Flexible M-PAM modulation format (FlexPAM). It is a hybrid of different M-PAMs in all four quadrature of the optical field. Although it providing less flexibility compared to TDHMF, FlexPAM has its unique advantage in two main aspect. Firstly, the inherently time consistent frame structure feature of FlexPAM may require an identical and simple transponder, which is very crucial from the operators point of view. Secondly, from the network perspective, the operators can assign each quadrature of FlexPAM to a specific network tributary and select an M-PAM according to the actual network conditions. Similar to TDHMF, both general characterization and theoretical formulation are discussed in detail. Then, the back-to-back performance of FlexPAM, including the comparison of different transmitter strategies that similar to the one of TDHMF, has been fully studied. The same BER strategy again provided a negligible SNR

penalty in contrast to the optimal strategy. At the same time, by using the same FEC code for both M-PAM, the same BER strategy may require a simpler signal processing procedure and reduce the complexity.

A subsequent work after the back-to-back analysis is the signal non-linear propagation evaluation of these two novel modulation formats. This thesis provide an extensive simulation analysis on the propagation of a Nyquist-WDM channel comb over an uncompensated and amplified fiber link. Due to the power unbalance in the time division (TDHMF) or in the polarization/quadrature (FlexPAM), the mixed modulation formats normally have some penalty against to the GN-model predictions. To improve their propagation performance, a simple polarization interleaving countermeasure is presented. It works well on TDHMF and has a significant impact on certain case of FlexPAM. Furthermore, the power ratio tuning is also proposed as an easy implemented and effective tool to improve the propagation performance. In the end, the propagation performance of both TDHMF and FlexPAM are compared in terms of the maximum reach versus system net bit rate, in addition, both with and without countermeasures conditions were considered. The results of this investigation showed that TDHMF has almost the same performance as the GN model predictions after the countermeasures employed. FlexPAM can provide a comparable propagation performance in contrast to the GN model predictions. Considering the advantages that mentioned before, the propagation performance of FlexPAM is acceptable.

Acknowledgements

When I registered for the Ph.D program in optical communication three years ago, I only have my interest and enthusiasm with me, but not a solid foundation of knowledge. In the past three years, I received many helpful advises and supports from lots of colleagues and friends. Hereby, I would like to show my gratitude to them.

First and the most, I would like express my deepest appreciation to all professors from OptCom group in Politecnico di Torino: Prof. Vittorio Curri, Prof. Andrea Carena, Prof. Pierluigi Poggiolini, Prof. Roberto Gaudino, Prof. Gabriella Bosco and Prof. Valter Ferrero. They are all quite kind and responsible to lead me into the world of optical communication. In particular, I owe a big debt of thanks to my advisors, Prof. Vitorrio Curri and Prof. Andrea Carena. They gave me lots of excellent advice, which is beneficial for lifetime. In every stage of my research, they provided me valuable guidance and innovative ideas. Without their impressive patience and kindness, I could not have completed this thesis.

Then, I would like to appreciate all researchers from ISMB, where I spent my first year. They are quite friendly and taught me lots of useful experiment knowledge.

I also would like to thank China Scholarship Council (CSC), which provided me the opportunity to study abroad and funded the first two years of my Ph.D program.

I would like to extend my appreciation to GARR consortium, which funded the last year of my Ph.D program.

Last but not least, I would like to thank all my friends who help me both in Italy and China. In particular, I would like to thank my family and my girlfriend, thank you for your understanding and supporting, without you I could not make this far.

Contents

List of Tables

List of Figures

XIV

Chapter 1

Introduction

1.1 Background

The Optical communication has evolved since the human history. The visual techniques such as smoke signals, beacon fires, hydraulic telegraphs, ship flags and semaphore lines were the earliest forms of the optical communications. Today, when people are talking about the optical communication, they mainly refer to the fiber-optic communication, which transmits information from one place to another by sending the pulses of light though an optical fiber.

Starting from 1966, Charles K. Kao and George Hockham first proposed the feasible optical fibers at STC Laboratories (STL) in Harlow, England, the optical transmission system has evolved five generations. The first generation systems operated at the wavelength around 0.8 μm and used the GaAs semiconductor lasers. The second generation systems operated at 1.3 μm, used the InGaAsP semiconductor lasers and first time used the single-mode fiber. The third generation systems operated at 1.55 μm and had the losses about 0.2 dB/km. In addition, the low loss fiber development was inspired by the discovery of Indium gallium arsenide. Eventually, the third generation systems could operate at 2.5 Gbit/s with a maximum reach equal to 100 km.

The fourth generation systems used the optical amplification device to reduce the need for repeaters and wavelength-division multiplexing (WDM) to increase the data capacity. WDM is similar to frequency division multiplexing (FDM) of radio systems technique, and it realized the system that can transmit more than one channel in the same fiber. In figure 1.1, it gives a schematic diagram of a WDM system, in which 9 channels are allocated on the same fiber but separated frequency bands.

After 2006, thanks to the advent of digital signal processing (DPS), the coherent optical transmission system becomes promising and meets the ever-increasing bandwidth needs. It has caused a dramatic revolution and one of its many aspects involves
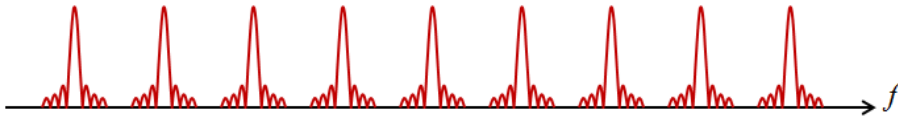
Figure 1.1.   A schematic diagram of a WDM system with 9 channels.

the possibility of fully removing the fiber chromatic dispersion (CD) compensation from the link.

As a result, the uncompensated transmission (UT) is possible to implement, and it has also largely changed the key futures of both the signal propagation and the non-linearity generation in the fiber. Actually, it brought an unexpected advantage from the coherent technology, in the novel UT propagation regime it appears to be possible to carry out the system performance prediction based on a relatively simple analytical non-linear propagation models [1].

1.2   Network Traffic Growth

The history of telecommunication told us that, the growing traffic needs are always the major motivation for all technology inovation. Hence, in this section, several main features of the traffic growth are introduced. From the beginning of this century, internet protocol (IP) has become the dominant traffic type. Consequently, from the end communication users point of view, it is a good measure of traffic demand. The dramatic IP traffic growth [2] in the foreseeable future is mainly due to the ever-increasing demand of emerging applications, for example, video sharing, high-definition video broadcasting, machine-to-machine communications, online gaming, mobile data and so forth.

Table 1.1 offers some historical measure of the internet traffic. In the past two decades, the global internet traffic has grew incredibly fast. About 25 years ago, in 1992, only 100 gigabytes traffic per day was carried by global network. Just 10 years later, instead of counting traffic by gigabytes per day, we counted the traffic by gigabytes per seconds, and the internet global traffic rose up to 100 gigabytes per second (GBps). In 2014, the internet traffic has increased 160 times compared to 2002 and reached 16,114 GBps. Moreover, according to the CISCO prediction, in 2019, this number will be tripled at least.

From 2014 to 2019, the IP traffic will have a compound annual growth-rate (CAGR) equal to 23% . In 2016, the annual global IP traffic will beyond the zettabyte (1000 exabytes) threshold. In addition, in 2019, this number will be doubled, and reaches two zettabytes. Figure 1.2 is also coming from the CISCO forecast, it reports the growth forecast of the fixed internet, the managed IP and the mobile data. It is worth to emphasize that the mobile data traffic will have a CAGR

Table 1.1. Historical Internet Context

Year	Global Internet Traffic
1992	100 GB per day
1997	100 GB per hour
2002	100 GBps
2007	2000 GBps
2014	16,144 GBps
2019	51,794 GBps

Source: Cisco VNI, 2015

of 57% from 2014 to 2019. A promoting factor of such increasing is the increasing percentage of the fourth-generation (4G) employment. It brings a convenient and fast connection to people and generate an unexpected amount of mobile data.
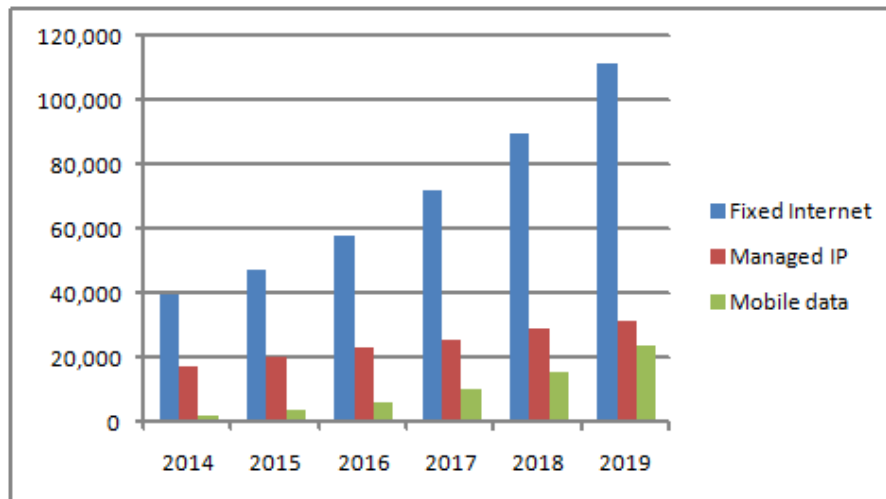
Figure 1.2. Global IP traffic forecast from 2014 to 2019, the unit of Y axis is Petabytes [PB] per Month.

Although the average IP traffic is predictable due to its steady growth pattern, the busy-hour traffic (or the traffic in the busiest 60-minutes period of the day) still has a dramatic growth and it increases much more fast than the average traffic. In 2014, the average traffic grew 29%, meanwhile, the busy-hour Internet traffic grew 37% [3]. It is mainly because the video and its related applications have claimed for 80 to 90 percent of total IP traffic. Their unique consuming patterns are the underlying reason for a much higher busy-hour traffic growth. The newly emerged Internet video sharing application also amplifies the gap between the peak and the average traffic, such as the live video, the ambient video and the video calling.

In order to guarantee the network operation, service providers plan the network

capacity according to the worst scenarios not the average one. This brings a big challenge to the metro network and the long-haul network, especially the metro network. The metro-only traffic is defined as traffic that traverses only the metro network and bypasses the long-haul traffic links. In the next five years, it will grow twice faster that long-haul traffic, mainly due to content delivery networks (CDNs) which carries 62 percent of the total Internet traffic by 2019.

The features of the traffic growth reveal several vital aspects of the future optical transmission systems. First, the optical transmission systems should satisfy the dramatic traffic growth with high bit rate choice. Second, due to the uncertain and unequal distribution of the traffic demands, the optical transmission systems should provide a certain degree of flexibility in terms of bit rate. In particular, the second aspect is the main concern of this thesis.

1.3 Legacy Paradigm: the IMDD Systems and Signal Regeneration Node

1.3.1 Intensity-Modulation Direct Detection System

Although today's core networks provide sufficiently enough capacities for the ongoing levels and types of traffic, the possibility of surging capacity at the edge of networks combined with the ever-increasing demand of applications, will accelerate the traffic growth over lots of applications and services that need high bandwidth and/or strict performance requirements. One of the key parts to keep the network advancement period, is to find the potential capability and the limitation of current technologies and architectures. Moreover, such study is helpful in determining what kind of technology advancement is needed by the next generation backbone networks.

Starting from the 1990s, the intensity-modulation direct detection (IMDD) systems have been commonly employed in the optical transmission system. As illustrated in figure 1.3, a typical IMDD system can modulate on the optical signal intensity, and the signal is detected by a photodetector at the receiver side.

The first key part of the IMDD systems is the modulation scheme. While the direct modulation IMDD with Fabry-Perot (FP) or distributed feedback (DFB) diode lasers design can offer a comparable modulation link gain in contrast to the external modulation [4] [5], the narrow passband drawback limits its commercial application. On the other hand, the external modulation has been commonly employed. The external modulation in a commercial IMDD system is based on the Mach-Zehnder interferometic (MZI) modulator that assembled in the inorganic material lithium niobate. In addition, it can offer a sufficient high frequency compared to the direct modulation. The lumped-electrode modulators can work at 150 MHz with a 0.65 V V_π [6].
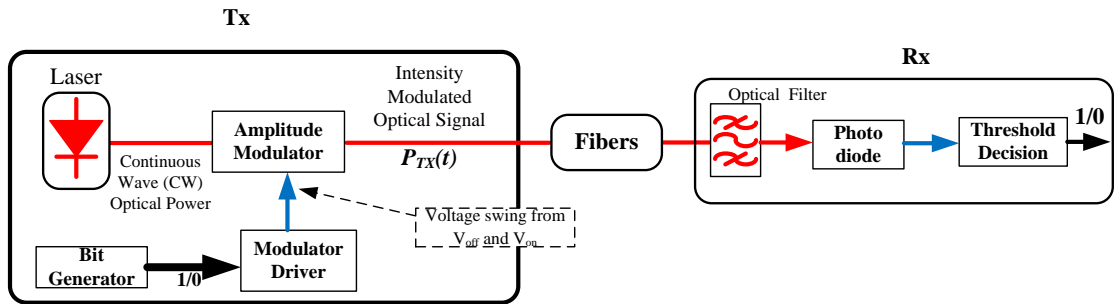
Figure 1.3.   The simplified IMDD scheme. It is basically an on-off keying system.

Another key part of the IMDD systems is the photodetectors. Any photodetectors that are available with a 3 dB bandwidth can satisfy the needs of most link applications [7]. The optical power of the photodetectors is a crucial parameter in both direct modulation and external modulation. In the direct modulation, the maximum modulation frequency is related to the optical power [8]. In the external modulation, although the larger optical power leads to more link gain, it also induces a large non-linearities over modulation-devices. Fortunately, such problem can be properly solved by increasing the bias [9].

For simplification, the previous discussion does not contain the amplifier. However, the practical implementation requires the optical amplifier to recover the fiber loss and enlarge the transmission distance. Furthermore, combined with the wavelength division multiplexing technique (WDM, similar to the frequency division multiplexing in the radio frequency communication) [10], the system's capacity can be largely amplified. Therefore, up to the present date, the WDM IMDD optical transmission system still provide service to many users around the world.

A typical link of such system is shown in figure 1.4. The uniformed multi-span is delpoyed in this link. The main issue of such link is the chromatic dispersion. In addition, both the polarization mode dispersion (PMD) and the polarization dependent loss (PDL) are also generated by the fiber non-linear effect. To properly handle these problems, the dispersion compensation unit (DCU) before the link, in the link and after the link are all mandatory. Moreover, an optimized dispersion map is needed to do dispersion management [11].

1.3.2   The Signal Regeneration Node

In the legacy paradigm, the backbone networks are typically optical-electrical-optical based [12]. Due to the existing of dispersion compensation in the optical link, the signal is completely regenerated from the optical to electrical and then to optical
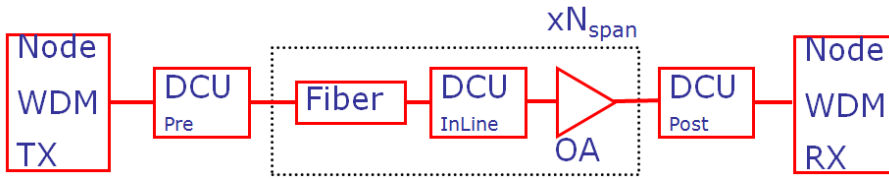
Figure 1.4.   A typical schematic diagram of WDM IMDD link. The DCU is refer to dispersion compensation unit.

again at each node as depicted in figure 1.5. All the routing work of the traffics are forced to finish in the electronic domain inside the node, no matter what is the destination of the traffic. The transponders can only work on a fixed wavelength. (a transponder is the element that sends and receives the optical signal from a fiber, and it is close to both the client side and the WDM signal network side.) It uses a large grooming switch which contains all the wavelengths enter into the node, and there is no way to implement all optical network on such a node.
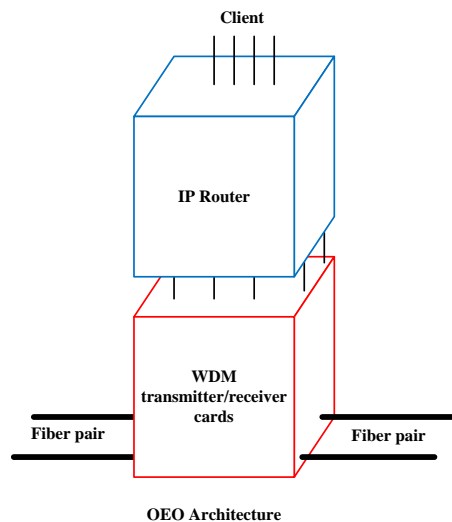
Figure 1.5.   A 2x2 OEO architecture.

1.4   Novel Paradigm: the Coherent Technology and Transparent Wavelength Routing

As pointed out in the previous section, the continue growth of current applications is the driving force behind the requirements for advanced technologies in the backbone

networks. Thanks to the modern transmission technologies, a novel paradigm is proposed to satisfy the traffic needs. The novel paradigm based on coherent optical transmission system can provide large bit rate choice mainly due to the employment of polarization multiplexed multilevel modulation format. A typical commercial PM-QPSK coherent optical transmission system has a 100 Gb/s per channel per fiber net bit rate [13], which is ten times the bit rate offered by the IMDD system.

Another important feature of the novel paradigm appears at the receiver side. Thanks to the powerful digital signal processing (DSP), now it is possible to compensate all the chromatic dispersion in an electronic way [14]. Inside the DSP, the chromatic dispersion can be compensated by a series of finite impulse response filters (FIR). In addition, the phase and polarization recovery can also be done in real time by the DSP. A second stage equalizer is employed to recover for the PMD, PDL and state of polarization (SOP). A typical coherent receiver structure is illustrated in the figure 1.6.
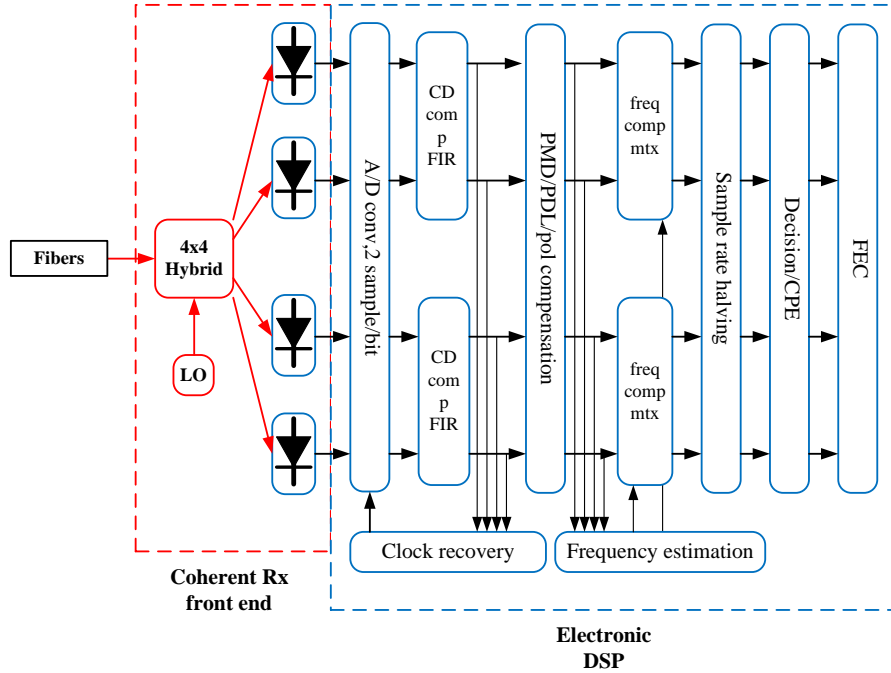
Figure 1.6. A dual stage equalizer structure is employed in the DSP. The first stage is constructed by two FFT-based FIR filters to compensate for the chromatic dispersion. The second stage contains a "butterfly" equalizer to recover other signal distortion.

As a result, there is no dispersion compensation in the optical link now. The signal now is passing from one node to another through several fiber spans as shown in figure 1.7. At the end of each span, an EDFA is employed to recover for the total

loss of the fiber span. In particular, this makes the transparent wavelength routing possible. Furthermore, the all-optical node is also possible in the novel paradigm. In contrast to the OEO node, it is both cost and power saving. Moreover, the optical reach of the all-optical node can be extended to 1500-4000 km, while the legacy networks can only realize a maximum reach of 500 km [12].
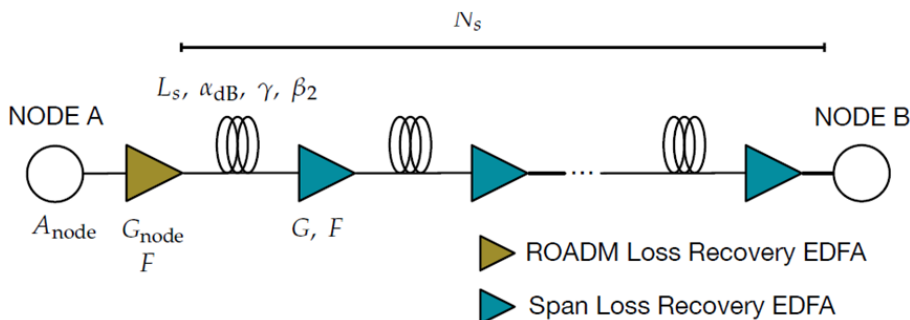
Figure 1.7. In the novel paradigm transmission link, there is no more dispersion compensation.

1.5 The Thesis Structure

In this thesis, in chapter 2 I discuss the necessity of the flexibility of optical network in the first place. Secondly, the channel spacing adjustment method is introduced as a promising approach to increase network flexibility. Thirdly, another approach called mixing standard modulation formats in different channels is analysed, and the back-to-back performance of such approach is studied. Although it not works well at the beginning, the back-to-back performance indicates that there is no interference between the channels with different modulation formats.

Then, in chapter 3, instead of combining different channel together to offer bit rate flexibility, I focus inside one channel and increase the spectral efficiency by hybrid two modulation formats in the time domain. With such a novel modulation formats, any arbitrary spectral efficiency can be achieved with a given symbol rate. Corresponding concepts and formulas are discussed first. After that, four transmitter operation strategies are proposed and evaluated. The same BER strategy is the winner of all operation strategies, especially from a practical point of view. As a complementary analysis, a more general hybrid scenario is studied, and the results indicate that particular hybrid combinations does have advantage in the back-to-back performance.

In chapter 4, building upon the TDHMF, we proposed another novel modulation format called flexible M-PAM modulation format (FlexPAM). Followed the same study manners, the FlexPAM has been deeply analysed. Similar to TDHMF, I first

introduced the characterization of FlexPAM and the related average BER formula. Then, four transmitter operation strategies similar to TDHMF are proposed and evaluated. The same BER strategy is chosen as the best operation strategy. A more general FlexPAM is also shown that some particular hybrid combinations have a better sensitivity performance.

Before jumping into the signal propagation discussion, a numerical model which predicts the system propagation performance is introduced in chapter 5. In addition, I explains the simulation system of this thesis and the methodology of my work.

In chapter 6, both TDHMF and FlexPAM propagation performances in non-linear uncompensated systems are examined. Due to their asymmetric and power unbalance frame structure, normally their propagation performance has some penalty against the model prediction. Several countermeasures are proposed to solve this issue. Then, I compare the propagation performance of both TDHMF and FlexPAM in a large bit rate range with or without countermeasures.

Finally, chapter 7 draws a conclusion.

Chapter 2

Flexibility Momentum in the Optical Network

2.1 Introduction

Induced by the ultra-high definition video broadcasting services and other high-speed broadband applications, the global IP traffic is expected to have a dramatic growth in the foreseeable future. Moreover, all these video related applications put a lot of pressure on the optical network, such as busy-hour traffic and the heterogeneity of the demands (huge gap between small and large demands). Despite the fact that there is a sufficiently broad spectrum, it is quite difficult to transmit the high-data-rate signal over long distances at high spectral efficiency .

On the hardware side, the state-of-the-art computer technology like multi-core processing, cloud storage and input-output convergence has pushed forward the standardization of higher speed Ethernet for industrial communication and the computing environment. In addition, all these advanced technology will strengthen the foundation for the next generation applications. As a result, the data flow of these applications will be definitely in a range from 10 Gb/s up to terabits (Tb) per second. To support such data flow, the operators must connect optical links that include 100 Gb/s bit rate class or even higher.

The overall traffic demands will be distributed uncertainly and unequally in the near future and result in a wide diversity of traffic demands ranging from 10 gigabits per second to terabits per second. Therefore, the network operators need to find a solution to satisfy such traffic demands in a cost-effective and scalable way.

To properly handle this problem, the operators need flexible and adaptive networks which contain flexible transponders and other network equipment that can adapt to the actual traffic demands. To this purpose, several possible methods have been proposed, including spectrum-sliced elastic optical network (SLICE) [15], baud rate

adaptation [16], rate-adaptive FEC [17], 4-D set-partitioned QAM [18–20] and flexible modulation format [21] [22]. In this chapter, first of all the channel spacing adjustment is introduced as a promising method. Secondly, one of the most straightforward methods, called mixing modulation formats in different channels, is analysed deeply.

2.2 Channel Spacing Adjustment

The recent innovative technologies in the optical transmission systems, like phase and multi-level modulation formats, polarization multiplexing, coherent detection and DSP, have laid a solid foundation for the commercial long-distance dense wavelength-division multiplexed (DWDM) transmission system with 100 Gb/s bit rate per channel. In addition, the optical signal can go through multiple nodes and links without signal regeneration (optical-electrical-optical, OEO). This makes the transparent wavelength routing becoming possible and brings advantages like removing both the space and power consuming OEO component and the automatically optical paths assignment. Nevertheless, the main concern regarding the transparent wavelength routing is the large fixed bandwidth. The main advantage of transparent wavelength routing is its efficient utilization of network capacity. Thus, it inherently conflicts with the current large fixed bandwidth in the International Telecommunication Union (ITU) rules.

In the current optical network, all the equipment is running with the 50 GHz ITU wavelength grids. According to the rules, the C-band (optical spectrum range from 1530 nm to 1565 nm) is divided into lots of fixed 50 GHz slots. The maximum bit rate that can be transmitted within such slot is 100 Gb/s. A bit rate higher than this number can not fit into this ITU scheme. Moreover, it requires all the optical links to work at their busiest moment all the time to avoide network crash. However, in many scenarios the traffic demands vary in a large range as indicated in previous paragraph. The network needs a finer granularity to allocate the spectrum resource. The channel spacing adjustment, also called flex grid [23], is one of the most promising approaches to handle this problem.

Being compatible with the current 50 GHz ITU grid, the 100-Gb/s-based transmission systems have commonly been employed in the last couple of years. In order to take full advantage of the existing system, the telecom and datacom industries are paying more attention to bit rate beyond 100 Gb/s, especially for the 400 Gb/s case. However, the spectral width of 400 Gb/s with standard modulation formats is larger than the 50 GHz ITU grid. Through using higher cardinality modulation format with higher spectral efficiency, the 400 Gb/s case can be put into the 50 GHz grid. On the other hand, it only allows a short transmission distance. Figure 2.1 gives a detailed description of the comparison between the exiting ITU grid and the flex grid.

Moreover, figure 2.2 from the past work [24] shows that in a flexible grid, systems
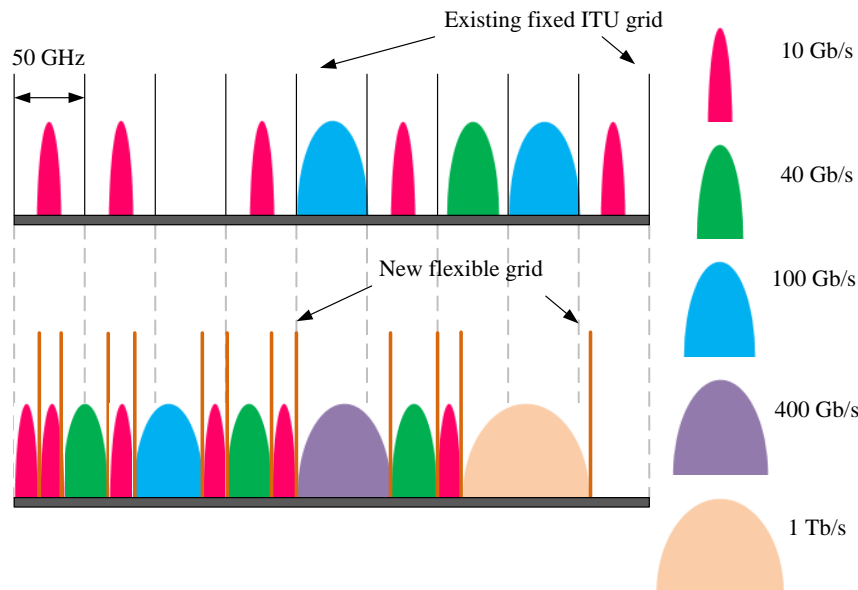
Figure 2.1.   Spectral widths of different bit rates relative to the ITU grid(for a given modulation format). Top: existing ITU 50 GHz grid; bottom: flex grid.

may have a lot of maximum reach plus system capacity combinations. In a fixed 50 GHz slots circumstance, there would only be one marker for each chosen modulation format, which limits the operators choice for designing the link and forces them to either sacrifice the system reach or the system capacity. However, when the flex grid is employed, it adds a lot of flexibilities into the network and offers a finer granularity between system reach and capacity.

In particular, such a new scheme will create a new network called the elastic optical network which has a number of distinguishing features. Firstly, it can satisfy higher bit rate beyond 100 Gb/s, such as 400 Gb/s and 1 Tb/s. Secondly, it can offer different bandwidth choices depending on the actual traffic condition. In addition, with a finer grid, the transmission system can use the existing spectrum resource more efficiently. At last, it allows dynamic network management.

However, on the network level, there are still some issues to resolve on the flexible spectrum allocation algorithm, the routing and non-uniform spectrum allocation scheme, and the network management. On the node level, corresponding technology, such as the otpical switching and the filtering device that provide a high resolution and steep performance, is not yet ready. Furthermore, from the operator's point of view, the network should be upgraded smoothly and economically [25]. But the flex grid will require a major change of the existing equipment that follows the current ITU grid. Therefore, during the evolution towards next generation networks, the current fixed grid networks will be upgraded only if they are no longer able to satisfy
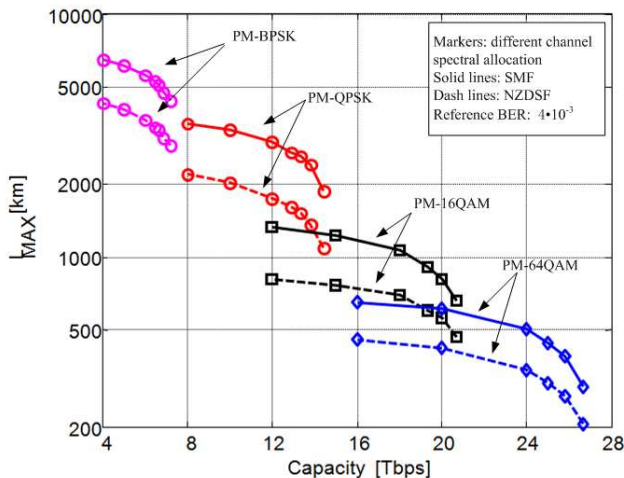
Figure 2.2.   The maximum reach of the system with different capacity. Different markers represent different channel spacing.

the traffic demands anymore. For some nodes/links, they will have a much faster traffic growth and traffic congestion [26]. So these nodes/links may be the first to be upgraded. Thus, the most-likely scenario is that, both fixed grid and flex grid scheme will operate at the same time. However, according to [27] [28] such a scenario will not happen for at least ten to fifteen years later. For those newly built data center or large content provider, flex-grid is still not an optimal choice for the current situation.

2.3   Mixing Standard Modulation Formats in Different Channels

2.3.1   Simplified Three Channel Model

The state-of-the-art transponder allows the transition of multiple standard modulation formats for different channels. In addition, different modulation formats can be assigned to different channels depending on the traffic demand and provide different bit-rate choices. This means through combining the bit rate of different channels, we can design a specific link to satisfy the unique traffic demands. Mixing different modulation formats in different channels is one of the most straightforward approaches for solving the network flexibility issue. In order to verify such approach, it is very important to testify that whether the different modulation formats deployed in different channels affect each other or not.

To this purpose, a simplified three channel model depicted in figure 2.3 was

studied. A typical coherent optical transmission system was considered here, details about the system layout can be seen in section 5.3.1. At the transmitter side, all the channels are shaped by a Nyquist filter with roll-off equals to α and the channel spacing allocation is equal to Δf. For simplification, only three channels were considered in this study, and they were the center channel and the two side channels. The K_S is defined in equation 2.1, where R_S is the symbol rate.
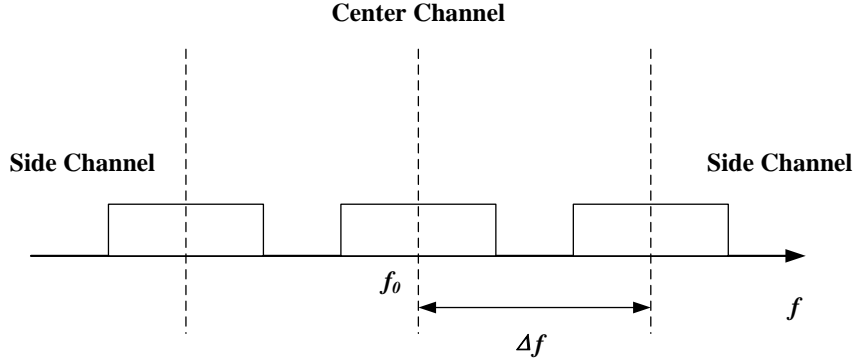
Figure 2.3. The transmission system has only three channels. And the center frequency is equal to f_0, channel spacing is equal to Δf. The filter's roll-off is equal to α.

$$K_S = \frac{\Delta f}{R_S} \tag{2.1}$$

2.3.2 Back-to-Back Performance

Four different standard modulation formats were considered. They are polarization multiplexed binary phase-shift keying (PM-BPSK), polarization multiplexed quadrature phase-shift keying (PM-QPSK), polarization multiplexed 16 quadrature amplitude modulation (PM-16QAM) and polarization multiplexed 64 quadrature amplitude modulation (PM-64QAM). One modulation format, for example PM-QPSK, was deployed in the center channel. Then another modulation format from the remaining three modulation formats, for example PM-16QAM, was chosen to be deployed on both side channels. At the receiver side, only the center channel performance was considered.

Furthermore, to testify the general behaviour of the mixing modulation formats in different channels, different values of the channel Nyquist filter roll-off α and channel spacing coefficient K_S were considered to represent different system operation conditions. The α ranged from [0,0.05,0.1,0.2,0.3] and the K_S ranged from [1.00,1.05,1.10,1.15,1.20]. The target BER is equal to 10^{-3}. More details about the

simulation system layout can be seen in section 5.3.1. Noted that, in the following discussion the bit-per-symbol (BpS) of a modulation format is used to represent the modulation formats which is deployed in the channel. Therefore, for PM-BPSK, BpS=2; for PM-QPSK, BpS=4; for PM-16QAM, BpS=8; and for PM-64QAM, BpS=12.

The back-to-back performance of such a simplified three channel system is shown in the following figures. In figure 2.4, the PM-BPSK is deployed in the center channel. All possible side channel modulation format choices have been concerned. With a given roll-off, for example in the $\alpha = 0.2$ case, the magenta curve ($K_S = 1.0$) gives the worst performance. It has the largest sensitivity for almost every given side channel modulation format cases except PM-BPSK. This is because too small channel spacing allocation would incur unnecessary inter channel interference. When the channel spacing increases (K_S increases), the back-to-back performance got improved. Till $K_S = 1.10$, which the channel spacing is 1.1 times larger than the symbol rate, the system can enjoy the benefit of enlarging the channel spacing. After this value, the green line, the blue line and the cyan line overlap with each other. Thus, the channel spacing won't make any impact on the system performance unless it is too small.

The black dash line is the back-to-back performance of only the center channel scenario. Therefore its sensitivity performance can be regarded as the reference. Normally, the three channel back-to-back performance should be worse than or at most equal to the reference. However, due to the simulation results fluctuation, some times the three channel system performance may slightly better than the reference. For instance, in figure 2.4 (a) and (c), there are some points below the reference. These fluctuations of the simulation results are mainly due to the interpolation algorithm in both the simulation software and the matlab DSP code.

It should be noted that, there is one exception in figure 2.4, when side channel is using PM-BPSK and the channel spacing is equal to the symbol rate, the system performance has some sensitivity advantages compared to other modulation formats deployed in the side channel cases. It seems like that, in a super channel circumstance, when the side channel is using PM-BPSK as its modulation format, the center channel will have an extra system margin as long as the filter roll-off is larger than 0. This phenomenon can be temporarily defined as the "PM-BPSK side channel advantage".

In figure 2.5, the PM-QPSK is deployed in the center channel. The impact of channel spacing on the system performance is similar to the center channel with PM-BPSK case. After a certain amount channel spacing increase, the sensitivity decrease benefit is not significant. In particular, the "PM-BPSK side channel advantage" appears again. The system has an extra margin about 1 dB or even higher compared to other modulation formats deployed in the side channels cases.

In figure 2.6 and figure 2.7, where PM-16QAM and PM-64QAM are deployed in the center channel respectively, some results of $K_S = 1.0$ and/or $K_S = 1.05$ cases are missing. This is because when the channel spacing is too small, the sensitivity

16
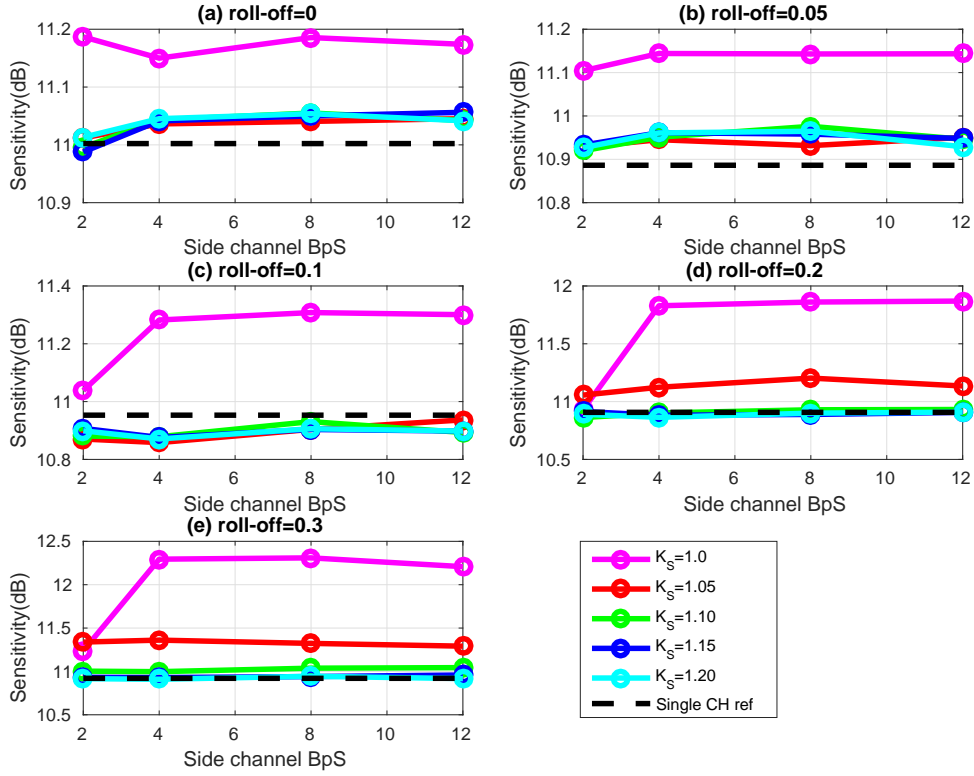
Figure 2.4.   The Center channel used PM-BPSK. And the BpS of side channel's modulation format varied from two to twelve. All five roll-offs are considered in each sub plot. Inside each sub plot, different curve represents different channel spacing.

is either too large to measure or cannot be measured at all. However, in figure 2.6 (d) and (c), when the channel spacing is equal to the symbol rate, the sensitivity of PM-BPSK deployed in both side channels cases can still be measured. This indicates that the "PM-BPSK side channel advantage" still exist.

For the filter roll-off, it may not affect the system performance. When the roll-off is equal to 0, all the signal is restricted inside the channel. Hence, the inter-channel interference is eliminated. That is why, the extra margin of side channel using PM-BPSK in a super channel circumstance does not happen in the roll-off equal to 0 case. However, it is not possible to have a real filter with 0 roll-off. There is always inter-channel interference in the real world. Therefore, the "PM-BPSK side channel advantage" may always exist in a super channel circumstances, and we may take advantage of this phenomenon.

In order to testify the advantage of side channel using PM-BPSK in a super

17
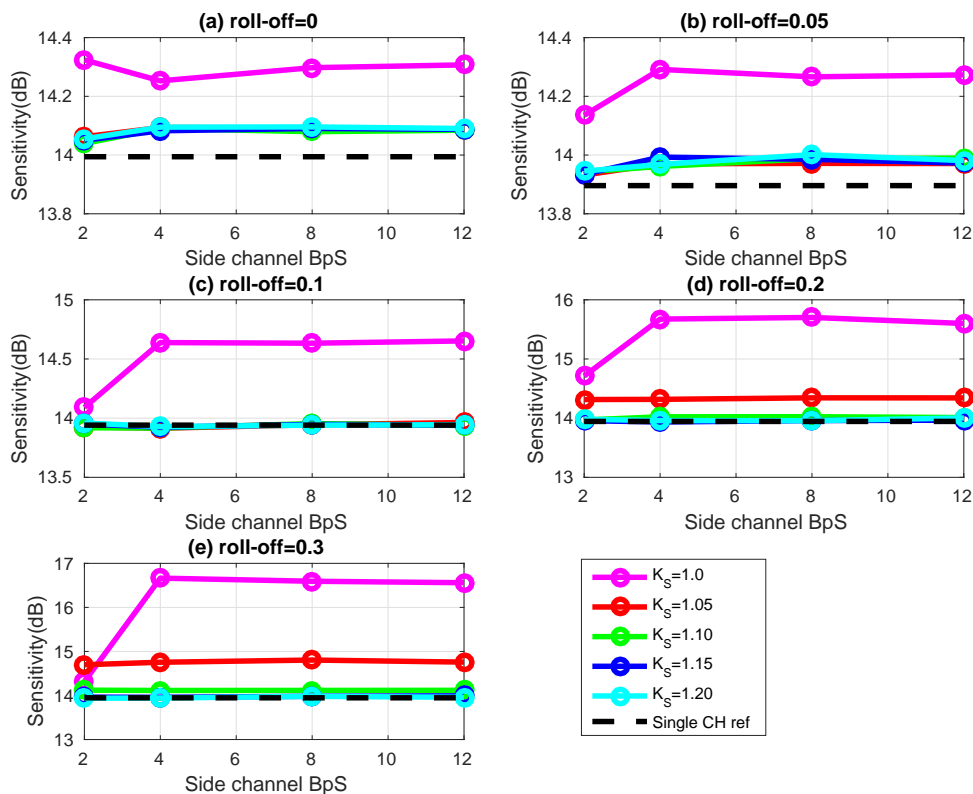
Figure 2.5.   The Center channel used PM-QPSK. And the BpS of side channel's modulation format varied from two to twelve. All five roll-offs are considered in each sub plot. Inside each sub plot, different curve represents different channel spacing.

channel circumstance, a series simulations had been operated, including adding dispersion before the receiver, different laser initial phase, noiseless simulation set-up and so on. After analysing the sensitivity, the probability density function (PDF) and the power spectrum density (PSD) of the signal in these simulations, the "PM-BPSK side channel advantage" still cannot be explained.

Fortunately, the reason of this "PM-BPSK side channel advantage" was found in the last moment, and it is because of the missing of the laser linewidth. The laser linewidth, typically in a single-frequency laser, is the full width at half maximum (FWHM) of its optical spectrum [29]. It has a strong relation with the temporal coherence, which is characterized by the coherence time or coherence length. More importantly, the laser linewidth can cause the phase noise problem. Previous simulations were all operated with an ideal laser which has 0 MHz laser linewidth.
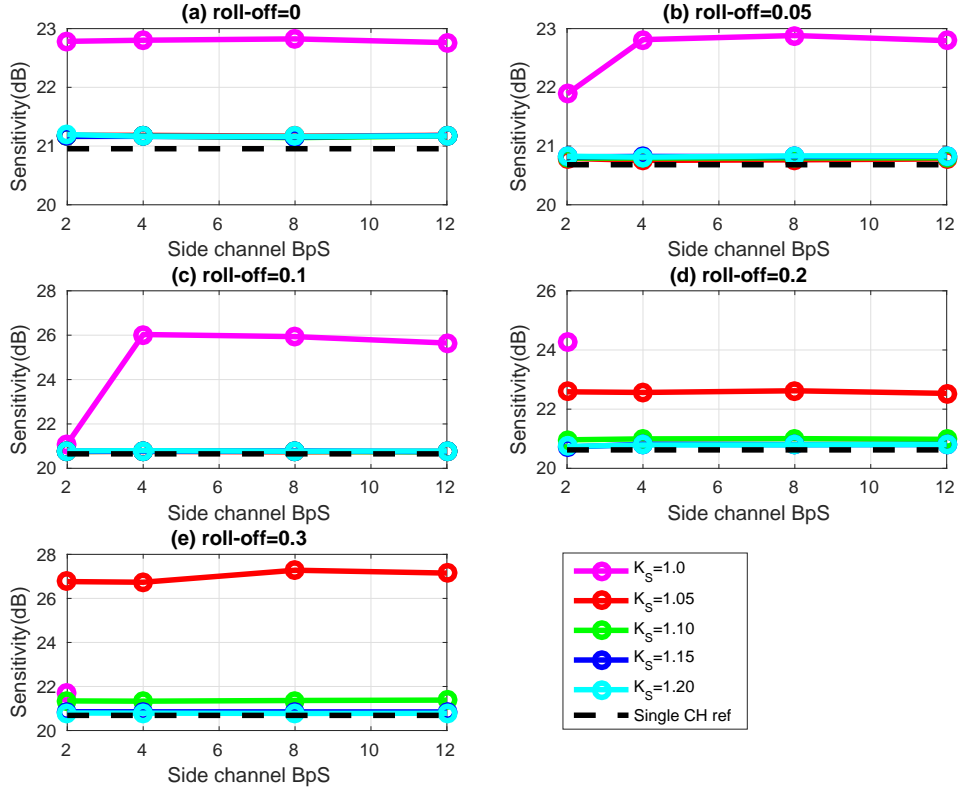
Figure 2.6. The Center channel used PM-16QAM. And the BpS of side channel's modulation format varied from two to twelve. All five roll-offs are considered in each sub plot. Inside each sub plot, different curve represents different channel spacing.

In figure 2.8, a 20 MHz laser linewidth is employed in the simulation system. In addition, in order to eliminate the interference caused by a specific laser initial phase, 100 different random seeds that related to the laser initial phase are applied to the laser. The channel spacing is equal to the symbol rate for simulating a super channel scenario . The filter roll-off is equal to 0.2. Moreover, in figure 2.8, the center channel is using the PM-QPSK, four sub figures refer to the side channel using different modulation format cases respectively.

The histogram of the simulation results represent the PDF of the sensitivity. It is clear that now the "PM-BPSK side channel advantage" is disappeared. The PDF of side channel using PM-BPSK case is almost the same as the other three cases, and the mean value difference is less than 0.1 dB. The red line is also the estimation of the PDF of the result based on a normal kernel function [30]. It gives a more
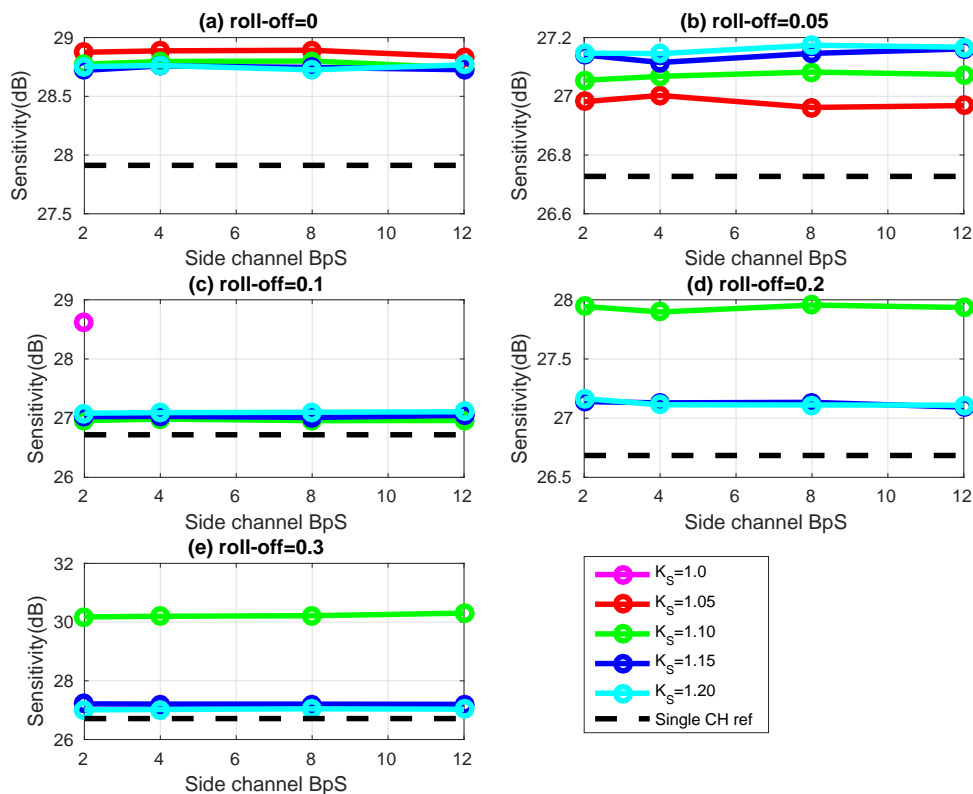
Figure 2.7. The Center channel used PM-64QAM. And the BpS of side channel's modulation format varied from two to twelve. All five roll-offs are considered in each sub plot. Inside each sub plot, different curve represents different channel spacing.

directly view of the PDF as a supplement to the histogram. Therefore, the extra margin brought by PM-BPSK is disappeared after the laser linewidth is employed. This is also true for other modulation formats deployed in the center channel cases.

So, from the previous analysis, it can be concluded that, mixing the standard modulation formats in different channels does not cause inter channel interference. For the center channel, it still has the same back-to-back performance as the all channel using uniform modulation format scenario. As a result, it won't cause a big difference in the propagation performance in contrast to the current single modulation format system. Thus, the optical signal non-linear propagation simulation is not discussed in this thesis.

Above all, by employing different modulation formats in different channels, the operators can obtain some flexibilities. In addition, this mixing modulation formats
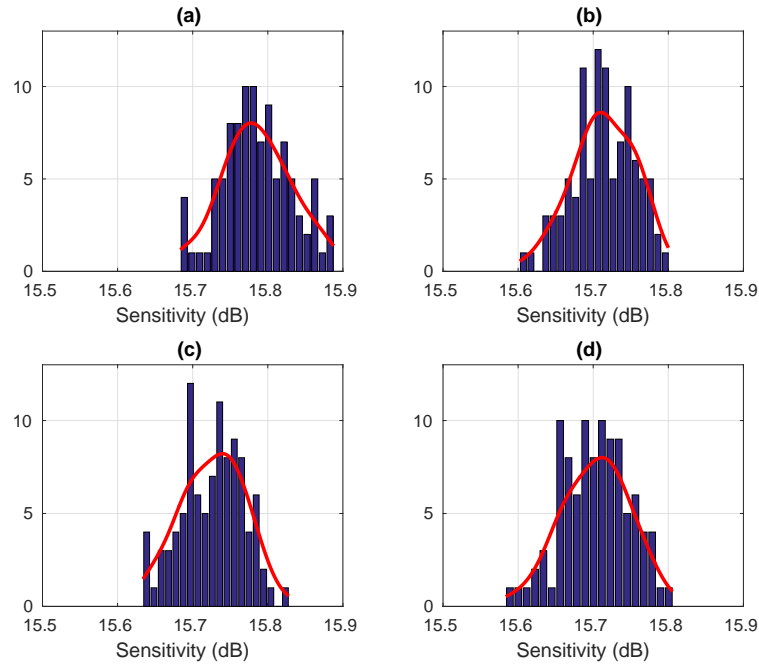
Figure 2.8.   Histogram of the results with different laser initial phase. (a) side channel: PM-BPSK; (b) side channel: PM-QPSK; (c) side channel: PM-16QAM; (d) side channel: PM-64QAM. The red curve is the estimation of PDF based on the normal kernel function.

in different channels approach won't induce an extra inter channel interference. Thus, it can be a possible solution for the network flexibility issue.

Chapter 3

Time Division Hybrid Modulation Formats

3.1 Introduction

To satisfy the exponential traffic growth in the back-bone network, the optical transmission system with wavelength division multiplexed (WDM) channels carrying 100 Gb/s has become available in the market. The physical capacity limit of such system with standard single mode fiber (SSMF) is now possible to be reached and a 100 Tb/s per fiber record has been realized [31]. However, the dramatic growth of the traffic is still considered a challenge with the existing optical network infrastructure. The Spatial division multiplexing (SDM) technologies as an alternative choice has already attracted much interest [32–34]. However, the SDM requires a large integration of both electronic and photonic equipments and a possible replacement of the existing fiber infrustructure. Needless to say, operators would definitely like to avoid large investments and to achieve more profit with the existing fiber. To take full advantage of the existing devices and fibers, researchers are paying much attention to the flexible optical networks, mainly because it can efficiently utilize the existing channel bandwidth [35] [36].

In such a scenario, the evolution of optical networks tends to maximize the time-flexibility. In fact, one of the key features of the transceivers is able to maximize spectral efficiency (SE) by adapting to the actual conditions of the network and the data rate for each given traffic demand [23]. In order to simplify the transceiver implementation, both the spectral allocation Δf of the channel and symbol rate R_S are kept as constants. Figure 3.1 shows the relationship between standard modulation formats and the maximum reach. The traditional use of the *standard* polarization multiplexing modulation formats with given bit-per-symbol (BpS) can not satisfy the enlarging spectral efficiency needs, because $SE = BpS \cdot \Delta f / R_S$. A flexible

transceiver which operates on demand with *N* different modulation formats could be a possible solution. However, the flexibility of such a transceiver is still limited by the N values corresponding to the modulation format *BpS*.

Bit Rate (Gb/s)

$BER_T = 2 \times 10^{-2}$

PM-64QAM: 300

PM-16QAM: 200

PM-QPSK: 100

PM-BPSK: 50

0

5.6 dB   6.1 dB   3 dB
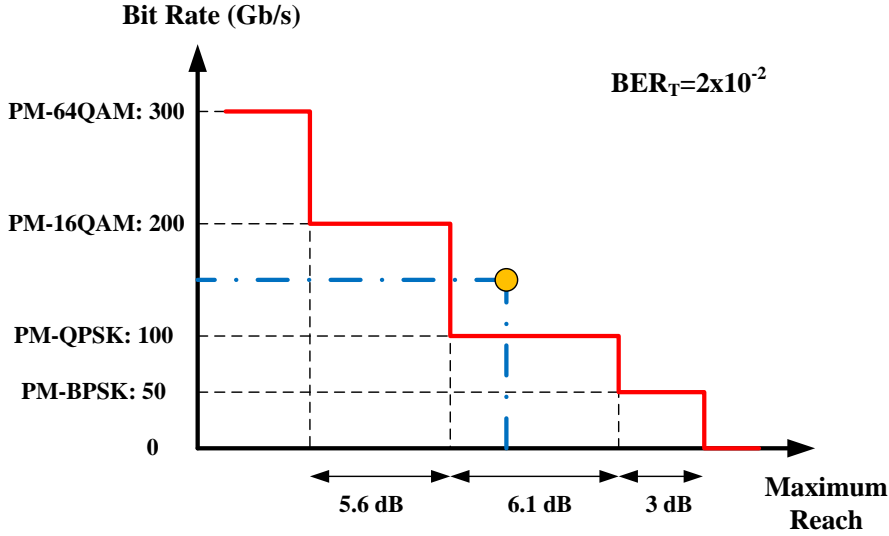
Maximum Reach

Figure 3.1.   The relationship between the bit rate and the system maximum reach. Suppose a system is required to work at the yellow spot. With traditional modulation format, we have to either sacrifice the system capacity or the system reach. The operators need a finer granularity to solve this problem.

The time-division hybrid modulation format (TDHMF) offers a solution that gives a more meticulous granularity for measuring *SE*. Although TDHMF leads to a trade-off with system maximum reach, it can offer arbitrary *SE* by hybrid two modulation formats in the time domain. This idea was first discussed in [37]. Moreover, it has been proved that TDHMF is feasible based on a pair of modulation formats in the square QAM family [38–44]. However, the transmitter operation strategy for TDHMF has not been fully studied in all previous research.

In this chapter, the general characterization and formula of TDHMF is discussed. Then, four different transmitter operation strategies are proposed and evaluated in term of sensitivity.

3.2 TDHMF Characterization and Theoretical Formulation

3.2.1 TDHMF Characterization

Generally, the TDHMF is a hybrid between two modulation formats (F_1 and F_2) in the time domain. Each format can be characterized by its power (P), SNR, BpS and the number of symbols in the entire frame (N). Both formats F_1 and F_2 operate at the same symbol rate R_S. The entire frame structure of TDHMF is depicted in figure 3.2.
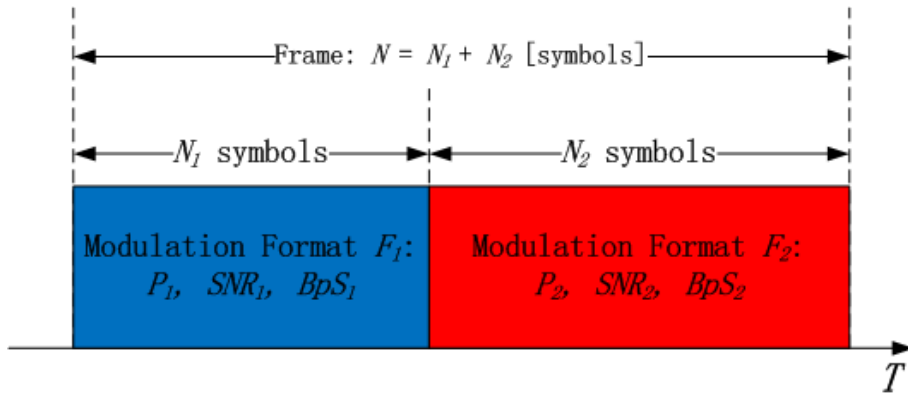
Figure 3.2. The frame structure of TDHMF in time-domain. It contains two modulation formats, which are characterized by its symbol number N_i, transmission power P_i, signal-to-noise ratio SNR_i and bit-per-symbol $BpS_i(i = 1,2)$. The total symbol in the frame is N.

Thus, the average BpS of TDHMF can be calculated in equation 3.1. It can be easily concluded from this equation that, TDHMF can achieve arbitrary BpS by properly choosing the pair of modulation formats and the frame length. As a result, with a given symbol rate, TDHMF can offer arbitrary bit rate choice. Thus, it can add a huge amount of flexibilities into the network and satisfy different traffic demands.

$$BpS_{TDHMF} = \frac{N_1 \cdot BpS_1 + N_2 \cdot BpS_2}{N} \qquad (3.1)$$

3.2.2 TDHMF Theoretical Formulation

Two key parameters, the format ratio κ and the power ratio PR, should be defined in the first place. The format ratio is equal to the number of symbols of format 1 divided by the number of the total symbols of the entire frame, $\kappa = \dfrac{N_1}{N}$. The power ratio is equal to the power of format 2 divided by the power of format 1,

25

$PR = \dfrac{P_2}{P_1}$. In the following sections, PR is described in a dB manner, which means $PR = 10 \cdot \log_{10}\left(\dfrac{P_2}{P_1}\right)$.

With these two parameters, the following frame related parameters can be derived. Firstly, The total signal power $P_{\mathrm{Tx}} = \kappa \cdot P_1 + (1 - \kappa) \cdot P_2$. Secondly, the SNR of the total signal is $SNR = \kappa \cdot SNR_1 + (1 - \kappa)SNR_2$. Thirdly, the average BpS in equation 3.1 can be rewritten as $BpS = \kappa \cdot BpS_1 + (1 - \kappa) \cdot BpS_2$.

Hence, the overall bit-error-rate (BER) of TDHMF is given by equation 3.2,

$$BER = \frac{1}{\kappa \cdot BpS_1 + (1 - \kappa) \cdot BpS_2} \cdot$$
$$\left\{ \kappa \cdot BpS_1 \cdot \Psi_1\left[\frac{\mathrm{SNR}}{(1 - \kappa) + \kappa \cdot PR}\right] + (1 - \kappa) \cdot BpS_2\Psi_2\left[PR\frac{\mathrm{SNR}}{(1 - \kappa) + \kappa \cdot PR}\right]\right\},$$
$$(3.2)$$

where $\Psi_1(x)$ and $\Psi_2(x)$ are the BER expression of format 1 and format 2 respectively. Although it does not appear in the equation 3.2, the frame length N has an impact on the optical signal propagation [21] and does not affect the back-to-back performance.

Although there are many possible TDHMF hybrid combinations, I did an in-depth study of a subset of the hybrid between two neighbouring square QAM modulation formats. These kind of combinations can still provide arbitrary BpS in a large range, and they are easy implemented. More details about this topic will be covered in the later section.

So now, considering about the two neighbouring square QAM modulation formats, they have the constellation sizes M^2 and $(2M)^2$ respectively, where M is the number of levels in each quadrature. In order to analyze the back-to-back performance of TDHMF, I take the advantage of using the analytical estimation of the bit error rate (BER) for an M^2-QAM modulation format [45], whose expression is:

$$\Psi_{\mathrm{QAM}}(\mathrm{SNR}, M) = \frac{M - 1}{M \cdot \log_2(M)}\mathrm{erfc}\left(\sqrt{\frac{3\mathrm{SNR}}{2(M^2 - 1)}}\right) \qquad (3.3)$$

where SNR is the signal-to-noise ratio (SNR) per symbol and $\mathrm{erfc}(\cdot)$ is the complementary error function which is defined as,

$$\mathrm{erfc}(x) = \frac{2}{\sqrt{\pi}}\int_x^\infty e^{-t^2}dt. \qquad (3.4)$$

After taking account of the characteristic format ratio κ and constellation size M^2, equation 3.2 could be rewritten as,

$$\Psi_{\mathrm{TDHMF}}(\mathrm{SNR}_1, \mathrm{SNR}_2, M, \kappa) = \frac{N}{N_{BpS}} \cdot$$
$$[\kappa \log_2(M)\Psi_{\mathrm{QAM}}(\mathrm{SNR}_1, M) + (1 - \kappa)(\log_2(M) + 1)\Psi_{\mathrm{QAM}}(\mathrm{SNR}_2, 2M)], \quad (3.5)$$

where N_{BpS} is the average number of bits per symbol encoded in the TDHMF frame

$$N_{\text{BpS}} = N \cdot (\log_2(M) + 1 - \kappa). \tag{3.6}$$

SNR_1 and SNR_2 represent the SNR perceived by each modulation format, and they determining the average SNR for the TDHMF frame, $\overline{\text{SNR}}$, which is given by,

$$\overline{\text{SNR}} = \kappa \text{SNR}_1 + (1 - \kappa)\text{SNR}_2. \tag{3.7}$$

In addition, the power ratio, PR, between two modulation formats can be defined as followed,

$$PR \text{ [dB]} = 10 \log_{10}\left(\frac{\text{SNR}_2}{\text{SNR}_1}\right). \tag{3.8}$$

The power ratio depends on the adopted transmitter operation strategy and determines the back-to-back performance of TDHMF.

3.3 TDHMF Transmitter Operation Strategies and Back-to-Back Performance Evaluation

3.3.1 Transmitter Operation Strategies

Once the pair of modulation formats is chosen, the overall BpS, N_{BpS}, is settle in the range of $[BpS_1 : BpS_2]$. With a given format ratio κ and proper frame length N, any BpS in this range can be achieved. As a result, the overall spectral efficiency is defined with a given channel spectral Δf. Then, according to equation 3.5, once the power ratio is settled, the TDHMF back-to-back performance can be easily obtained. Therefore, the only remaining degree of freedom for setting the transmitter operation is the choice of the power ratio PR. To this purpose, the following four different transmitter operation strategies can be implemented.

1. *Constant Power* (PR = 0 dB): it keeps two hybrid modulation formats constant power during the transmission($P_1 = P_2 = P_{\text{Tx}}$), therefore the power ratio between two formats is $PR = 0\ dB$ and the SNR perceived by each format is $\text{SNR}_1 = \text{SNR}_2 = \dfrac{\overline{\text{SNR}}}{2}$. By substituting PR and SNR_i into equation 3.5, the following BER expression can be obtained,

$$\Psi_{\text{TDHMF}}(\text{SNR}, M) = \frac{N}{N_{\text{BpS}}} \cdot$$

$$\left[\kappa\frac{M-1}{M}\text{erfc}\sqrt{\frac{3\overline{\text{SNR}}}{4(M^2-1)}} + (1-\kappa)\frac{2M-1}{2M}\text{erfc}\sqrt{\frac{3\overline{\text{SNR}}}{4(4M^2-1)}}\right] \tag{3.9}$$

The constant power strategy is the simplest transmitter operation strategy. Only the largest constellation size modulation format $(2M)^2$ works at the forward-error correction (FEC) BER cliff, while the other format is basically working error free. However, it is not the optimal choice, which will be shown later. It is because that the constant power strategy leads to inefficiency in two aspects, the performance(large back-to-back penalties) and the receiver side complexity. Two QAM formats operate at completely different BERs, therefore it may requires two sets of FEC codes.

2. *Same Euclidean Distance* $(d_1 = d_2)$: the minimum Euclidean distance d_i(i=1,2) is kept equal for both modulation formats. So as to guarantee the same Euclidean distance, the power-ratio must be constant and depends only on the chosen pair of modulation formats. Assuming d represents Euclidean distance, and it is the same for PM-QPSK, PM-16QAM and PM-64QAM. Therefore, the average powers can be respectively considered as $\frac{1}{2}d^2$, $\frac{5}{2}d^2$ and $\frac{21}{2}d^2$. Consequently, the power ratio between two neighbouring square QAM is set. The SNR of perceived by each of the QAM is respectively given by,

$$\text{SNR}_1 = \frac{\overline{\text{SNR}}}{\kappa \cdot PR + (1 - \kappa)}, \tag{3.10}$$

and

$$\text{SNR}_2 = \frac{PR \cdot \overline{\text{SNR}}}{\kappa \cdot PR + (1 - \kappa)}. \tag{3.11}$$

By substituting both equation 3.10 and 3.11 into the BER expression 3.5, the final expression will be a function of $\overline{SNR}$, M and κ yields.

3. *Same BER* $(\Psi_1 = \Psi_2)$: both modulation formats are forced to operate at the same BER. In order to guarantee both modulation formats in TDHMF frame operate at the same BER, the required SNR must be determined by the target BER, Ψ_{target}, which the system needs to achieve. The required SNR can be obtained by inverting the BER expression of equation 3.3,

$$\text{SNR}_1^{\text{req}} = \frac{2(M^2 - 1)}{3} \cdot \left[\text{erfc}^{-1} \left(\Psi_{\text{target}} \frac{M \log_2(M)}{M - 1} \right) \right]^2, \tag{3.12}$$

and

$$\text{SNR}_2^{\text{req}} = \frac{2(4M^2 - 1)}{3} \cdot \left[\text{erfc}^{-1} \left(\Psi_{\text{target}} \frac{2M \log_2(2M)}{2M - 1} \right) \right]^2. \tag{3.13}$$

Hence, the power-ratio is consequently defined by,

$$PR = 10 \log_{10} \left(\frac{\text{SNR}_2^{\text{req}}}{\text{SNR}_1^{\text{req}}} \right). \tag{3.14}$$

The average BER of the whole TDHMF frame is then obviously given by Ψ_{target}, and the average SNR can be derived by substituting $\text{SNR}_1^{\text{req}}$ and $\text{SNR}_2^{\text{req}}$ in equation 3.7.

4. *Minimum BER* ($\Psi_{\min}$): through finding the optimum SNR pair, $[\text{SNR}_1^{\text{opt}}, \text{SNR}_2^{\text{opt}}]$, which minimizes the estimated BER of expression of equation 3.5, it is able to achieve the global minimum BER. Since in equation 3.7, with a given $\overline{\text{SNR}}$, the value of SNR_2 is automatically determined by the value of SNR_1. The following optimization procedure can be applied to determine $\text{SNR}_1^{\text{opt}}$,

$$\begin{aligned}
\text{SNR}_1^{\text{opt}} &= \left\{ \text{SNR}_1 : \Psi_{TDHMF} \left(\text{SNR}_1, \frac{\overline{\text{SNR}} - \kappa}{1 - \kappa}, M \right) \right\} \\
&= \min \left[\Psi_{TDHMF} \left(\text{SNR}_1, \frac{\overline{\text{SNR}} - \kappa}{1 - \kappa}, M \right) \right], \quad (3.15)
\end{aligned}$$

then $\text{SNR}_2^{\text{opt}}$ is given by,

$$\text{SNR}_2^{\text{opt}} = \frac{\overline{\text{SNR}} - \kappa \text{SNR}_1^{\text{opt}}}{1 - \kappa}. \tag{3.16}$$

The average BER of the whole TDHMF frame is then given by,

$$\begin{aligned}
\Psi = \frac{N}{N_{\text{BpS}}} \cdot \\
\left[\kappa \frac{M-1}{M} \text{erfc} \sqrt{\frac{3 \text{SNR}_1^{\text{opt}}}{2(M^2 - 1)}} + (1 - \kappa) \frac{2M-1}{2M} \text{erfc} \sqrt{\frac{3 \text{SNR}_2^{\text{opt}}}{2(4M^2 - 1)}} \right] \quad (3.17)
\end{aligned}$$

3.3.2 Back-to-Back Performance

In the last section, I explain that the power ratio is different when different transmitter operation strategy is employed. It also depends on both the chosen pair of modulation formats and the BER target. Therefore, in this section, the power ratio of different transmitter operation strategies are evaluated and compared in the first place. Then, at the given BER target, the sensitivity performance of each transmitter operation strategy is also discussed.

The square QAM family in this thesis contains PM-QPSK, PM-16QAM and PM-64QAM. In addition, PM-BPSK is also considered as a hybrid candidate, due to its resemblance to the PM-QPSK. Therefore, TDHMF now can offer arbitrary BpS from BpS=2 (PM-BPSK) to BpS=12 (PM-64QAM). In both figure 3.4 and figure 3.3, the BER target is $2 \cdot 10^{-2}$. BpS at 2, 4, 8 and 12 are standard square QAM modulation formats respectively, and they are PM-BPSK, PM-QPSK, PM-16QAM and PM-64QAM. The values between BpS=4 and BpS=8, they are the hybrid between PM-QPSK and PM-16QAM with different format ratios. For instance, BpS=5 is TDHMF operated with $\kappa = 0.75$; BpS=6 is TDHMF operated with $\kappa = 0.50$; and BpS=7 is TDHMF operated with $\kappa = 0.25$. A similar story happens from BpS=8 to BpS=12 but with PM-16QAM and PM-64QAM.

In figure 3.3, it compares the power ratio of different transmitter operation strategies. Since the constant power strategy has a 0 dB power ratio, it is not shown in the figure. Both the same Euclidean distance strategy and the same BER strategy have a constant power ratio as discussed in the last section. In these two strategies, different hybrid combinations have different power ratios. It should be noticed that, when TDHMF is the hybrid between PM-BPSK and PM-QPSK, all three strategies have the same power ratio. It is because PM-BPSK and PM-QPSK have very similar constellation structure, and PM-QPSK carries double bit rate compared to PM-BPSK. The same Euclidean distance strategy has the largest power ratio for a given BpS, then is the same BER strategy. The minimum BER strategy varies the power ratio with different BpS, but the power ratio is still smaller than the one of the previous two strategies. All these three strategies imply power unbalance along the time domain, and it induces a non-linear impairment on the signal propagation performance, which will be covered in the later chapters.

In figure 3.4, it compares all four operation strategies in terms of sensitivity. The blue line refers to the constant power strategy, the red line refers to the same Euclidean distance strategy, the green line refers to the same BER strategy, and the black line refers to the minimum BER strategy. It is obvious that the constant power is a suboptimal strategy. It has a much higher sensitivity at given BpS. The Minimum BER has the optimal performance. Although minimum BER has the best performance, the same Euclidean distance strategy and the same BER strategy have a comparable performance, and the difference is less than 0.2 dB. The minimum BER strategy implies more complexity, because each format delivers a different pre-FEC BER and should work with a specifically designed FEC. From a practical point of view, the same BER strategy may has a much simpler signal processing procedure because it allows using the same FEC for both modulation formats. At the same time, it has a negligible SNR penalty compared to the minimum BER strategy.
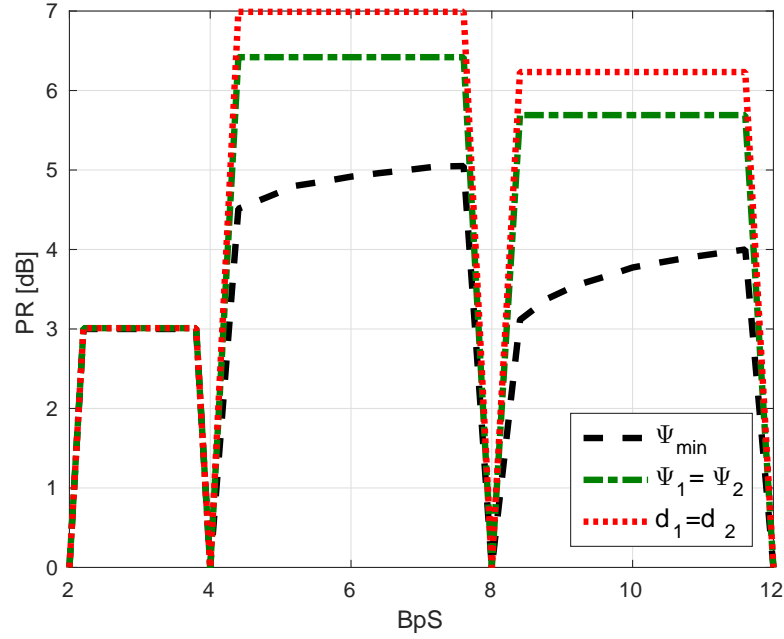
Figure 3.3. The power ratio of different operation strategies at different BpS.

3.4 Arbitrary Two Square QAM Hybrid

In the previous sections, the TDHMF back-to-back performance is estimated with two neighbouring square QAM modulation formats combinations. However, there is one question still remaining unsolved: why two neighbouring square QAM modulation formats are chosen as the hybrid combination?

Before answering this question, I would like to discuss about why I choose the square QAM family. The square QAM family can offer BpS in a large range. BpS above 12 (PM-64QAM) is possible to achieve and corresponding technologies have been fully developed. In this thesis, with the help of transmitter DSP and the digital-to-analog converter (DAC) followed by a linear modulator drivers, arbitrary modulation formats electrical signal can be generated. Then, with a quad-parallel Mach-Zehnder (QPMZ) electrical-to-optical converter, the optical signal with arbitrary modulation format is generated.

Actually, for a given BpS, there are many possible hybrid combinations. Among them, two neighbouring square QAM hybrid combinations offer the optimal back-to-back performance. In figure 3.5, it compares the sensitivity performance of the TDHMF hybrid between PM-QPSK and the other three modulation formats. Since the constant power strategy is a suboptimal strategy, it is not discussed here. At BpS=6, it can be a hybrid either between PM-QPSK and PM-16QAM or PM-QPSK

31
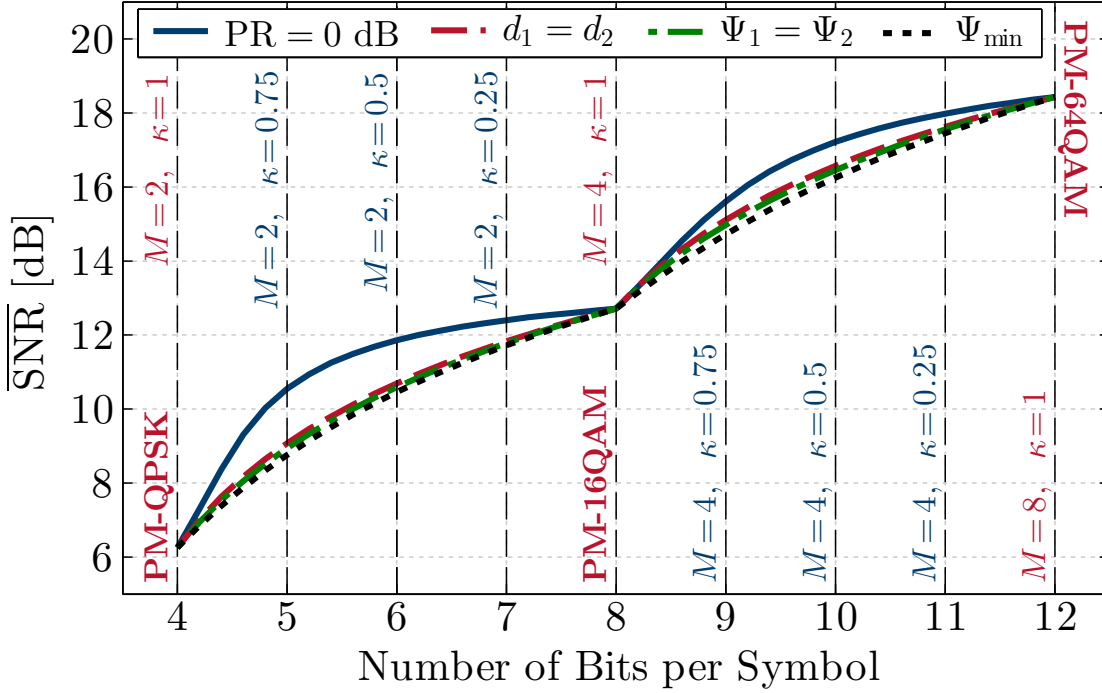
Figure 3.4.   Back-to-back sensitivity performance of TDHMF with four different transmitter operation strategy for a number of bits per symbol ranging from 4 (PM-QPSK) up to 12 (PM-64QAM). The constant power strategy is the suboptimal choice, the minimum BER strategy has the optimal performance, and the same Euclidean distance strategy and the same BER strategy have almost the same performance as the minimum BER strategy. The BER target $\Psi_{\text{target}} = 2 \times 10^{-2}$.

and PM-64QAM. The hybrid between PM-QPSK and PM-16QAM has much better performance, the SNR penalty is at least 2 dB (with the minimum BER strategy).

In addition, in figure 3.6, it compares the sensitivity performance of the TDHMF hybrid between PM-16QAM and the other three modulation formats. Again, at BpS=6 case, the hybrid between two neighbouring square QAM modulation formats has the optimal performance. The hybrid between PM-16QAM and PM-QPSK has an advantage about 1 dB compared to the hybrid between PM-16QAM and PM-BPSK.

The two SNRs perceived by two neighbouring square QAM have less difference with a given BER target. It is mainly due to the BER expressions. As a result, the overall $\overline{\text{SNR}}$ of the signal of two neighbouring square QAM hybrid combinations are smaller than the one of arbitrary hybrid combinations. Thus, for a given BpS, the two neighbouring square QAM combinations are the optimal choice. It should be pointed
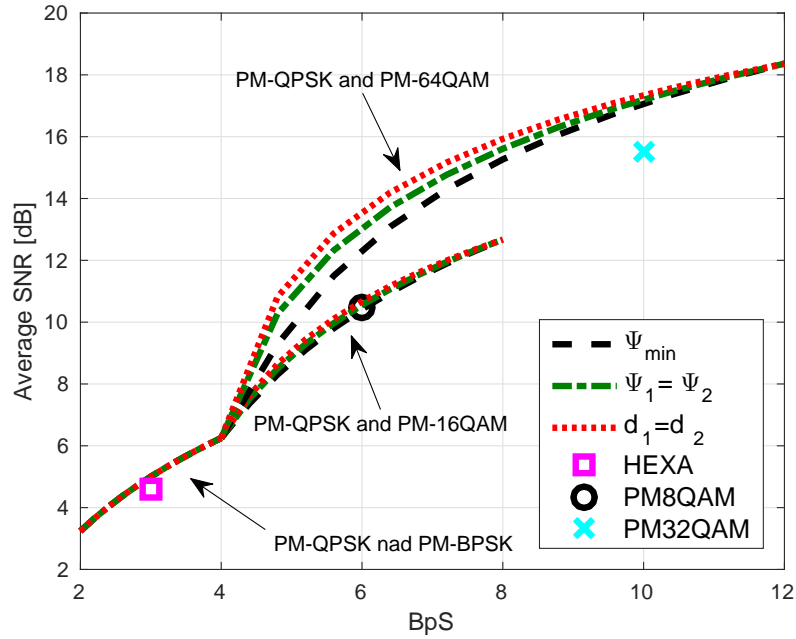
Figure 3.5. Hybrid PM-QPSK with PM-BPSK, PM-16QAM and PM-64QAM. Transmitter operates with the minimum BER strategy, the same BER strategy and the same Euclidean distance strategy. Three modulation formats with a fixed bit per symbol are compared to TDHMF.

out that, in both figure 3.5 and 3.6, three traditional modulation formats, HEXA [46], PM-8QAM and PM-32QAM, are compared to the TDHMF. The comparison results indicate that TDHMF has a negligible SNR penalty in contrast to these three modulation formats. This implies the potential of TDHMF replacing those standard modulation formats at a given BpS.
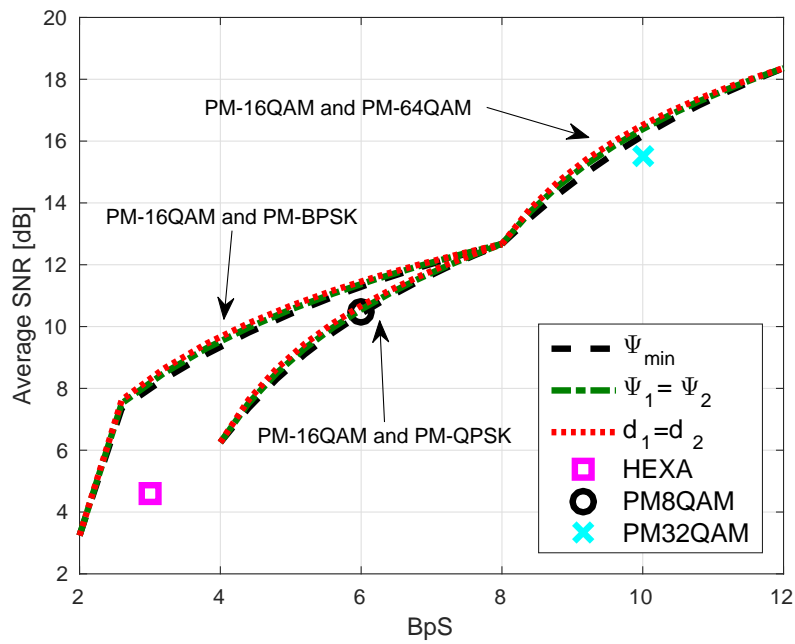
Figure 3.6. Hybrid PM-16QAM with PM-BPSK, PM-QPSK and PM-64QAM. Transmitter operates with minimum BER, same BER and same Euclidean distance strategies. Three modulation formats with a fixed bit per symbol are compared to TDHMF.

Chapter 4

Flexible M-PAM based Modulation Format

4.1 Introduction

Nowadays, the optical networks tend to increase their level of flexibility. Therefore, a transceiver that has the following feature will become favourable. Firstly, it could maximize the spectral efficiency. Secondly, it could also adapt to the actual conditions of network and data rate for every given traffic demand [23]. To simplify the transceiver implementation, it is convenient to keep the channel spacing Δf and the symbol rate R_S as constant. It has already been shown in figure 3.1 that the standard multi-level PM-MQAM modulation formats only allow a limited amount of flexibilities. Since $SE = BpS \cdot \dfrac{R_S}{\Delta f}$, those fixed BpS standard modulation formats can only offer a fixed spectral efficiency and cannot satisfy the flexibility requirement. One possible solution, which has been discussed in the previous chapter, is the Time-Division Hybrid Modulation Formats (TDHMF), which combines two different standard multi-level modulation formats in the time domain. In such a new scheme, a very large amount of flexibilities can be achieved. On the other hand, an increased transceiver complexity is required especially at receiver side when de-multiplex the two generating formats.

In this chapter, the flexible M-PAM based modulation formats (FlexPAM) is proposed and analysed. FlexPAM deploys four M-PAM modulation formats for each dimensions of the optical field (in-phase and quadrature on both polarizations). Although, FlexPAM can only work at integer BpS, which means a reduction of the flexibility compared to TDHMF, transceivers will benefit from employing FlexPAM for two main reasons: firstly, it simplify the transmitter and receiver structure because does not vary the format in time; secondly, from a networking perspective, it can assign each dimension to a specific tributary and select the M-PAM order based

on the traffic demand.

First of all, this chapter discusses the general characterization of FlexPAM and the corresponding theory formulation. Then, several transmitter operation strategies that similar to TDHMF are proposed and evaluated. In the last part, the back-to-back performance of FlexPAM is reviewed.

4.2   FlexPAM Characterization and Theoretical Formulation

4.2.1   FlexPAM Characterization

Thanks to the state-of-the-art transponder, we are able to modulate on each quadrature of the optical field. Figure 4.1 gives an example of FlexPAM constellation. In X-polarization in-phase, it uses a 4-PAM; and on quadrature, it uses an 8-PAM. In Y-polarization, the in-phase is a 4-PAM; and the quadrature is a 2-PAM. FlexPAM is the hybrid in the quadrature domain, and it takes advantage of all four quadratures in optical field. For the FlexPAM, it can be characterized by the power P_i, BpS_i and SNR_i ($i = $ 1,2,3,4)of each M-PAM. Since the $BpS_{symbol} = BpS_{XI} + BpS_{XQ} + BpS_{YI} + BpS_{YQ}$, with different M-PAMs combinations, it can offer many possible BpS. As a result, FlexPAM can add a lot of flexibilities into the optical network.

In figure 4.2, it gives several FlexPAM frame structure examples. It also shows that, there are many possible FlexPAM hybrid combinations for a given BpS. For example, for FlexPAM BpS=6, it can be a combination composed by the 2-PAM plus the 4-PAM plus the 8-PAM and the 0-PAM (nothing is transmitted in that quadrature). Another possible combination can be composed by the 2-PAM plus the 8-PAM plus the 2-PAM and the 8-PAM. Normally, the FlexPAM symbol structure is asymmetric. This would result in the polarization power unbalance and leads to a penalty in the signal propagation. Instead of studying arbitrary hybrid combinations, this thesis focus on the combinations with two neighbouring M-PAM. The reason of this focus will be mentioned in the later section.

Unlike TDHMF, FlexPAM is kept constant in the time domain. Therefore, one symbol can tell the whole story of the frame. Compared to TDHMF, FlexPAM can only offer integer BpS in a certain range. This is because FlexPAM has s consistent frame structure in time domain. Therefore, FlexPAM offers less flexibility in contrast to TDHMF for sure. On the other hand, this time consistent frame structure would result in an identical and simple transponder structure, which is very crucial for the operators. In addition, from the network point of view, it can assign each quadrature to a specific tributary and select an M-PAM based on the traffic demand. Thus, considering the advantage in transponder structure and network traffic assignment,
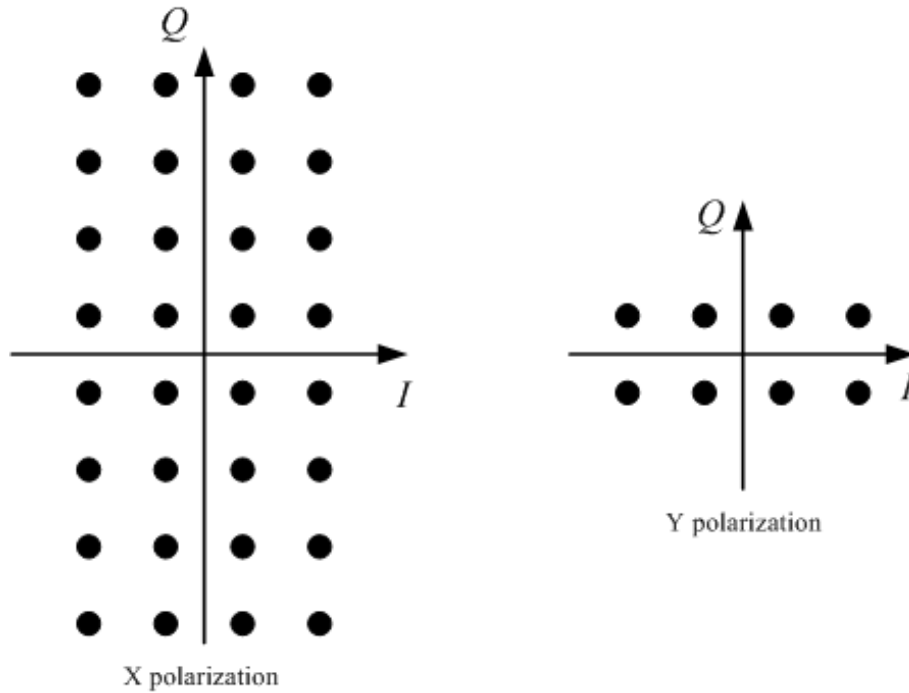
Figure 4.1.   The constellation of FlexPAM with 8 bits per symbol.

		BpS=8	BpS=6	BpS=6	BpS=11
X polarizatin	I	4-PAM	2-PAM	2-PAM	4-PAM
	Q	8-PAM	4-PAM	8-PAM	8-PAM
Y polarizatin	I	4-PAM	8-PAM	2-PAM	8-PAM
	Q	2-PAM	0-PAM	8-PAM	8-PAM

Figure 4.2.   FlexPAM symbol structure. The FlexPAM can be represented by a vector, whose elements are the cardinality of corresponding M-PAM in each quadrature. Four cases are shown here, BpS=8 ([2 3 2 1]), BpS=6 ([1 2 3 0]), BpS=6 ([1 3 1 3]) and BpS=11 ([2 3 3 3]). Since the thesis considered only 2-PAM, 4-PAM and 8-PAM, integer bits per symbol in the range of [4:12] can be achieved.

the lack of flexibility compared to TDHMF is totally acceptable.

4.2.2   FlexPAM Theoretical Formats

To analyse the back-to-back performance of FlexPAM, we may use the BER estimation equation of an M-PAM modulation format [45].

$$\Psi_{\text{PAM}}\left(\text{SNR}, M\right) = \frac{M-1}{M\log_2(M)}\text{erfc}\left(\sqrt{\frac{3\text{SNR}}{M^2-1}}\right) \qquad (4.1)$$

Starting from 4.1, two key parameters, the power ratio PR and the format ratio κ, are defined similar to TDHMF. The power ratio is equal to the power of PAM_2 divided by the power of PAM_1, thus $PR = \dfrac{P_2}{P_1}$. The format ratio is equal to the number of bits of PAM_1 divided by the number of total bits of the FlexPAM symbol, thus $\kappa = \dfrac{BpS_1}{BpS_{total}}$. In addition, the average BER of FlexPAM can be estimated by individually accounting for the BER incurred in each of its four orthogonal quadratures as ,

$$\Psi_{\text{FlexPAM}} = \sum_{i=1}^{4} \frac{M_i}{\sum_{i=1}^{4} M_i} \cdot \Psi_{\text{PAM}}\left(\text{SNR}_i, M_i\right), \qquad (4.2)$$

where M_i is the cardinality of each M-PAM.

By substituting the BER expression of the two chosen neighbouring M-PAM into equation 4.2, we can have the overall BER expression of FlexPAM as,

$$\Psi_{\text{FlexPAM}}\left(\text{SNR}_1, \text{SNR}_2, M, \kappa\right) = \frac{1}{\log_2(M) + 1 - \kappa}.$$
$$\left[\kappa\log_2(M)\Psi_{\text{PAM}}\left(\text{SNR}_1, M\right) + (1-\kappa)\left(\log_2(M)+1\right)\Psi_{\text{PAM}}\left(\text{SNR}_2, 2M\right)\right]. \qquad (4.3)$$

The power ratio between two M-PAM can also be calculated as,

$$\text{PR} = 10\log_{10}\left(\frac{\text{SNR}_2}{\text{SNR}_1}\right). \qquad (4.4)$$

In contrast with TDHMF, the average $\overline{\text{SNR}}$ is given by,

$$\overline{\text{SNR}} = 2\left(\kappa\text{SNR}_1 + (1-\kappa)\text{SNR}_2\right), \qquad (4.5)$$

with SNR_1 and SNR_2 is corresponding to the SNR locally perceived by each PAM format in a single quadrature, as opposed to equation 3.7, where SNR_1 and SNR_2 are measured over both in-phase and quadrature.

Note that the factor of 2 between the average $\overline{\text{SNR}}$ equation of 3.7 and 4.5 compensates for the factor of 2 between denominators in the arguments of the $\text{erfc}(\cdot)$ function of expression 3.5 and 4.1. Consequently, the back-to-back performance of both strategies is exactly equivalent.

4.3 FlexPAM Operation Strategy and Back-to-back Evaluation

4.3.1 Transmitter Operation Strategies

Similar to TDHMF, by properly choosing the power ratio, different strategies can be employed on the transmitter. Four transmitter operation strategies, the constant power strategy, the same Euclidean distance strategy, the same BER strategy and the minimum BER strategy, are all considered in this thesis.

1. *Constant Power* (PR = 0 dB): In order to guarantee the constant power for both M-PAM modulation formats that composing the FlexPAM, the power ratio between the two formats must be PR = 0 dB. In such a scenario, the SNR perceived by each formats is the same, and it can be calculated according to equation 4.5. Thus, $\text{SNR}_1 = \text{SNR}_2 = \overline{\text{SNR}}/2$. Then, by substituting the overall $\overline{\text{SNR}}$ into equation 4.3, the following BER expression can be obtained,

$$
\Psi_{\text{FlexPAM}} = \frac{1}{\log_2(M) + 1 - \kappa} \cdot
$$
$$
\left[\kappa(M-1)\text{erfc}\left(\sqrt{\frac{3\overline{\text{SNR}}}{2(M^2-1)}} \right) + (1-\kappa)\left(M - \frac{1}{2}\right)\text{erfc}\left(\sqrt{\frac{3\overline{\text{SNR}}}{2(4M^2-1)}} \right) \right].
$$
$$
(4.6)
$$

   Similar to TDHMF, the constant power strategy is the simplest transmitter operation strategy but an inefficient one. The higher cardinality M-PAM component works at the FEC BER cliff, and the other component actually works error free. Two M-PAM modulation formats operate at different BERs, thus FlexPAM has the potential of requiring two dedicated FEC codes for each formats. However, it is contrary to FlexPAM original intention, which is having a simpler and identical transmitter and receiver. Moreover, the sensitivity performance shows that the constant power strategy has large back-to-back penalties compared to other strategies.

2. *Same Euclidean Distance* ($d_1 = d_2$): In order to keep the minimum Euclidean distance of the two M-PAM modulation formats (d_1 and d_2) the same, the power ratio between two M-PAM must be constant. In addition, the SNR perceived by each M-PAM modulation formats is respectively given by,

$$
\text{SNR}_1 = \frac{M^2 - 1}{(8 - 6\kappa)M^2 - 2}\overline{\text{SNR}}, \tag{4.7}
$$

and

$$\text{SNR}_2 = \frac{4M^2 - 1}{(8 - 6\kappa)\, M^2 - 2}\overline{\text{SNR}}. \tag{4.8}$$

Thus, according to equation 4.4, the power ratio PR can be easily obtained. Moreover, by substituting 4.7 and 4.8 into the overall BER expression in equation 4.3 and after reducing all its terms as functions of $\overline{\text{SNR}}$, M and κ yields, the final expression of BER in the same Euclidean distance strategy can be obtained,

$$\Psi_{\text{FlexPAM}} = \frac{M - \dfrac{\kappa + 1}{2}}{M\, (\log_2(M) + 1 - \kappa)} \text{erfc}\left(\sqrt{\frac{3\overline{\text{SNR}}}{(8 - 6\kappa)\, M^2 - 2}}\right). \tag{4.9}$$

3. *Same BER* ($\Psi_1 = \Psi_2$): In order to force the two M-PAM modulation formats in the FlexPAM frame to operate at the same BER, one must determine the required SNR of each format in order to achieve the target BER, Ψ_{target}. The required SNR can be obtained by inverting the BER expression of 4.1 with a given Ψ_{target} as,

$$\text{SNR}_1^{\text{req}} = \frac{M^2 - 1}{3}\text{erfc}^{-1}\left(\frac{M \log_2(M)}{M - 1}\Psi_{\text{target}}\right)^2, \tag{4.10}$$

and

$$\text{SNR}_2^{\text{req}} = \frac{4M^2 - 1}{3}\text{erfc}^{-1}\left(\frac{2M \log_2(2M)}{2M - 1}\Psi_{\text{target}}\right)^2. \tag{4.11}$$

The average BER of the entire frame is then obviously given by Ψ_{target}, whereas the average SNR can be obtained by substituting $\text{SNR}_1^{\text{req}}$ and $\text{SNR}_2^{\text{req}}$ into equation 4.5. In the end, the power ratio between two PAM formats is given by,

$$\text{PR} = 10 \log_{10}\left(\frac{\text{SNR}_2^{\text{req}}}{\text{SNR}_1^{\text{req}}}\right). \tag{4.12}$$

4. *Minimum BER* (Ψ_{min}): So as to achieve the minimum global BER requires to find the optimum SNR pair, $[\text{SNR}_1^{\text{opt}}, \text{SNR}_2^{\text{opt}}]$, that minimizes the estimated BER of expression 4.3. Considering that for any given $\overline{\text{SNR}}$, the value of SNR_2 is automatically determined by the value of SNR_1 through 4.5. Thus, the

40

following optimization procedure can be applied to determine $\mathrm{SNR}_1^{\mathrm{opt}}$,

$$
\begin{aligned}
\mathrm{SNR}_1^{\mathrm{opt}} &= \left\{ \mathrm{SNR}_1 : \Psi_{\mathrm{FlexPAM}} \left(SNR_1, \frac{\dfrac{\overline{\mathrm{SNR}}}{2} - \kappa \mathrm{SNR}_1}{1 - \kappa}, M \right) \right\} \\
&= \left\{ \min \left[\Psi_{\mathrm{FlexPAM}} \left(\mathrm{SNR}_1, \frac{\dfrac{\overline{\mathrm{SNR}}}{2} - \kappa \mathrm{SNR}_1}{1 - \kappa}, M \right) \right] \right\}, \quad (4.13)
\end{aligned}
$$

whereas $\mathrm{SNR}_2^{\mathrm{opt}}$ is given by,

$$
\mathrm{SNR}_2^{\mathrm{opt}} = \frac{\overline{\mathrm{SNR}}/2 - \kappa \mathrm{SNR}_1^{\mathrm{opt}}}{1 - \kappa}. \tag{4.14}
$$

The average BER of the entire FlexPAM frame is then obtained,

$$
\begin{aligned}
\Psi_{\mathrm{FlexPAM}} = {} & \frac{1}{M \left(\log_2(M) + 1 - \kappa \right)} \cdot \\
& \left[\kappa(M - 1)\mathrm{erfc}\left(\sqrt{\frac{3\mathrm{SNR}_1^{\mathrm{opt}}}{M^2 - 1}} \right) + (1 - \kappa)\left(M - \frac{1}{2} \right) \mathrm{erfc}\left(\sqrt{\frac{3\mathrm{SNR}_2^{\mathrm{opt}}}{4M^2 - 1}} \right) \right].
\end{aligned}
$$
$$(4.15)$$

4.3.2 Back-to-Back Performance

From the last section, it can be concluded that FlexPAM has the same back-to-back performance as TDHMF. Therefore, instead of showing all possible BpS back-to-back performance, this section shows the detail of a specific FlexPAM case, which has BpS=6 and is a hybrid between 2-PAM and 4-PAM with 0.5 format ratio.

In figure 4.3, it compares all four strategies in FlexPAM back-to-back performance and gives the relation between BER and SNR. Obviously, the constant power strategy (the blue line) is still a suboptimal choice. It has about a 1.2 dB SNR penalty against to the other three strategies at the BER target $(2 \cdot 10^{-2})$. The minimum BER strategy still has the best performance. All the other curves are on the right side of the black solid curve which refers to the minimum BER strategy. The same BER and the same Euclidean distance strategies, again, have negligible SNR penalty compared to the minimum BER strategy. Similar to TDHMF, the minimum BER strategy has the optimal performance but has the potential of requiring a more complex system set-up. Two different and specific designed FEC codes maybe necessary for the deployment of both M-PAM modulation formats. The same BER strategy offers

a comparable performance in contrast to the minimum BER strategy, and it may require a much easier implementation. Because, a same FEC code can be used for both M-PAM at the same time. In addition, with only one FEC code employed, it can eliminate the potential DSP interference that coming from two different sets of FEC codes. Therefore, the same BER strategy can be considered as a conservative choice.
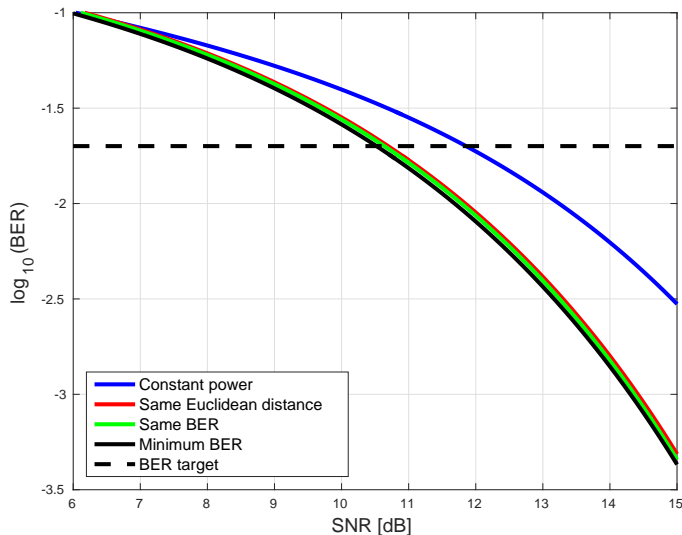
Figure 4.3. FlexPAM BpS equal to 6 case. Two modulation formats are 2-PAM and 4-PAM, format-ratio $\kappa = 0.5$. BER target, Ψ_{target}, is equal to $2 \cdot 10^{-2}$. the required SNR in the constant power strategy is 11.86 dB, the required SNR in the same Euclidean distance strategy is 10.69 dB, the required SNR in the same BER strategy is 10.63 dB and the required SNR in the minimum BER strategy is 10.52 dB.

Complementary to the sensitivity analysis of figure 4.3, the frame structure, power ratio and required SNR of FlexPAM is described in detailed in table 4.1 for a BpS ranging from 4 to 12. Since it can play a key role on the signal performance after non-linear fiber propagation, besides the power ratio between M-PAM formats, the correspondent power ratio between polarization tributaries, PR_{pol}, is also indicated in table 4.1. It is defined as the power ratio between the Y polarization (assuming the highest power polarization) and the X polarization. In particular, the vectors in the "$\log_2(M)$" column refers to the FlexPAM symbol structure. It is also called the BpS vector. Each element in the BpS vector refers to the number of bits of the correspondent quadrature.

Since FlexPAM has the same back-to-back performance as the TDHMF, those analysis for FlexPAM BpS=6 case are also correct in other FlexPAM BpS cases that listed in table 4.1. Thus, other BpS cases are not discussed here.

4.4 Arbitrary M-PAM Hybrid

As discussed in the previous section, FlexPAM has a huge amount of possible combinations with different M-PAM for a given BpS. The previous sections only consider on those combinations with two neighbouring M-PAM modulation formats. In this section, a more general picture of FlexPAM hybrid combinations is presented.

In the figure 4.4, it shows the back-to-back performance of all possible FlexPAM combinations. Three M-PAM modulation formats were considered. They are 2-PAM, 4-PAM and 8-PAM. Hence, the average BpS of the symbol ranged from 1 to 12. The order of a specific M-PAM in the BpS vector does not affect the back-to-back performance. For instance, when BpS=5, [1,1,1,2] and [1,2,1,1] have exactly the same performance. For a given BpS, the optimum combination is the one with two neighbouring M-PAM modulation formats. For example, in the BpS=6 case, BpS vector [1,2,1,2] has the optimal back-to-back performance. Those suboptimal choices are either having more than two kinds of M-PAMs or transmitting nothing on more than one quadratures, such as [1,2,3,0]. It should be noted that TDHMF is regarded as the reference sensitivity performance for a given BpS. Those optimum combinations of FlexPAM should have the exactly same performance as TDHMF according to the previous theoretical formulation analysis.

Therefore, instead of studying arbitrary FlexPAM hybrid combinations, I spent most of my time in studying those combinations with two neighbouring M-PAM modulation formats. In the rest of this thesis, the hybrid combinations of FlexPAM are limited in the two neighbouring M-PAM modulation formats range.
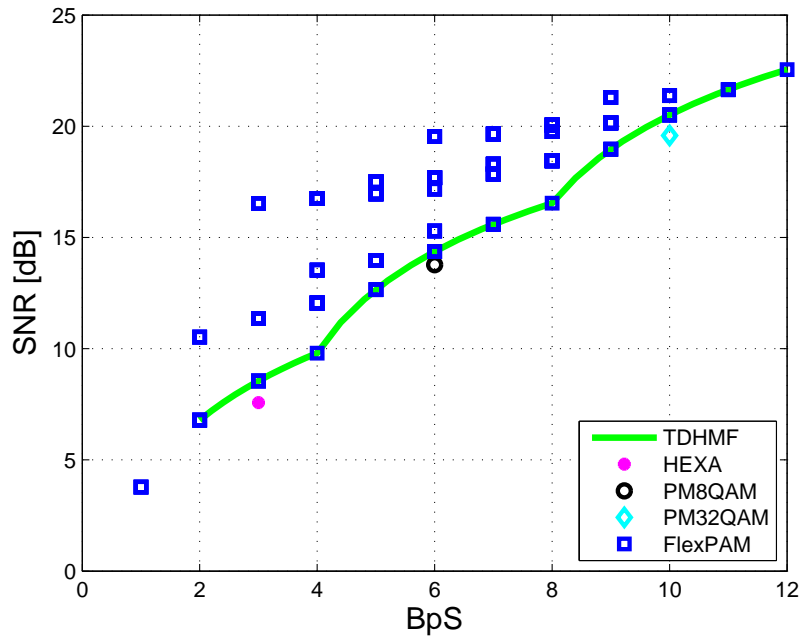
Figure 4.4. Sensitivity B2B performance of FlexPAM arbitrary M-PAM hybrid. TDHMF is operated with same BER strategy. Note that HEXA, PM-8QAM and PM-32QAM are indicated in the figure only as equivalent spectral efficiency solution for BpS=3, BpS=6 and BpS=10 respectively.

Table 4.1. FlexPAM frame structure, power-ratio and required SNR for different transmitter operation strategies, considering a target BER of 2×10^{-2}. In addition, the units for SNR_{req}, PR_{pol} and SNR_{req} are dB. Noted that, for a given BpS, TDHMF has the same PR as FlexPAM.

N_{BpS}	$\log_2(M)$	Format	M	κ	$d_1 = d_2$			$\Psi_1 = \Psi_2$			Ψ_{min}		
					SNR_{req}	PR	PR_{pol}	SNR_{req}	PR	PR_{pol}	SNR_{req}	PR	PR_{pol}
4	[1 1 1 1]	PM-QPSK	2	1	6.25	0	0	6.25	0	0	6.25	0	0
5	[1 1 1 2]		2	0.75	9.07	7	4.78	8.94	6.46	4.33	8.76	4.87	3.08
6	[1 2 1 2]	PM-8QAM	2	0.5	10.69	7	0	10.59	6.46	0	10.46	5	0
7	[1 2 2 2]		2	0.25	11.83	7	2.22	11.78	6.46	2.13	11.72	5.09	1.84
8	[2 2 2 2]	PM-16QAM	4	1	12.71	0	0	12.71	0	0	12.71	0	0
9	[2 2 2 3]		4	0.75	15.11	6.23	4.15	14.98	5.72	3.74	14.72	3.69	2.23
10	[2 3 2 3]	PM-32QAM	4	0.5	16.57	6.23	0	16.45	5.72	0	16.25	3.9	0
11	[2 3 3 3]		4	0.25	17.62	6.23	2.08	17.56	5.72	1.98	17.45	4.04	1.57
12	[3 3 3 3]	PM-64QAM	8	1	18.43	0	0	18.43	0	0	18.43	0	0

Chapter 5

The Gaussian Noise Model and Mixed Formats Simulation System

5.1 Introduction

In the past few years, the coherent optical transmission systems have made steady progress, and achieved the ever-increasing propagation performance records. The outstanding format, PM-QPSK, has been proved that it has a better propagation performance in [47] and [48]. In addition, the PM-16QAM has attracted considerable interest [49]. At the same time, some attention has been put on other even higher cardinality formats [50], [31].

Obviously, these record-broken systems are all operated over uncompensated transmission links. Earlier works, both simulation [51] [52] and experimental results [53], have already predicted such a scenario, that the optical transmission systems have a better propagation performance without optical dispersion compensation.

It is a common agreement that not only the newly built link but also the upgrade of the existing link, should implement the uncompensated transmission link. In such a scenario, it is very important to understand the theoretical limitations of the uncompensated transmission link and have an accurate and convenient prediction tool.

Actually, there are two main factors that limit the long-haul transmission systems' propagation performance. They are the amplified spontaneous emission (ASE) noise due to the optical amplifier and the non-linear interference (NLI) generation due to the fiber Kerr effect. The ASE noise has been fully studied. As for the other one, although the non-linear signal propagation in a dispersion-managed transmission system has been studied for many years, there is no way to have a simple, easy-understanding, and accurate analytical solution to describe the system performance. However, in the context of uncompensated transmission, it is now possible to achieve

such a goal.

In this chapter, the signal propagation properties and the Gaussian noise model derivation are introduced in the first place. Then, the simulation methodology of this thesis is described in detail, including the simulation system architecture and the simulation steps. After that, a simulation example with the GN-model prediction is presented in the last part.

5.2 Gaussian Noise Model

5.2.1 The Signal Propagation in Uncompensated Transmission

In the dispersion-managed transmission, the signal is kept the same at the end of each span by using dispersion compensation. However, in the uncompensated transmission, the signal is heavily affected by chromatic dispersion. The four electric field components of the signal become an identical, statistically-independent and zero-mean Gaussian like signal after several spans propagation. Figure 5.1 from [54] shows that the signal after uncompensated transmission becomes Gaussian like.

As long as the uncompensated transmission started, every frequency component of the signal become phase-scrambled because of the chromatic dispersion. The signal's matching phase is destroyed by the phase-scrambling and then generates many random data symbols. The signal can be considered as the sum of many random independent contributions, and then converges to Gaussian. This appearance implies that the signal can be regarded as a sort of non-linear disturbance which is Gaussian-noise-like. As a result, it is much easier to handle the signal in a statistical approach.

In addition, [55] has proved that even without ASE noise, the signal components appear to be Gaussian like. In particular, there is no statistically dependency among any components in this result. Figure 5.2 shows the scattering diagram of the signal after DSP.

This phenomenon has also been testified in an experimental environment [56]. Two different transmitted power, the low power $P_L = -3$ dBm and the high power $P_H = +4$ dBm, can realized the experimental environment that only have the ASE noise or only have the fiber non-linear interference respectively. Figure 5.3 shows that in the high transmitted power scenario, the noise fits the Gaussian probability density function well of both real and imaginary parts, which means that the non-linear interference can be considered as a Gaussian noise.

Therefore, in both simulation and experiment ways, the signal distribution appears to be Gaussian like even without ASE noise. That is to say, the non-linear interference can be considered as an excess additive Gaussian noise. Consequently,
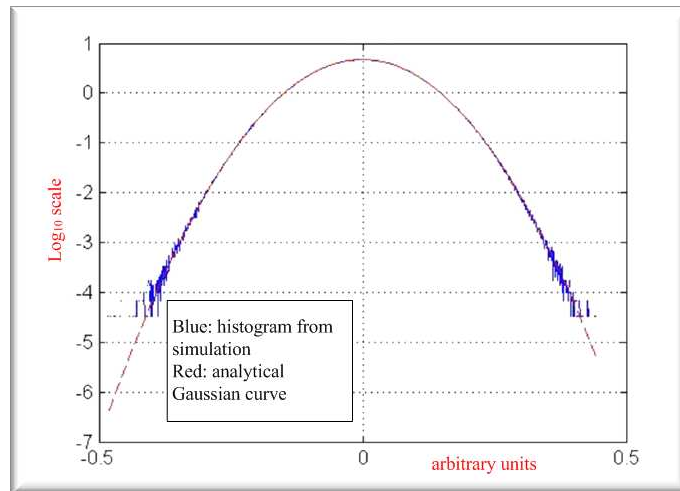
Figure 5.1.   Optical field samples after 500 km of single mode fiber propagation, the system symbol rate is 32 GBaud and using PM-QPSK.
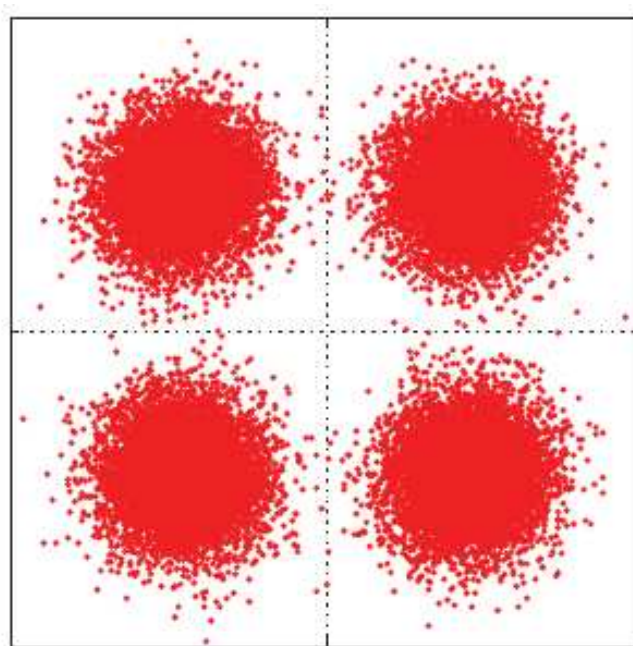
Figure 5.2.   WDM simulation over 3000 km of single mode fiber, the system symbol rate is 28 GBaud, with 9 channels, 50 GHz channel spacing and using PM-QPSK. The transmitted power per channel is set to 3 dBm and simulated without ASE.

the impact of non-linear interference on the systems can be estimated through an alter signal-to-noise-ratio by simply adding the non-linear interference noise to ASE noise.

49
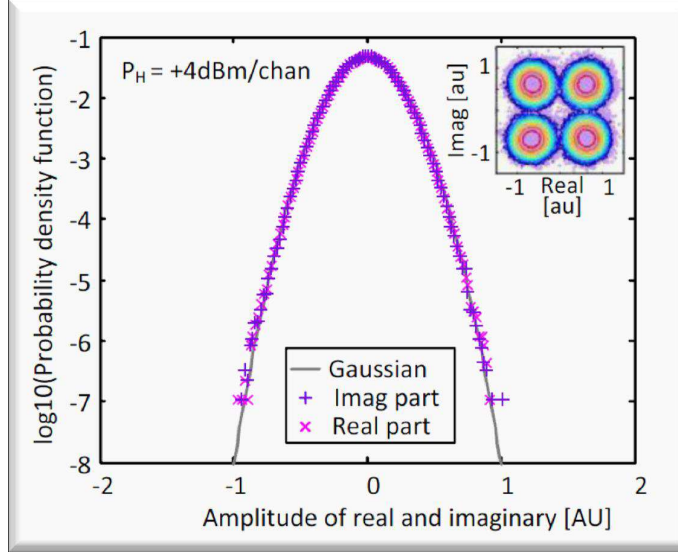
Figure 5.3. Experiment was carried on a system with 80 channels and the channel spacing is 50 GHz (full C band). The system has 15 uniformed fiber spans, which are all SSMF with 100 km span length. The transmitted power is set to 4 dBm per channel.

5.2.2 Gaussian Noise Formula Derivation

In the context of uncompensated transmission, the transmission link can be equivalent to the model which is depicted in figure 5.4. The ASE noise is coming from the optical amplifier and the non-linear interference is coming from the fiber Kerr effect. From the previous section, we can know that non-linear interference is Gaussian-like and additive. In addition, it is uncorrelated with either ASE or the signal. Thus, the optical signal-to-noise-ratio (OSNR) can be characterized in equation 5.1.
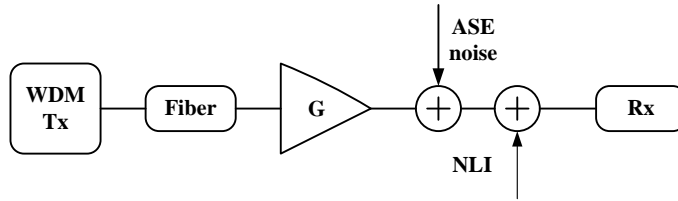
Figure 5.4. In the simplified uncompensated transmission link model, there is no more dispersion compensation unit. The ASE noise and the non-linear interference are added at the end of each span. The amplifier fully recovers the fiber span loss.

$$\text{OSNR} = \frac{P_{\text{ch}}}{P_{\text{ASE}} + P_{\text{NLI}}} \tag{5.1}$$

Since the BER can be a function of OSNR (BER = Ψ(OSNR)), once the OSNR is obtained, the system performance can be predicted. In equation 5.1, the channle power P_{ch} is easily obtained and determined by the system set-up. The ASE noise power can be obtained as $P_{\text{ASE}} = \int_{B_{\text{OSNR}}} G_{\text{ASE}} \, df$. Thus, finding the non-linear interference power is the prior target. Since the non-linear interference power $P_{\text{NLI}} = \int_{B_{\text{OSNR}}} G_{\text{NLI}}(f) \, df$, the key part is to find the power spectrum density for the non-linear interference power.

The first job to derive the solution for the non-linear interference power spectrum density is to find a suitable Gaussian-noise signal model. Each channel of the WDM comb can be regarded as a Gaussian random process. In order to use a four-wave-mixing like approach to assess the non-linear interference, the signal spectrum must be made up of spectral lines. For such a goal, the signal model can be described as equation 5.2 and depicted as figure 5.5.

$$N_{\text{WDM}}(f) = \sum_{n=-\infty}^{+\infty} \xi_n \sqrt{f_0 G_{\text{WDM}}(nf_0)}\delta(f - nf_0) \tag{5.2}$$
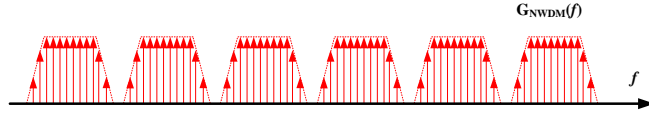
Figure 5.5.   The average power spectrum of the Gaussian noise.

With the spectral line signal model, it is possible to find the linear propagation solution for the Non-linear Schrödinger Equation (NLSE). Then, the Kerr term can be generated by using the linear solution of NLSE. Using the Kerr term as a source term, the non-linear interference field can be found. At the same time, the power spectrum density of the non-linear interference field is also found. After looking up for the frequency-continuous limit and taking the multi-span and the dual-polarization into account, the Gaussian Noise Reference Formula (GNRF) in equation 5.3 can be derived to measure the non-linear interference. More detail derivation can be found in [57].

$$G_{\text{NLI}}(f) = \frac{16}{27}\gamma^2 L_{\text{eff}}^2 \int_{-\infty}^{+\infty} \int_{-\infty}^{+\infty} G_{\text{WDM}}(f_1)G_{\text{WDM}}(f_2)G_{\text{WDM}}(f_1 + f_1 - f)\cdot$$

$$\left| \frac{1 - e^{-2\alpha L_S}e^{j4\pi^2\beta_2 L_S(f_1-f)(f_2-f)}}{1 - j2\pi^2\beta_2\alpha^{-1}(f_1 - f)(f_2 - f)} \right|^2 \frac{\sin^2\left(2N_S\pi^2(f_1 - f)(f_2 - f)\beta_2 L_S\right)}{\sin^2\left(2\pi^2(f_1 - f)(f_2 - f)\beta_2 L_S\right)}df_1 df_2 \tag{5.3}$$

51

In particular, the power spectrum density of the non-linear interference in a single span is in equation 5.4. Furthermore, it has been proved that the non-linear interference power spectrum density $G_{\text{NLI}(f)}$ is approximately flat in any given WDM channel over the bandwidth [1]. Figure 5.6 shows that, in a RS-SMF system with 11 channels and 20 span, the $G_{\text{NLI}(f)}$ shape is close to the shape of signal spectrum at the center channel. As a result, the non-linear interference noise can be regarded as Gaussian-like, additive and locally white. Since the full bandwidth integration is complex and time-consuming, the locally white feature of $G_{\text{NLI}(f)}$ can effectively simplify the numerical calculation process.
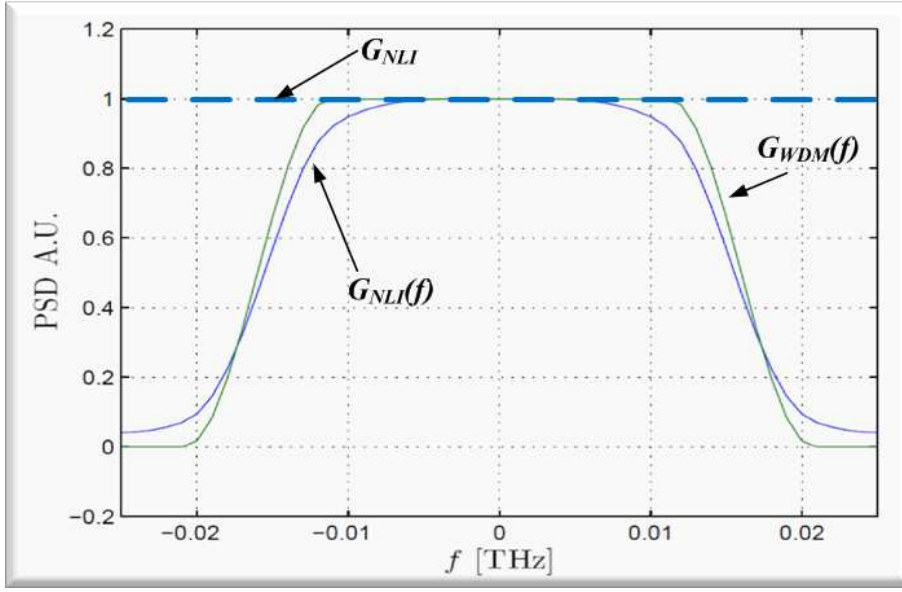
Figure 5.6.   Enlarge figure of one channel. $G_{\text{NLI}}(f)$ is almost the same as $G_{\text{WDM}}(f)$. Moreover, it can be considered as rectangular shape, and only the center frequency is concerned.

$$G_{\text{NLI}}^{1span}(f) = \frac{16}{27}\gamma^2 L_{\text{eff}}^2 \int\limits_{-\infty}^{+\infty}\int\limits_{-\infty}^{+\infty} G_{\text{WDM}}(f_1)G_{\text{WDM}}(f_2)G_{\text{WDM}}(f_1 + f_1 - f)\cdot$$

$$\left| \frac{1 - e^{-2\alpha L_S}e^{j4\pi^2\beta_2 L_S(f_1-f)(f_2-f)}}{1 - j2\pi^2\beta_2\alpha^{-1}(f_1 - f)(f_2 - f)} \right|^2 df_1 df_2 \quad (5.4)$$

Therefore, the power spectrum density of non-linear interference can be simplified to equation 5.5,

$$G_{\text{NLI}}^{1span} \approx \gamma^2 G_{\text{WDM}}^3 L_{\text{eff}}^2 \left(\frac{2}{3}\right)^3 \frac{\text{asinh}\left(\frac{1}{2}\pi^2|\beta_2|L_{\text{eff,a}}B_{\text{WDM}}^2\right)}{\pi|\beta_2|L_{\text{eff,a}}}, \quad (5.5)$$

where $L_{\text{eff,a}} = \dfrac{1}{2\alpha}$, $L_{\text{eff}} = \dfrac{1 - e^{(-2\alpha L_S)}}{2\alpha}$, and β_2 is the dispersion with the of $[\text{ps}^2\text{km}^{-1}]$. Now the power of non-linear interference can be approximately calculated as,

$$P_{\text{NLI}} \approx G_{\text{NLI}} \cdot B_{OSNR}. \tag{5.6}$$

Actually, figure 5.6 gives the worst performance of $G_{\text{NLI}(f)}$. Other channels' $G_{\text{NLI}(f)}$ are all smaller than the one of the center channel. For simplification, the power spectrum density of non-linear interference at the center channel is assumed to represent all the other power spectrum densities. Even if this assumption would result in a worse system propagation performance prediction, the prediction offers a good enough accuracy within a short calculation time.

5.2.3   Non-linear Interference Noise Accumulation

After the derivation of $G_{\text{NLI}(f)}$ in one span, an important question needs to be addressed urgently. How does the NLI noise accumulate along the fiber spans? Does it relate to the optical signal bandwidth B_{WDM}, or the number of channels N_{ch}, or the number of spans N_s.

Since the non-linear interference is added at the end of each span, it is possible to have a roughly estimation of the total non-linear interference with the incoherent law. Therefore, the non-linear interference grows exactly as the number of span N_S in equation 5.7.

$$G_{\text{NLI}} \approx G_{\text{NLI}}^{1span} \cdot N_S \tag{5.7}$$

The incoherent non-linear interference accumulation just provides a rough prediction of the total non-linear interference. Simulations proved that actual total non-linear interference is larger than the number calculated with incoherent law. And numerical studies suggest that the coherent non-linear interference accumulation can be modelled through the "ε-law" in equation 5.8.

$$G_{\text{NLI}} \approx G_{\text{NLI}}^{1span} \cdot N_S^{1+\varepsilon} \qquad \varepsilon > 0 \tag{5.8}$$

The "ε-law" is quite accurate in measuring the coherent non-linear interference summation. And the ε can be calculated in equation 5.9.

$$\varepsilon \approx \frac{3}{10} \cdot \log_e \left(1 + \frac{6}{L_S} \frac{L_{\text{eff,a}}}{\text{asinh}\left(\frac{1}{2}\pi^2|\beta_2|L_{\text{eff,a}}B_{\text{WDM}}^2\right)} \right) \tag{5.9}$$

53

5.3 Mixed Formats Simulation System

5.3.1 Simulation System Layout

The coherent optical transmission system for this thesis is built within MATLAB and OptSim. MATLAB (matrix laboratory) is a multi-paradigm numerical computing environment and fourth-generation programming language. OptSim is a software for design and simulation of the optical transmission system.

The bit and electrical signal generation are realized in MATLAB. The Pseudo Binary Bit Sequence (PRBS) is used to generate the original bit sequence. In addition, the degree of PRBS is $k_{\mathrm{PRBS}rm}$, i.e., the maximum sequence length is $2^{k_{\mathrm{PRBS}}} - 1$. The gray coding is used to map the bit sequence into the electrical voltage signal. In particular, all these electrical signal is Non Return to Zero (NRZ). Then, four series of electrical voltage signal represented the four components of the electrical field are saved and passed to OptSim.

The optical transmission link is built inside the OptSim. The transmitter architecture is shown in figure 5.7, four parallel Mach-Zehnder modulators are used to modulate on each quadrature of the optical field. The Nyquist filter is employed as the shaping filter. It is used to generate a squared of raised-cosine spectrum, thus the ISI can be removed from the system. It also can compensate for the "sinc" shape of NRZ pulses. The transfer function of Nyquist filter is in equation 5.10.

$$H(f) = \frac{\sqrt{rcos_\alpha(f)}}{\mathrm{sinc}\left(\pi\dfrac{f}{R_S}\right)} \tag{5.10}$$

Where the R_S is the symbol rate and the $rcos_\alpha(f)$ is the raised-cosine function with a roll-off α. The $rcos_\alpha(f)$ is described in equation 5.11.

$$rcos_\alpha(f) = \begin{cases} T, & |f| \leq \dfrac{1-\alpha}{2T} \\ \dfrac{T}{2}\left[1 + cos\left(\dfrac{\pi T}{\alpha}\left[|f| - \dfrac{1-\alpha}{2T}\right]\right)\right], & \dfrac{1-\alpha}{2T} < |f| \leq \dfrac{1+\alpha}{2T} \\ 0, & \text{otherwise} \end{cases} \tag{5.11}$$

With a Polarizing Beam Splitter (PBS), the two polarization optical signal are combined together and passed through the fiber channel, and then pumped into the fiber span link. The coherent link architecture is shown in the figure 5.8. The channel comb is composed by 13 Nyquist WDM channel, where the channel spacing Δf is 50 GHz. In addition, each channel has its own 12 PRBSs with a degree equal to 16. In particular, all these PRBSs are different and uncorrelated. The system has a gross symbol rate $R_S = 32$ Gbaud, which assumes a 28% overhead due to
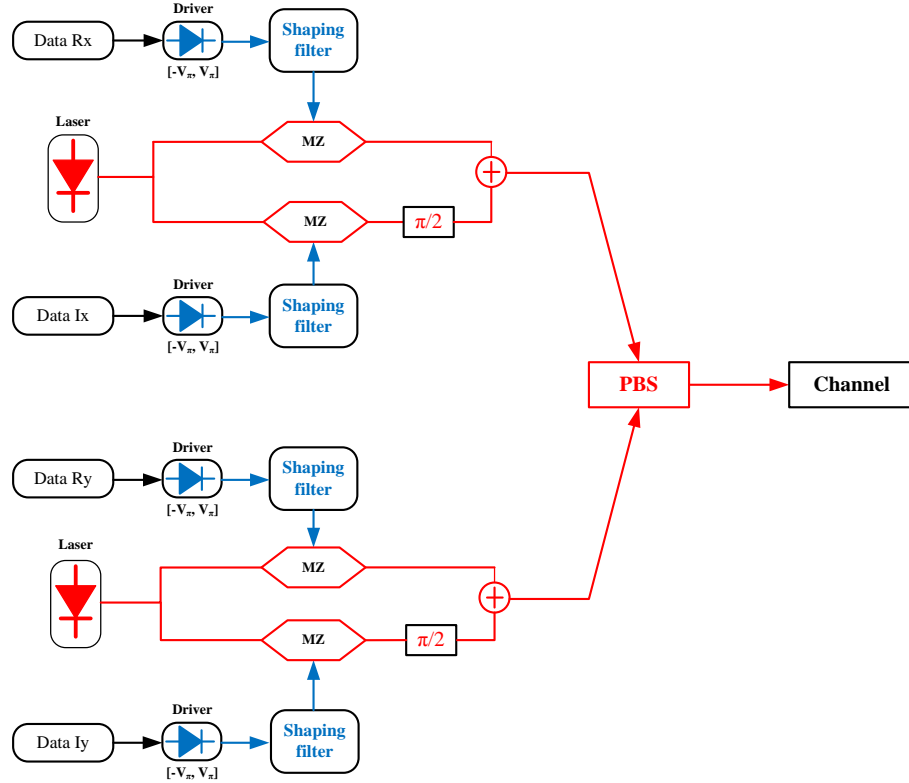
Figure 5.7. Transmitter structure of the simulation system in OptSim. MZ is the Mach-Zehnder modulator. PBS is the Polarizing Beam Splitter.

the protocol and the FEC coding. Thus, each channel carries a net symbol rate $R_S = 25$ Gbaud, and the corresponding net bit rate is $R_b = R_S \cdot \text{BpS}$, where the BpS is determined by the chosen modulation format. It should be pointed out that in the following chapter, instead of using BpS, the net bit rate R_b is used to represent every specific mixed formats case.

Inside the fiber span, the standard single model fiber (SSMF) is employed, whose dispersion $D = 16.7$ ps/nm/km, loss $\alpha = 0.22$ dB/km, fiber non-linearity coefficient $\gamma = 1.3$ 1/W/k and the effective area is 83 μm^2. The span length $L_S = 100$ km. The Erbium Doped Fiber Amplifier (EDFA) is employed at the end of each span, and it has a noise figure $F = 5$ dB. It should be pointed out that the ASE noise of EDFA is added at the receiver side instead of the end of each span as depicted in 5.4. The fiber span loss is completely recover by the amplifier.

The receiver architecture is depicted in figure 5.9. The local oscillator (LO) is combined with the incoming signal and then sent into two 90-degree hybrids (one for each polarization, and more detail about this component is shown in figure 5.10). The LO is assumed ideal and has the same frequency as the center channel. In
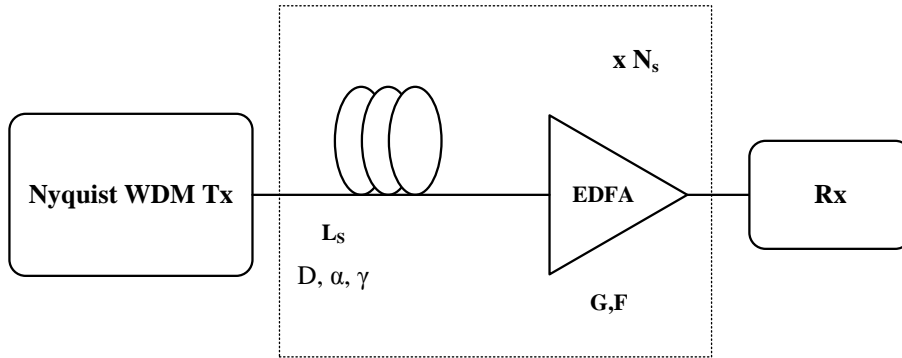
Figure 5.8. 13 Nyquist WDM channels with 50 GHz channel spacing are combined together and transmitted through the coherent link. The SSMF is employed. The fiber span lose is fully recovered by the amplifier.

particular, all the laser linewidth in this simulation is 0, thus there was no phase noise in the simulation. All the signal components were received and detected by four balanced photo-detectors (BPDs). Then, four 5th order low-pass Bessel filters are used to filter each components, and the filter -3 dB bandwidth is equal to 16 GHz. All the chromatic dispersion is compensated electronically in a compound component inside OptSim. After that, all the signal is sampled at 2 samples per symbol for digital data processing (DSP). It should be point out that, quantization effects are neglected here.

The DSP is also realized in MATLAB. An equalizer with 51-taps FIR filters was employed, and its training sequence length was 30000. In addition, the equalizer coefficients were adjusted according to the least-mean-square (LMS) algorithm, and it is followed by a threshold-based decision. All the data processing was done off-line within MATLAB.
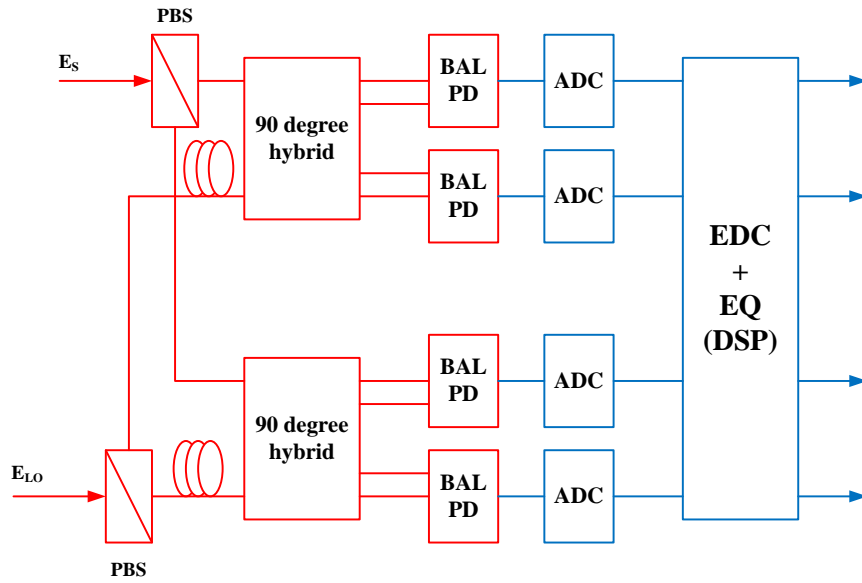
Figure 5.9.   The simulation receiver architecture. Four balanced photo-detectors are used in the coherent front-end. The electric dispersion compensation unit is integrated inside the OptSim.
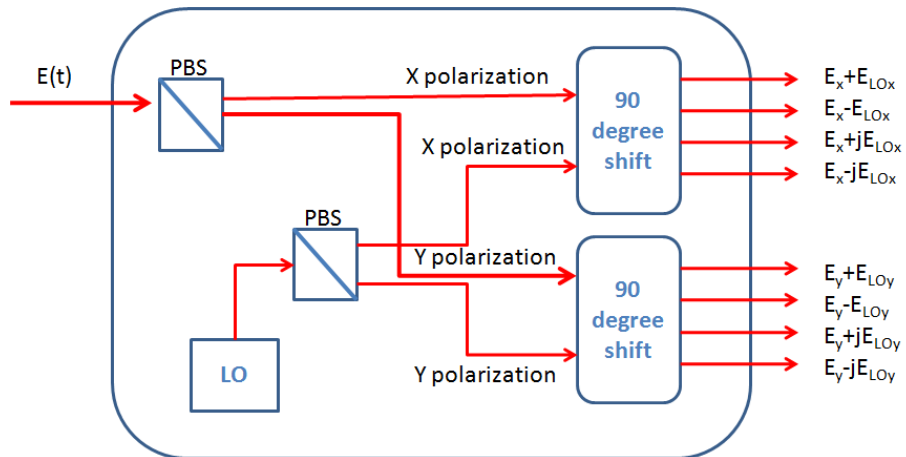
Figure 5.10.   The local oscillator has the same frequency as the center channel. Every component is assumed to work in an ideal condition.

57

5.3.2   Simulation Methodology

In this section, a complete simulation procedure is presented to explain the simulation methodology of the thesis. PM-16QAM is chosen as the modulation format. The BER_{target} is $2 \cdot 10^{-2}$. Calculating the required SNR of the system is the first job. According to equation 5.12, the required SNR in theory is 12.6705 dB [45].

$$\Psi_{\text{PM}-16\text{QAM}} = \frac{3}{8}\text{erfc}\left(\sqrt{\frac{3\text{SNR}}{10}}\right) \tag{5.12}$$

It should be pointed out that, instead of using OSNR, SNR is used here for easy understanding. The relation between OSNR and SNR is given in equation 5.13, where B_n is the OSNR bandwidth. This formula only works under the condition that the receiver has a matched filter, if not, the relationship between OSNR and SNR will become more complex.

$$OSNR = \frac{R_S}{B_n}SNR \tag{5.13}$$

In both theory analysing and system back-to-back performance evaluating, the B_n is assumed equal to R_S. But in propagation simulation, the B_n is always 12.48 GHz (0.1 nm).

In a back-to-back simulation, the optical signal is directly passed from the transmitter to the receiver, the fiber does not participate in this part. The back-to-back simulation runs several times by varying different ASE noise at the receiver side. At each run, the BER performance is recorded. With the linear interpolation algorithm, the required SNR in back-to-back performance can be obtained. Normally, the simulation required SNR and the theory required SNR are almost the same. However, when the modulation format has a over large constellation size like PM-64QAM, the error floor is obvious. At the BER target, the simulation required SNR is larger than theory required SNR. In such a scenario, the simulation required SNR is regarded as the required SNR for the following simulation steps. More details about the error floor can be found in [58].

After obtaining the required SNR, the system propagation performance can be predicted based on GN-model that realized in MATLAB. As depicted in figure 5.11, the black solid line refers to the incoherent GN-model prediction and the black dash line refers to the coherent GN-model prediction. The GN-model prediction provides information about the optimum transmitted power per channel and how far the system can reach, which both are quite important in the simulation. Otherwise, too much time is spent on finding the proper simulation parameters. In this example, the optimum transmitted power is around 0.5 dBm and the system maximum reach is around 19 span. Previous analysis showed that the same BER strategy offers good

enough back-to-back performance in contrast to other strategies. In this thesis, all the following propagation simulations use the same BER strategy as the transmitter operation strategy.
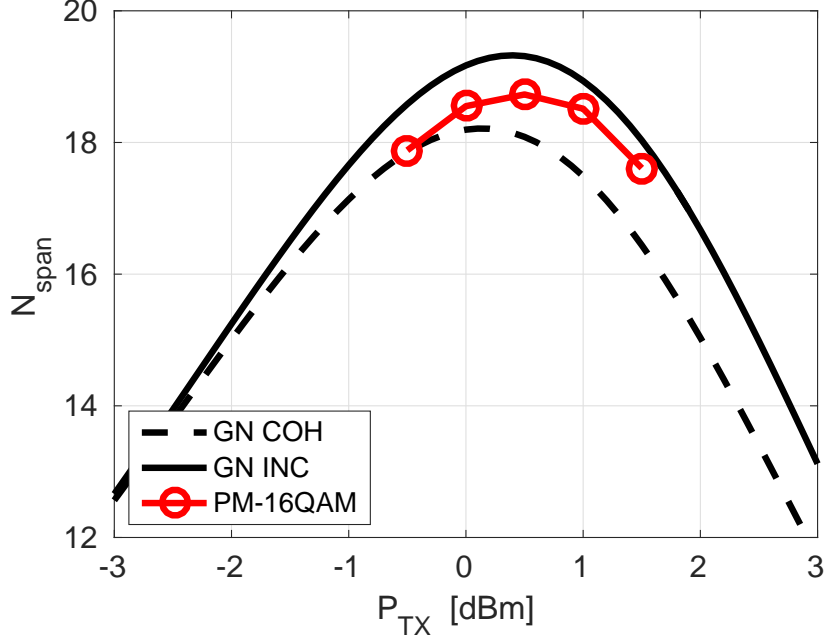
Figure 5.11. Example of PM-16QAM in non-linear uncompensated propagation. Incoherent GN-model has higher maximum reach than coherent GN-model, because of $G_{\text{NLI,COH}}$ is larger than $G_{\text{NLI,INC}}$ which could be proven by Eq. 5.7 and 5.8. GN-model offers a relatively precise prediction without excessive CPU cost.

Five transmitted power around the optimum transmitted power are chosen. In this example, the five chosen values are -0.5, 0, 0.5, 1.0 and 1.5 dBm. For each transmitted power, a series fiber spans are simulated. At the end of each span, a standard receiver followed by the LMS algorithm equalizer and the threshold-based decision is employed to detect the signal and obtain the BER. By applying the linear interpolation algorithm, the maximum span numbers giving the BER below the BER target can be found. The largest maximum reach of all these transmitted powers is regarded as the system maximum reach.

It should be pointed out that, the linear interpolation algorithm generates the maximum transmitted span with a fractional number, such as 9.5 span. The fractional number can not be consider as a full span in the practical implementation. However, it can be considered as as a sort of system margin. The increase in the fractional number, for instance from 9.1 to 9.8, implies that the system can obtain an extra margin. Such an extra system margin although can not counted as a full fiber span,

it can be useful in reducing the system sensitivity requirement.

Chapter 6

Mixed Formats Non-Linear Uncompensated Propagation

6.1 Introduction

After the back-to-back performance analysis, the subsequent reseach was to evaluate the propagation performance of both TDHMF and FlexPAM in an uncompensated non-linear coherent optical transmission system. All the simulation carried in this chapter were operated within the same system which is decribed in section 5.3.1. Since the GN-model is developed based on the standard square QAM modulation formats, the asymmetric frame structure and power unbalanced features of both TDHMF and Flex-PAM may incur some penalties compared to the GN-model preditions. In additon, such speculation has been proved experimentally [44].

The blue line in the schematic figure 6.1 shows that without any countermeasure, the non-linear propagation performance of mixed formats may has some penalties against to the GN-model prediction. Thus, a main concerning in this chapter is to find countermeasures for the mixed formats, which can improve the system propagation performance and move system working area from the blue line to the red line.

In this chapter, the non-linear propagation performance of THDMF is discussed in the first place. Then, three feasible countermeasures are presented and evaluated, and they are polarization interleaving, power ratio tuning and pre distortion. Secondly, similar countermeasures are applied on the FlexPAM propagation simulation, and their effectiveness on the FlexPAM propagation have also been testified. In the end, the propagation performance of all possible bit rate cases are discussed, and in particular, propagation with countermeasures and without countermeasure are both contained in the discussion.
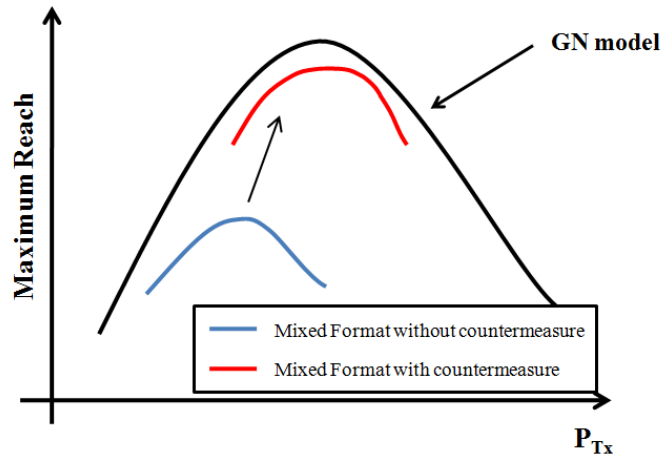
Figure 6.1.   The schematic diagram of a mixed format propagation performance.

6.2 TDHMF Non-linear Propagation and Countermeasures

6.2.1 Polarization Interleaving

Since all the square QAM family is polarization symmetric, the TDHMF composed by two neighbouring square QAM also should be polarization symmetric. In figure 6.2, it displays an example of TDHMF with two modulation formats, F_1 and F_2, with a 0.5 format ratio. The X polarization of TDHMF is exactly the same as the Y polarization.
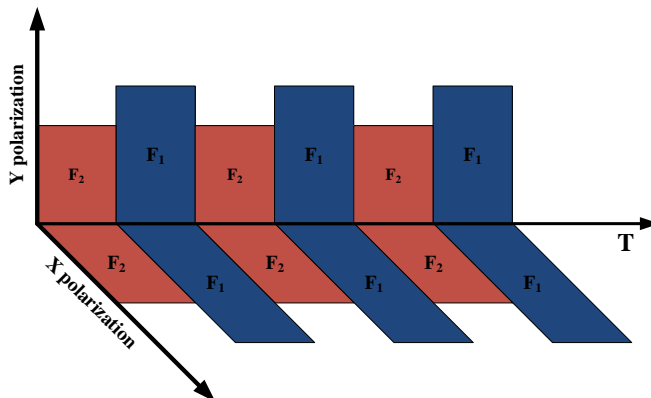
Figure 6.2.   A pictorial description of TDHMF without polarization interleaving applied. F_1 and F_2 represent the two hybrid modulation formats.

Since the same BER strategy is applied as the transmitter operation strategy, the higher cardinality format has a much higher power than the lower cardinality format (see figure 3.3). In such a scenario, the signal power is unequally distributed along the time domain. For each polarization, the signal power goes up and down along the time domain. In addition, the polarization symmetric feature of TDHMF makes the situation even worse.

In order to reduce the power unbalance along the time domain, the polarization interleaving (PI) is applied. In figure 6.3, it is the TDHMF in figure 6.2 after applying PI. The whole Y polarization is shifted to the right by the number of the symbols of format F_1. As a result, it creates a much better power balanced frame structure along the time domain, and reduces the non-linear impairment.
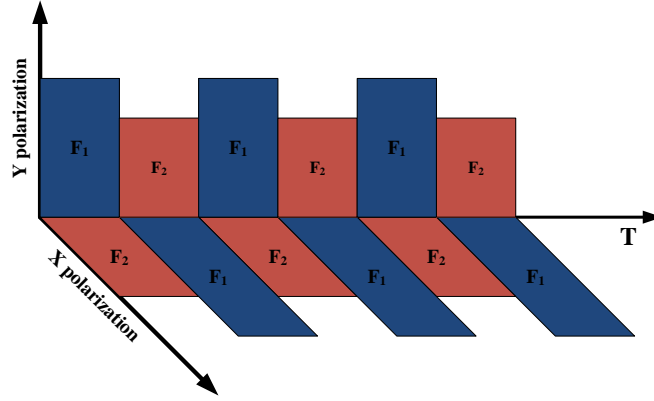
Figure 6.3. A pictorial description of polarization interleaving in TDHMF. F_1 and F_2 represent the two hybrid modulation formats.

Certainly, the PI can be extended to other format ratio cases. Assuming the frame length is equal to four, the figure 6.4 presents how to apply PI when the format ratio is equal to 0.75 and 0.25. In the case of polarization interleaving, for $\kappa = 0.75/0.25$, instead of aligning "2M"/"M" at the beginning/ending of the Y polarization frame, they are locating at the second/third symbol of the Y polarization frame. It should be pointed out that, there is no analytical solution for applying the PI on a TDHMF with a frame length equal to N. It depends on both the format ratio κ and the frame length N.

To illustrate the advantage of PI, three bit-rate cases are presented here, and they are TDHMF 225G, 250G and 275G. They are all the hybrid between PM-16QAM and PM-64QAM with $\kappa = 0.75/0.50/0.25$ respectively. In figure 6.5, a 0.25 dB gain is obtained in the 225G case after applying PI. In figure 6.6, a 0.17 dB gain is obtained in the 250G case after applying PI. In the figure 6.7, although the system performance does improved after applying PI in the 275G case, the improvement is

		$N_{\mathrm{BpS}} = 4\log_2(M)$	$N_{\mathrm{BpS}} = 4\log_2(M)+1$	$N_{\mathrm{BpS}} = 4\log_2(M)+2$	$N_{\mathrm{BpS}} = 4\log_2(M)+3$
x-pol	**I**	$\kappa = 1$ $\boxed{M}$	$\kappa = 0.75$ $\boxed{M}\ \boxed{2M}$	$\kappa = 0.5$ $\boxed{M}\ \boxed{2M}$	$\kappa = 0.25$ $\boxed{M}\ \boxed{2M}$
	Q	$\boxed{M}$	$\boxed{M}\ \boxed{2M}$	$\boxed{M}\ \boxed{2M}$	$\boxed{M}\ \boxed{2M}$
y-pol / **without PI**	**I**	$\kappa = 1$	$\kappa = 0.75$	$\kappa = 0.5$	$\kappa = 0.25$
	Q	$\boxed{M}$	$\boxed{M}\ \boxed{2M}$	$\boxed{M}\ \boxed{2M}$	$\boxed{M}\ \boxed{2M}$
		$\boxed{M}$	$\boxed{M}\ \boxed{2M}$	$\boxed{M}\ \boxed{2M}$	$\boxed{M}\ \boxed{2M}$
with PI	**I**	$\boxed{M}$	$\boxed{M}\boxed{2M}\ \boxed{M}$	$\boxed{2M}\ \boxed{M}$	$\boxed{2M}\ \boxed{M}\boxed{2M}$
	Q	$\boxed{M}$	$\boxed{M}\boxed{2M}\ \boxed{M}$	$\boxed{2M}\ \boxed{M}$	$\boxed{2M}\ \boxed{M}\boxed{2M}$
		$\kappa = 1$	$\kappa = 0.75$	$\kappa = 0.5$	$\kappa = 0.25$
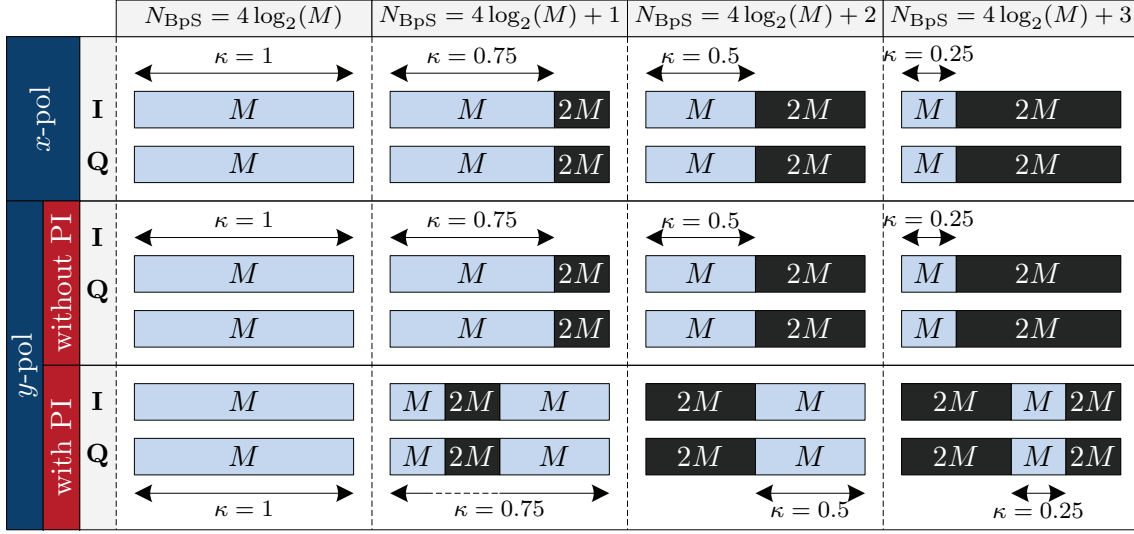
Figure 6.4. Four typical format ratio values are include in this figure. The number of symbol per frame is 4. Therefore, $\kappa = 1$ is pure square QAM; $\kappa = 0.75$ is represented both 125G and 225G cases; $\kappa = 0.75$ is represented both 150G and 250G cases; $\kappa = 0.75$ is represented both 175G and 275G cases.

insignificant and limited in a small range.

In the 275G case, the format ratio is 0.25, which means the higher cardinality format dominates the TDHMF overall performance. As long as the total frame length is four, no matter where to align the three symbols of PM-64QAM, they always contribute over 90% of the total signal power. In such a scenario, with or without PI does no make a huge impact on reducing the power unbalance along the time domain. For the same reason, both TDHMF 275G with or without PI cases have almost the same performance as the GN-model prediction, which is totally impossible for the previous two bit rate cases.

TDHMF 125G, 150G and 175G are not shown here, they have the similar performance as these three cases. It should be pointed out that, the polarization interleaving frame structure does not affect the back-to-back performance. For all bit rate cases, with or without PI cases have exactly the same back-to-back performance.
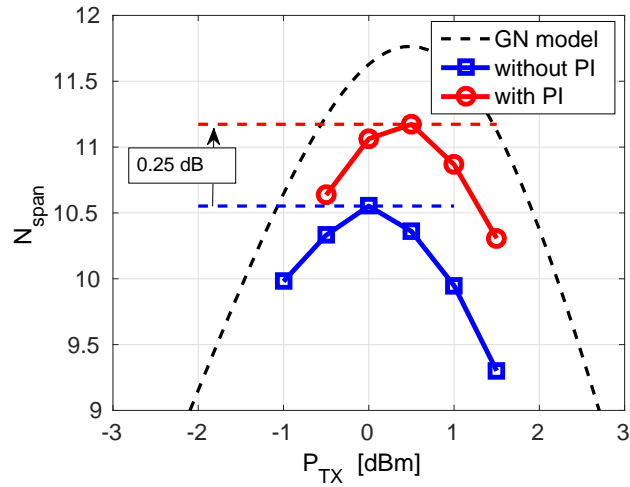
Figure 6.5. TDHMF 225G case, which contained PM-16QAM and PM-64QAM with format ratio $\kappa = 0.75$, with or without PI both are reported. Through using PI, system obtains approximately 0.25 dB gain, and gets closer to the GN-model prediction. Noted that, after applying PI the optimum working power is shifted from 0 dBm to 0.5 dBm.
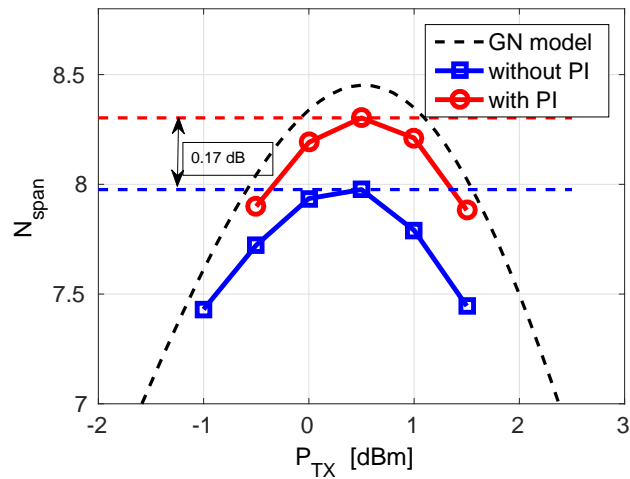
Figure 6.6. TDHMF 250G case, which contained PM-16QAM and PM-64QAM with format ratio $\kappa = 0.50$, with or without PI both are reported. Through using PI, system obtains approximately 0.17 dB gain, and gets closer to the GN-model prediction.
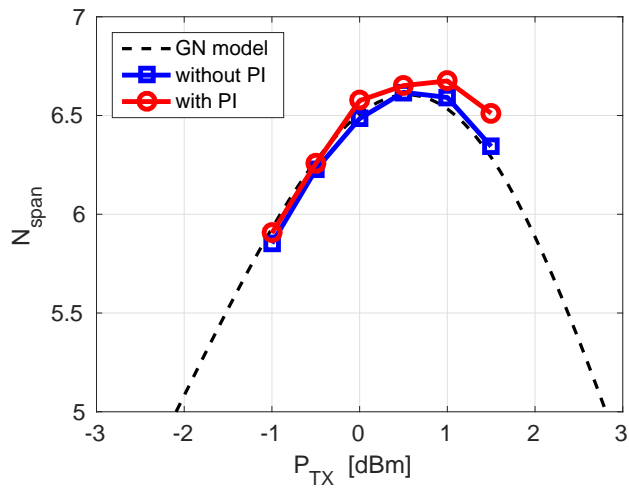
Figure 6.7.   TDHMF 275G case, which contained PM-16QAM and PM-64QAM with format ratio $\kappa = 0.25$, with or without PI both are reported. In this case, TDHMF with PI has almost the same performance as the one without PI.

6.2.2 Power Ratio Tuning

Besides the polarization interleaving, the power ratio tuning is proposed to improve the propagation performance of TDHMF.

By slightly tuning away from the TDHMF optimum working PR, we can improve the system performance in some cases. Here, the optimum working PR refers to the PR that can force the two modulation formats to operate with same BER in the back-to-back performance. The exact number of the optimum working PR for every bit rate cases can be seen in table 4.1.

When the format ratio κ is equal to 0.75, in the figure **??**, the 125G case is obtained a 0.11 dB gain after tuning PR from 6.4 dB to 6.8 dB. In addition, at the bottom part of the figure, the 225G case is obtained a 0.19 dB gain after tuning PR from 5.7 dB to 6.3 dB.
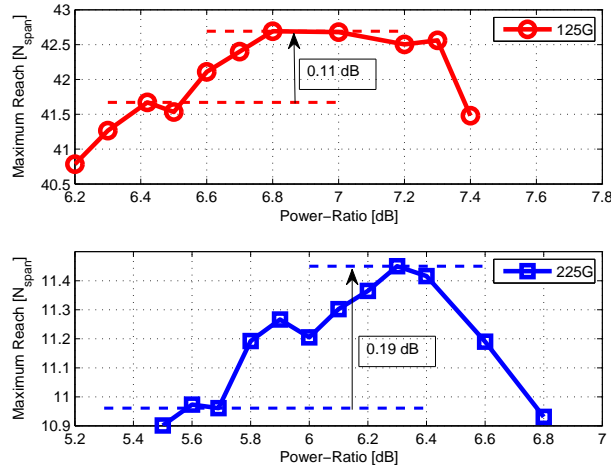
Figure 6.8.   The propagation performance after applying power ratio tuning of both 125G (top) and 225G (bottom) cases, which both have $\kappa = 0.75$. After tuning up the power ratio, system maximum reach has increased 0.11 dB for 125G and 0.19 dB for 225G.

However, the PR tuning advantage is not that significant when the format ratio is equal to 0.5. In figure 6.9, the 150G case, after tuning away from the optimum working PR, it just has a slight gain, and the performance is not stable. In the 250G case, an improve momentum is observed when tuning up the PR, but the improvement is limited.

When the format ratio is equal to 0.25, as shown in figure 6.10 the advantage of PR tuning have disappeared. When the same amount of PR is tuned as before, the system performance becomes bad. In the 175G case, at the PR equal to 6.8 dB case, the system performance has a negative gain compared to the one with
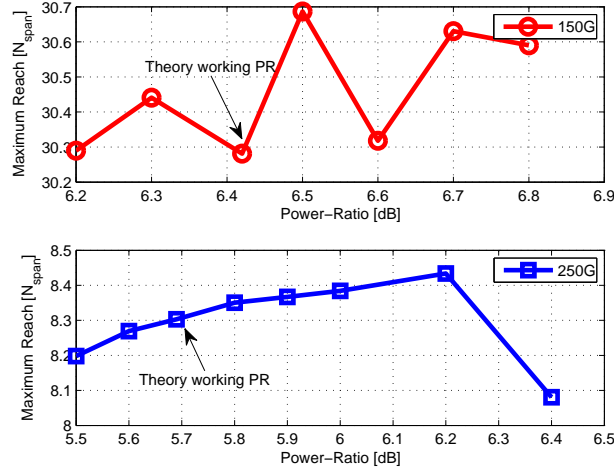
Figure 6.9.   Power ratio tuning in both 150G (top) and 250G (bottom) cases, where $\kappa = 0.50$. After tuning up the power-ratio, both system maximum reach have a slightly increasing, however when keeps tuning up power-ratio, the system performance decrease.

the optimum working PR. In the 275G case, all the increase and decrease of the propagation results vary in a small range. Neither 175G nor 275G had improvement after tuning PR.
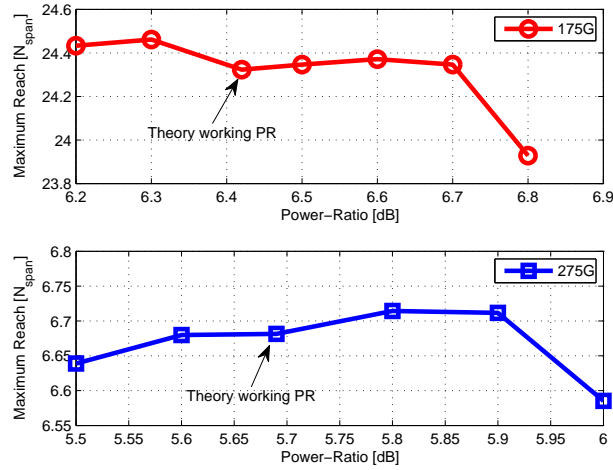
Figure 6.10.   Power ratio tuning in both 175G (top) and 275G (bottom) cases, where $\kappa = 0.25$. Power-ratio has little impact on these two cases, increasing of N_{span} is barely count, over tuning power-ratio, they system performance would decrease.

Actually, more than one thing can affect the effectiveness of PR tuning, and

each factor counteracts each other. First, inside the TDHMF, the higher cardinality component suffers the most from nonlinear interference. Figure 6.11 shows that inside the TDHMF 225G, under the optimum working PR conditions, the two components performs in a different way. The red line, PM-16QAM, has a much better propagation performance than the blue line, PM-64QAM. In addition, table 6.1 shows that in most of the PR cases the lower cardinality component has a better propagation performance.
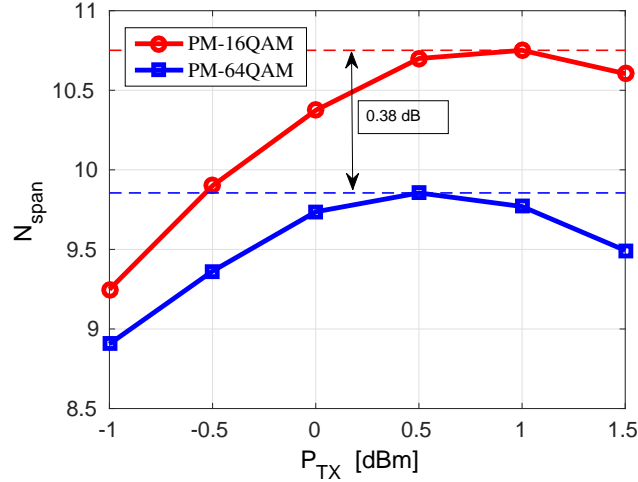
Figure 6.11. Individual propagation performance of PM-16QAM and PM-64QAM in the TDHMF 250G case. PM-64QAM suffers more from fiber nonlinearity and becomes the lower performance component.

Second, when tuning up the PR, it is basically pumping more power into the higher cardinality component and improving its propagation performance. To fully understand the benefit of the tuning PR, the non-linearity must be removed from the simulation. If the fiber non-linearity is fully cancelled, the two componets of TDHMF have the same propagation performance. In figure 6.12, the two components of TDHMF 225G case, PM-16QAM has the same performance as the PM-64QAM after each span under the optimum working PR conditions. After tuning up the PR, the two curves split. The PM-64QAM (red dash line) has outperformed PM-16QAM (blue dash line) when the fiber non-linearity is removed.

As a result, in the low transmitted power region (where the fiber non-linear effect is negligible), the higher cardinality modulation format's propagation performance got improved after tuning PR. Although higher cardinality format suffers more from fiber non-linearity, its overall propagation performance obtains a certain amount of gain after tuning PR. In table 6.1, the maximum reach of PM-64QAM inside TDHMF 225G has been steadily enhanced after tuning up the PR.
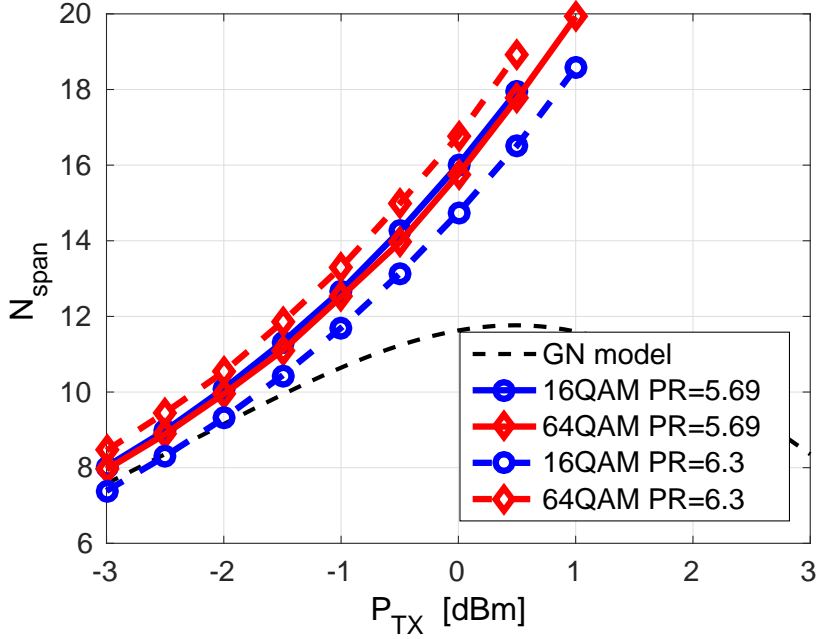
Figure 6.12. Simulation result of TDHMF 225G in linear fiber propagation. Since $\Psi_{\text{target}} = 2 \cdot 10^{-2}$, system theory working power-ratio is equal to 5.69. In such scenario PM-16QAM and PM-64QAM have same performance for different transmission power. When the power-ratio is increased, more power is pumped into PM-64QAM. In this linear propagation, PM-64QAM has a better performance than PM-16QAM. For each transmitted power P_{Tx}, it has about 2 N_{span} advantage.

Power-Ratio [dB]	5.5	5.6	5.69	5.8	5.9	6.0
MR 16QAM [N_{span}]	12.7885	12.6320	12.4131	12.2963	12.1373	11.94418
MR 64QAM [N_{span}]	10.9015	10.9733	10.9614	11.1922	11.2665	11.2049
Overall MR [N_{span}]	10.9015	10.9733	10.9614	11.1922	11.2665	11.2049
Power-Ratio [dB]	6.1	6.2	6.3	6.4	6.6	6.8
MR 16QAM [N_{span}]	11.8684	11.7034	11.6109	11.4289	11.1901	10.9313
MR 64QAM [N_{span}]	11.3021	11.3651	11.4502	11.4159	11.6619	11.7335
Overall MR [N_{span}]	11.3021	11.3651	11.4502	11.4159	11.1901	10.9313

Table 6.1. TDHMF 225G cases power-ratio tuning detail maximum reach data. The optimum working PR is 5.69 dB.

Furthermore, operating with the same BER strategy implies that the worst performance of the two components of TDHMF determines the maximum reach of the TDHMF. As illustrated in table 6.1, as long as the PM-64QAM's maximum reach is shorter than PM-16QAM, it determines the maximum reach of TDHMF

225G.

Moreover, tuning away from the optimum working PR implies an extra SNR penalty, and this will cancel the PR tuning gain. As a result, one can not continuously enlarge the PR to improve the system performance. Therefore, for certain cases of TDHMF, like 125G and 225G, PR tuning is an effective tool in improving performance. For some cases, like 175G and 275G, it does not work.

6.2.3 Pre Distortion Application

No matter in the IMDD system or the coherent optical transmission system, the chromatic dispersion is the main issue in optical fiber transmission system. In the IMDD systems, the dispersion compensation unit is added into the link to provide substantial performance gains. In the new era of coherent systems operating over the uncompensated transmission links, lots of studies have been carried to prove that the chromatic dispersion pre-compensation is also quite useful in this novel scheme, in both simulations [59] [60] and experiments [61] [62] [63].

Instead of pre compensating dispersion before the link, previous work [21] have shown that for TDHMF, adding an extra chromatic dispersion (pre distortion) before the propagation can significantly improve the system performance. However, simulations in [21] were operated with the minimum BER strategy. In this section, the effectiveness of pre distortion is testified again, but with the same BER strategy.

A fiber grating component is employed before the fiber in order to add pre distortion. In addition, the extra chromatic dispersion ranged from 0 to 30000 ps/nm. Unfortunately, pre distortion does not work when the transmitter is operated with the same BER strategy. Figure 6.13 shows the impact of pre distortion on the system performance for both the 150G and the 175G cases. In the TDHMF 150G case, an insignificant gain is obtained with a small amount of pre distortion. But when the pre distortion increases, the system performance obtain negative gain. In the 175G case, the pre distortion technique is still not effective in improving the system performance. Other bit rate simulations also did not have a significant gain after employing the pre distortion technique.

Then, to have a more general picture of the pre distortion technique effectivenees, the PI was also considered. In figure 6.14, both TDHMF 250G with or without PI cases are taken into account. In both cases, the system performance decreases when the pre distortion increases. For the TDHMF 250G with PI case, the maximum reach lost about 0.5 N_{span} when the pre distortion is equal to 30,000 [ps/nm]. For the TDHMF 250G with PI case, the maximum reach lost about 0.3 N_{span} when the pre distortion equal to 20,000 [ps/nm]. Other TDHMF bit rate with/without PI comparison simulations all showed a similar behaviour. Hence, with or without PI can not affect the effectiveness of pre distortion on TDHMF.

Actually, too much pre dispersion will distort the signal heavily and increase the

71
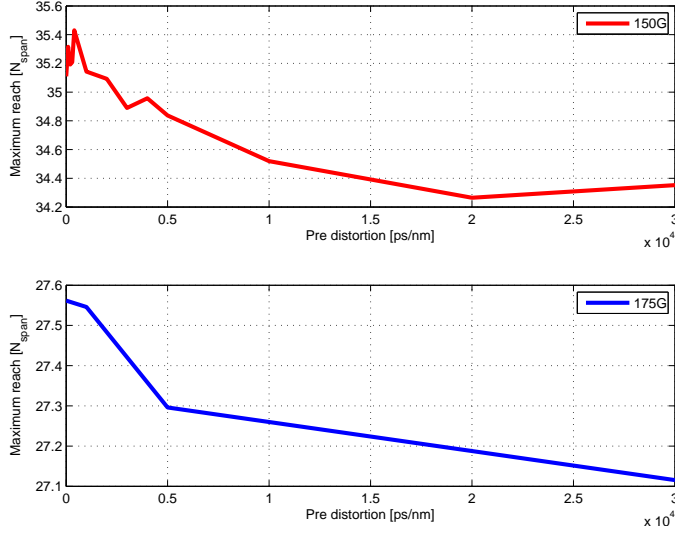
Figure 6.13. Top: TDHMF 150G with PI case, when pre-distortion raised up to 400 ps/nm, system performance obtained 0.04 dB gain, after 1000 ps/nm, system performance keeps decreasing; bottom: TDHMF 175G case, with pre distortion increasing, the system maximum reach keeps decreasing.
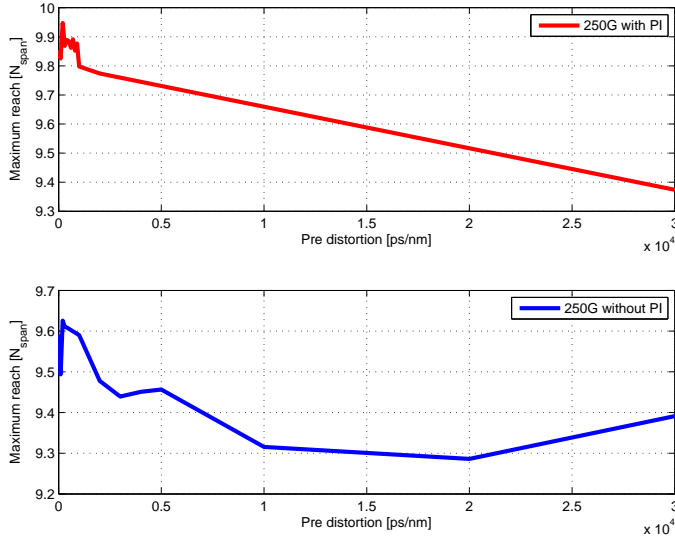
Figure 6.14. Top: TDHMF 250G with PI case, system performance fluctuated in a small range (about 0.2 N_{span}), and keeps decreasing when pre distortion increases; bottom: TDHMF 250 without PI case, system performance has an inverse relation with pre distortion.

complexity of the receiver. For TDHMF with same BER strategy, the pre distortion is not an effective tool in mitigating the non-linear interference.

72

6.3 FlexPAM Non-linear Propagation and Countermeasures

6.3.1 Polarization Interleaving

Since the FlexPAM has a time constant frame structure, the polarization interleaving that similar to the TDHMF cannot be employed on FlexPAM. But, when the format ratio $\kappa = 0.5$, there actually exists two types of frame structure, which are depicted in figure 6.15. The first one, which is defined as the without PI type, has the two M-PAMs that aligning in different polarizations. The second one, which is defined as the with PI type, has the two M-PAMs that interleaving with each other in both polarizations. Apparently, FlexPAM with PI has a symmetric polarization symbol structure. This property gives a big advantage in the non-linear uncompensated signal propagation. It should be pointed out that, both frame structure type of the format ratio $\kappa = 0.5$ cases have the same back-to-back performance, which means that the polarization interleaving does not affect the back-to-back performance.

| | | $N_{\mathrm{BpS}} = 4\log_2(M)$ | $N_{\mathrm{BpS}} = 4\log_2(M) + 1$ | $N_{\mathrm{BpS}} = 4\log_2(M) + 2$ | | $N_{\mathrm{BpS}} = 4\log_2(M) + 3$ |
				without PI	with PI	
x-pol	**I**	M	M	M	M	M
	Q	M	M	M	$2M$	$2M$
y-pol	**I**	M	M	$2M$	M	$2M$
	Q	M	$2M$	$2M$	$2M$	$2M$
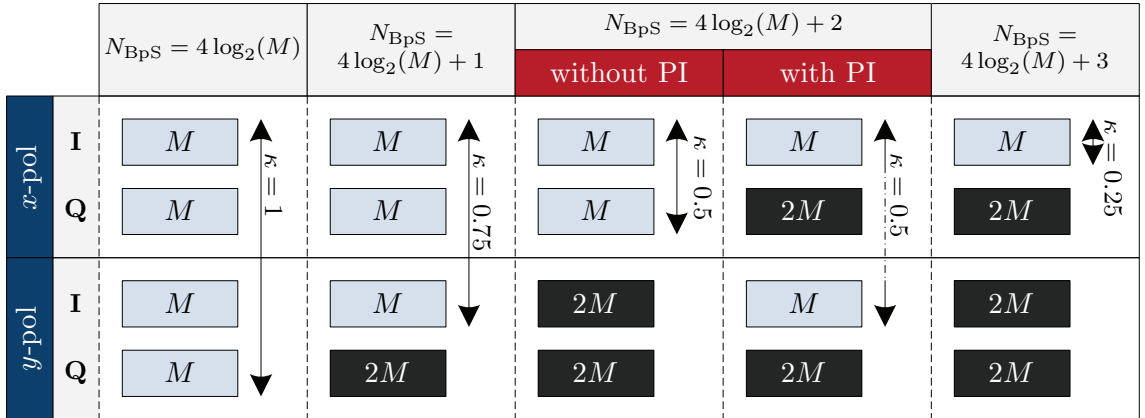
Figure 6.15. The entire frame structure of FlexPAM composed by two neighbour M-PAMs. In this thesis, $\kappa = 1$ represents pure format, $\kappa = 0.75$ represents FlexPAM 125G and 225G cases, $\kappa = 0.5$ represents FlexPAM 150G and 250G cases, and $\kappa = 0.25$ represents FlexPAM 175G and 275G cases. In the back-to-back simulation, for $\kappa = 0.5$ case, FlexPAM with PI has the same performance as the one without PI.

The FlexPAM 150G propagation performance is shown in figure 6.16. It is a hybrid between 2-PAM and 4-PAM with format ratio $\kappa = 0.5$. The FlexPAM with PI structure has a 1.3 dB N_{span} advantage compared to the one without PI.

The FlexPAM 250G case has the same format ratio $\kappa = 0.5$, but it is composed by 4-PAM and 8-PAM. Figure 6.17 reports a 1 dB N_{span} advantage of the FlexPAM
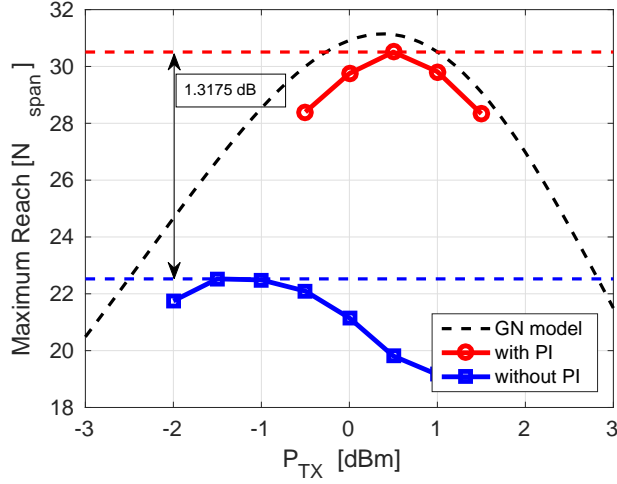
Figure 6.16.   The maximum reach versus the launched power per channel for FlexPAM 150G case, including both with and without PI cases. FlexPAM 150G is composed by 2-PAM and 4-PAM with format ratio $\kappa = 0.5$. The overall bits per symbol is 6.

250G after applying PI.
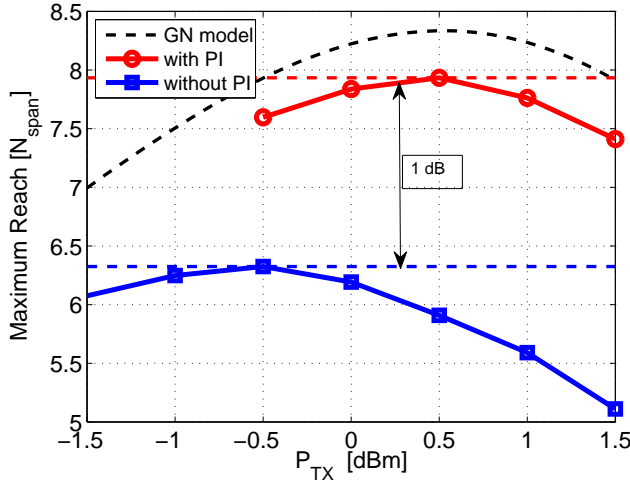
Figure 6.17.   The maximum reach versus the launched power per channel for FlexPAM 250G case, including both with and without PI cases. FlexPAM 250G is composed by 4-PAM and 8-PAM with format ratio $\kappa = 0.5$. The overall bits per symbol is 10.

When the format ratio is equal to 0.5, the system performance of FlexPAM with PI has a significant improvement, and gets closer to the GN-model prediction.

It should be pointed out that, there is no difference of both FlexPAM symbol structure in the back-to-back performance. A more polarization power balanced symbol structure can definitely mitigate the fiber non-linear interference.

6.3.2 Power Ratio Tuning

Instead of tuning up the PR to obtain improvement like TDHMF, the FlexPAM tunes down the PR to improve the system performance. In figure 6.18, the PR tuning technique is employed to both 125G and 225G cases. In the 125G case, a 0.25 dB gain is obtained after tuning down the PR to 6 dB. In the 225G case, a 0.31 dB gain is obtained after tuning down the PR to 5.2 dB. Noted that both cases have a format ratio $\kappa = 0.75$.
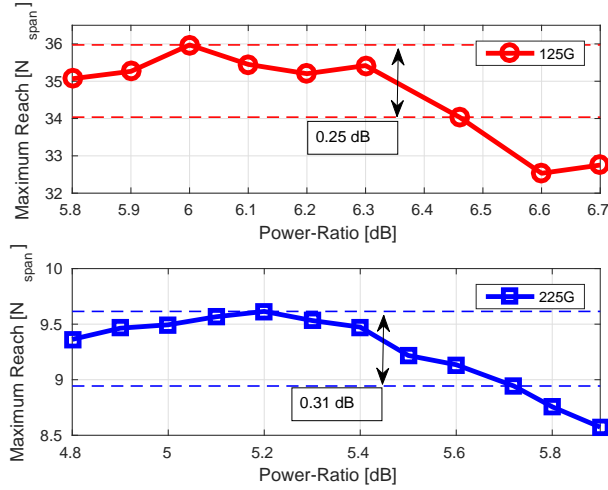
Figure 6.18. The power-ratio tuning in Flex-PAM 125G and 225G, whose format-ratio $\kappa = 0.75$. After power-ratio tuning, the system performance has 0.25 dB and 0.31 dB gain respectively.

When the format ratio $\kappa = 0.50$, both FlexPAM 150G and 250G benefit from the PR tuning even after PI is applied. In figure 6.19, a 0.24 dB gain is reported in the 150G case after tuning down the PR to 6.1 dB; and a 0.40 dB gain is reported in the 250G case after tuning down the PR to 5.2 dB.

However, when the format ratio is equal to 0.25, no obvious gain is obtained from the PR tuning. It is reported that in figure 6.20, the result of both the 175G and the 275G cases vary in a small range. In addition, these amount of data variation can be ignored.

To provide a more in-depth analysis of the system performance after applying the tuning PR technique, in figure 6.21, the SNR penalty ΔSNR is shown. It is incurred by sweeping the power ratio between formats. Indeed, the optimum back-to-back

75
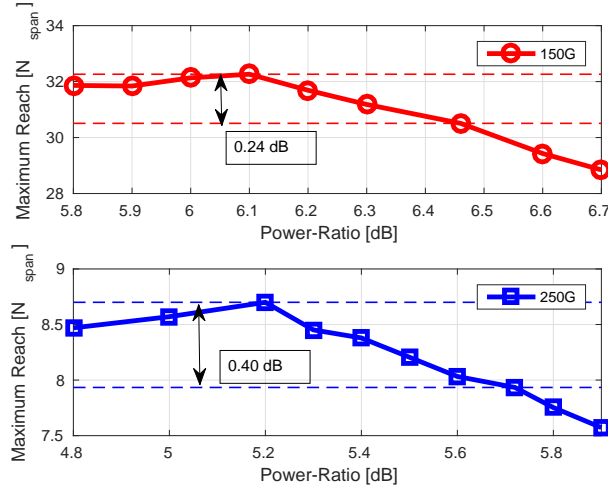
Figure 6.19. The power-ratio tuning in Flex-PAM 150G and 250G, whose format-ratio $\kappa = 0.50$. After power-ratio tuning, the system performance has 0.24 dB and 0.40 dB gain respectively. Note that, for both 150G and 250G cases polarization-interleaving have already applied.
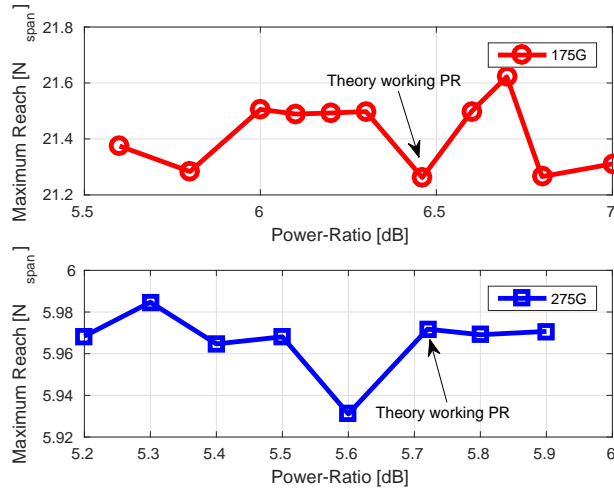
Figure 6.20. Power-ratio tuning in Flex-PAM 175G and 275G, whose format-ratio $\kappa = 0.25$. System performance did not benefit from the power-ratio tuning.

performance (ΔSNR = 0dB) is obtained at the theoretical values listed in table 4.1, 6.46 dB for M=2 and 5.72 dB for M=4. The slope of the curves in figure 6.21 represents how fast does ΔSNR evolves with ΔPR, and it strongly depends on the format ratio κ. For the power ratio lower than the optimum, the growth of ΔSNR evolves slower with lower κ, whereas the opposite is true for power ratios larger than

the optimum. If the maximum SNR penalty is 0.2 dB, one will have an approximate 2.5 dB PR reduction tolerance for the $\kappa = 0.25$ case. Whereas only an approximate 0.5 dB PR reduction tolerance is allowed for the $\kappa = 0.75$ case.

Note that, although from the back-to-back perspective, it does not make sense to tune the PR, for the signal propagation in the fiber, reducing the PR can be an effective tool for the mitigation of non-linear effects. In contrast with TDHMF, the distribution of the optical power is inherently constant over time for FlexPAM. However, it suffers from the power unbalance between polarization tributaries, which can only be solved through PI for the $\kappa = 0.5$ case (see figure 6.15). In the remaining cases ($\kappa = 0.25$ and $\kappa = 0.75$), it is not possible to avoid optical power unbalance by simply rearranging the PAM formats among the four quadratures. In such a scenario, reducing PR is a possible way to counteracting polarization power unbalance. As a result, the SNR penalty is incurred in figure 6.21.
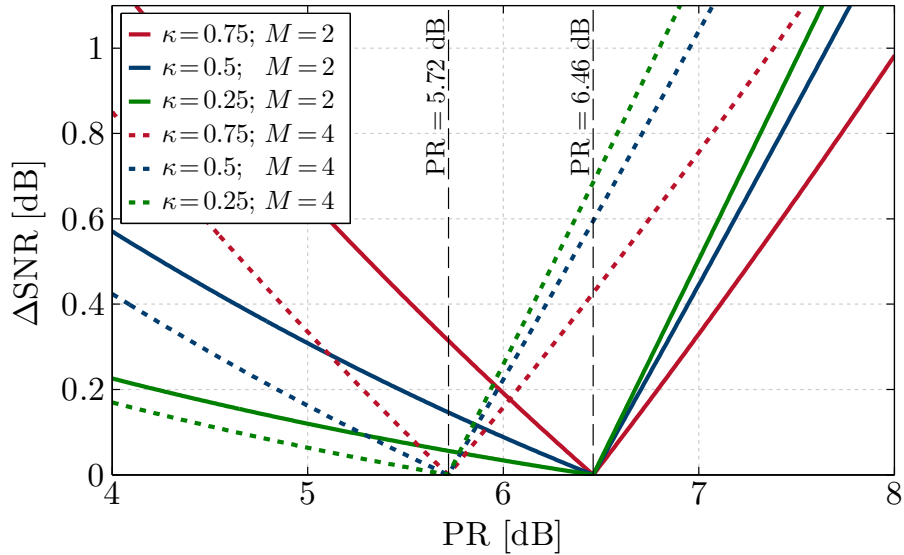
Figure 6.21. The SNR penalty (ΔSNR) is suffered in back-to-back by tuning the power ratio around its optimum value when operating with the same BER strategy. The target BER is 2×10^{-2}.

The relationship between the quadrature power ratio, PR, and the polarization power ratio, PR_{pol}, is illustrated in figure 6.22 for different FlexPAM configurations. Note that PR_{pol} is not depend on M, but on both PR and format ratio. It is also worth emphasizing that, similar to the behaviour depicted in figure 6.21, any changes on the polarization power ratio are less sensitive for the $\kappa = 0.25$ case. That's why for both FlexPAM 175G and 275G, the effectiveness of PR tuning is not that obvious. When $\kappa = 0.75$, while PR_{pol} decreases with decreasing PR at a rate of 0.7 dB/dB, there is only an approximate 0.2 dB of PR_{pol} variation for $PR_{pol} \in [5,6]$dB.

Therefore, for the FlexPAM 125G and 225G cases, the PR tuning has a significant impact on the system performance improving.
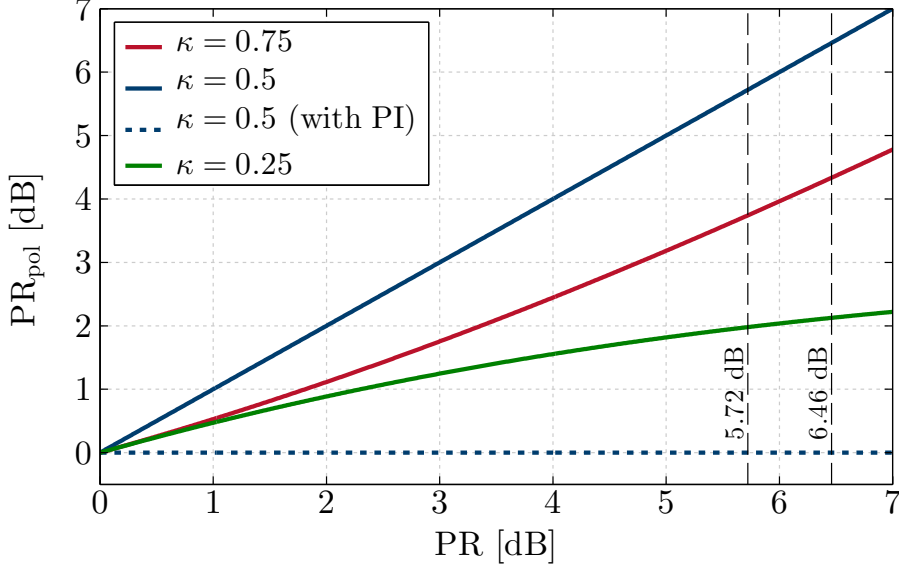
Figure 6.22. FlexPAM: the impact of PR tuning on the power unbalance between polarization tributaries (or equivalently, the polarization power-ratio PR_{pol})

6.3.3 Pre Distortion Application

The effectiveness of pre distortion technique is testified again in this section but with FlexPAM.

Still, the pre distortion technique can not improve the system performance in the FlexPAM propagation(see figure 6.23). The results have some fluctuation in first couple of hundreds pre distortion. After 1000 ps/nm pre distortion, the system performance decreases with pre distortion increasing. Other bit rate cases also do not benefit from pre distortion.

Similar to TDHMF, the PI is considered to have a better understanding of the pre distortion technique. In figure 6.24, it displays how the maximum reach evolves when the pre distortion increases of both FlexPAM 250G with and without PI cases. For FlexPAM 250G without PI case, the maximum reach decrease about 0.6 N_{span} when the pre distortion is equal to 30000 ps/nm. For the FlexPAM 250G with PI case, all the simulation results vary in a small range about 0.1 N_{span}. No significant improvement is obtained after applying PI.

Since the FlexPAM has an asymmetric symbol structure, more pre distortion could further distort the signal. Hence, the pre distortion technique does not work on FlexPAM either.

78
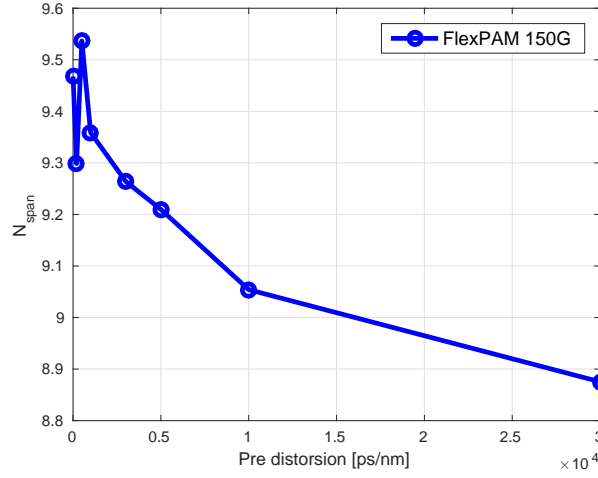
Figure 6.23. The maximum reach of FlexPAM 150G in different pre distortion. Noted that the target BER is 10^{-3} in this case.
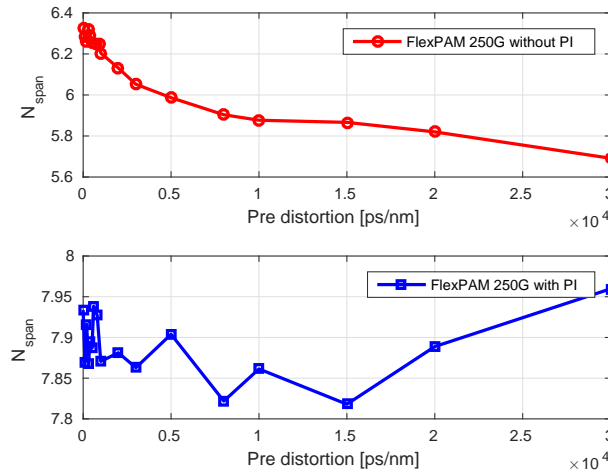
Figure 6.24. The maximum reach of FlexPAM 250G in different pre distortion cases, including both with and without PI conditions. Noted that the target BER is $2 \cdot 10^{-2}$ in this figure.

6.4 Non-linear Propagation Comparison

6.4.1 Propagation without countermeasures

The first step of this section analysis is to evaluate the maximum transmission distance that can be achieved for each considered modulation strategy - TDHMF and FlexPAM - without applying any countermeasures for non-linear impairments.

The maximum reach is defined in terms of the maximum number of fiber spans, N_{spans}, along which the signal can propagate, while still guaranteeing the operation below the given target BER. The results of this simulation campaign are shown in the figure 6.25, in terms of maximum reach versus net channel bit rate.

Figure 6.25. The maximum reach achieved by TDHMF and Flex-PAM for different bit-rates ranging from 100G to 300G without any nonlinear mitigation countermeasures. Note that both PM-8QAM and PM-32QAM are indicated in the figures only as equivalent spectral efficiency solutions for 150G and 250G.

As expected, without the implementation of any non-linear mitigation techniques, both TDHMF and FlexPAM perform worse than the GN-model predictions due to the power unbalance in time (TDHMF) and in polarization (FlexPAM). In particular, FlexPAM performs much worse, especially at 150G and 250G. The higher power level needed by the higher cardinality format generates an extra non-linear impairment in fiber propagation, compared to a transmission technique based on constant power. Consequently, the maximum reach is significantly reduced with respect to the GN-model predictions.

It is important to refer that TDHMF has been tested with a frame composed of only 4 symbols (or 4 time slots), thus approximately reaching its maximum performance. Note that in [21] it has been shown that TDHMF tends to significantly degrade its non-linear propagation performance with increasing frame-size.

Focusing on the FlexPAM results and considering M = 2, one can observe a shortening of the maximum reach of about 25% (1.25 dB) for $\kappa = 0.75$, whereas a smaller penalty of approximately 11.5% (0.5 dB) is found for the case of $\kappa = 0.25$. This can be justified by the fact that the polarization power unbalance of FlexPAM

is inherently lower for $\kappa = 0.25$ - approximately 2 dB - as shown in the table 4.1. The same exact pattern can be observed for the case of M = 4, but with a reduced penalty: 24% (1.2 dB) and 9.5% (0.4 dB) for $\kappa = 0.75$ and $\kappa = 0.25$, respectively. In addition, this slight penalty reduction is well matched with the correspondent reduction of PR_{pol} in table 4.1 from M = 2 to M = 4. It therefore becomes apparent that polarization power unbalance plays a critical role in the non-linear propagation performance of FlexPAM.

6.4.2 Propagation with countermeasures

In order to counteract the fiber non-linearity and improve system propagation performance, the PI and PR tuning techniques are applied to both TDHMF and FlexPAM. The overall effectiveness of the proposed non-linear mitigation countermeasures is summarized in figure 6.26, which shows the maximum reach versus net bit-rate for the two hybrid modulation techniques including non-linear impairments' countermeasures. The GN-model predictions are also plotted as a performance benchmark.
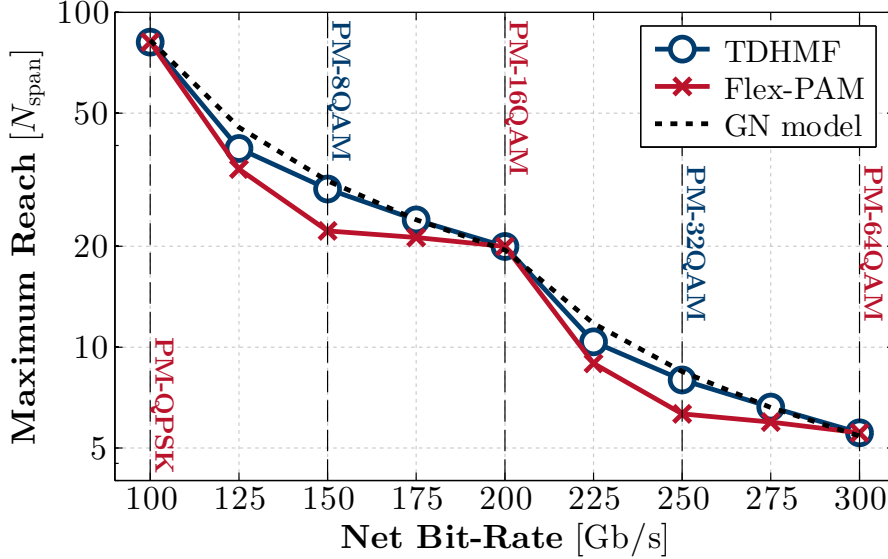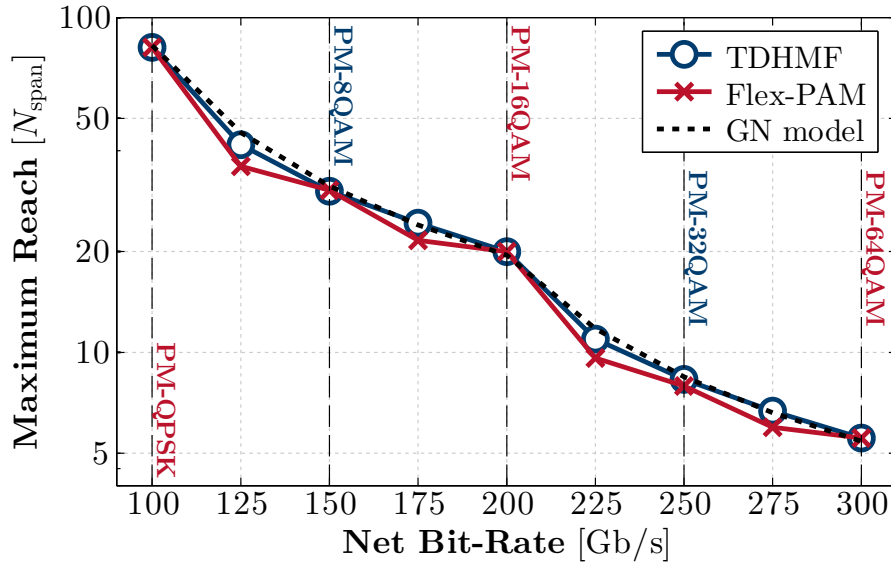

Figure 6.26. The maximum reach achieved by TDHMF and Flex-PAM for different bit-rates ranging from 100G to 300G when applying nonlinear mitigation countermeasures: PI and PR tuning. Note that both PM-8QAM and PM-32QAM are indicated in the figure only as equivalent spectral efficiency solutions for 150G and 250G.

As a direct comparison with the result of figure 6.25, figure 6.26 reveals that both TDHMF and FlexPAM got an improvement and getting closer to the GN-model predictions due to the reduction of non-linear effects.

For TDHMF, after applying PI and PR tuning, it almost has the same performance as the GN-model predictions for all the tested bit rates. For FlexPAM, the PI is an very effective tool in improving the system propagation performance when the format ratio is equal to 0.5. Unfortunately, it cannot be applied to the other two format ratio cases. But with the PR tuning, they can partially shorten the gap to the GN-model predictions. It is worth of emphasizing that, even if PR tuning is less effective for $\kappa = 0.25$, its associated reach reduction is significantly lower than that of $\kappa = 0.75$, regardless of the constellation size, due to a lower polarization power unbalance. Consequently, FlexPAM is generally less impaired by non-linearities for $\kappa = 0.25$. After applying the PI and the PR tuning to FlexPAM, the obtained reach reduction compared to the GN-model predictions is less than 3% for $\kappa = 0.5$, 10% for $\kappa = 0.25$ and 20% for $\kappa = 0.75$.

Finally, it is important to stress out that, although TDHMF has been applied with a short frame-size (4 symbols) in order to achieve a near-optimum performance, its practical implementation may require a longer frame-sizes to keep a feasible DSP complexity at the receiver. This may come at the expense of a degraded non-linear propagation performance. On the contrary, the Flex-PAM frame is of fixed length (4 symbols) and is inherently constant over time, thereby it has the potential of simplifying all receiver side processing and enabling lower chip area and power consumption.

Chapter 7

Conclusion

In order to take full advantage of the existing spectral resource in the meshed networks with fast-varying traffic demands, it is important to develop a transponder which adapts its bit rate according to the actual traffic conditions. This thesis has argued that by using both TDHMF and FlexPAM, the optical transmission system can provide many bit rate flexibilities to the networks. These two promising flexible modulation techniques have been theoretically and numerically compared in both back-to-back and signal propagation perspectives.

Building upon the well-known TDHMF technique, which exploits the time-varying modulation, we proposed and numerically assessed the FlexPAM concept. The FlexPAM allows integer bit-per-symbol granularity resorting to hybrid M-PAM modulation among the four orthogonal quadratures in a dual-polarization optical signals. The implementation complexity maybe tackled by associating the time consistent property of FlexPAM with a common-mode BER transmitter operation strategy ($\Psi_1 = \Psi_2$). This may allow for a simpler receiver-side processing of the electrical signal and shared FEC decoding of the result bit-stream. The numerical simulations have confirmed that, both TDHMF and FlexPAM have an equivalent back-to-back performance at a given integer bit-per-symbol.

The simulation results of this thesis indicate that, the signal propagation performance of both TDHMF and FlexPAM is dominated by rather different non-linear phenomena, which also associated with the specificities of their different frame structures. The polarization interleaving is proved to be a simple and effective non-linear impairment countermeasure for TDHMF and also for FlexPAM with a 50% format ratio. Considering the fact that it is impossible to apply PI to FlexPAM with 25% and 75% format ratio, we assessed a simple power ratio tuning procedure, which can reduce the power unbalance between polarizations and thereby mitigate the non-linearities. Although the PR tuning was only found to be partially effective for the case of 75% format ratio case, it was also shown that the non-linear penalty incurred at 25% format ratio is inherently smaller, due to its correspondent FlexPAM

frame structure. In addition, the effectiveness of pre distortion technique was testified for both TDHMF and FlexPAM. However, the system propagation performance did not obtain a significant improvement after applying this technique.

In general, it seems that both TDHMF and FlexPAM incurred penalties against the GN-model predictions in terms of signal maximum reach. The gap to the GN-model predictions can be shorten by employing appropriate non-linear propagation countermeasures. Relatively to TDHMF, FlexPAM may provide some benefits of allowing simpler receiver-side processing, which may be a crucial advantage from the practical implementation point of view.

This thesis extends our knowledge of mixed modulation formats, especially on the topic of transmitter operation strategy implementation. It will serve as a base for future studies of the network level. More research is needed to have a better understanding of the relation between power balance (both time and polarization/quadrature)and the propagation performance. A natural progression of this work is to explore the possibility of developing a GN-model-like analytical tool for the mixed modulation format.

Bibliography

[1] Pierluigi Poggiolini. The gn model of non-linear propagation in uncompensated coherent optical systems. *Journal of Lightwave Technology*, 30(24):3857–3879, 2012.

[2] I Cisco. Cisco visual networking index: Forecast and methodology, 2014–2019. *CISCO White paper*, 2015.

[3] Cisco Visual Networking Index. The zettabyte era: trends and analysis. *Cisco white paper*, 2013.

[4] CH Cox III, DZ Tsang, LM Johnson, and GE Betts. Low-loss analog fiber-optic links. In *Microwave Symposium Digest, 1990., IEEE MTT-S International*, pages 157–160. IEEE, 1990.

[5] E Ackerman, D Kasemset, S Wanuga, R Boudreau, J Schlafer, and R Lauer. A low-loss ku-band directly modulated fibre-optic link. *Photonics Technology Letters, IEEE*, 3(2):185–187, 1991.

[6] CH Cox III, Edward I Ackerman, and GE Betts. Relationship between gain and noise figure of an optical analog link. In *Microwave Symposium Digest, 1996., IEEE MTT-S International*, volume 3, pages 1551–1554. IEEE, 1996.

[7] Charles Cox, Edward Ackerman, Roger Helkey, and Gary E Betts. Techniques and performance of intensity-modulation direct-detection analog optical links. *IEEE Transactions on Microwave theory and techniques*, 45(8):1375–1383, 1997.

[8] Winston I Way. Large signal nonlinear distortion prediction for a single-mode laser diode under microwave intensity modulation. *Lightwave Technology, Journal of*, 5(3):305–315, 1987.

[9] Keith J Williams, Ronald D Esman, and Mario Dagenais. Nonlinearities in pin microwave photodetectors. *Lightwave Technology, Journal of*, 14(1):84–96, 1996.

[10] Charles A Brackett. Dense wavelength division multiplexing networks: Principles and applications. *Selected Areas in Communications, IEEE Journal on*, 8(6):948–964, 1990.

[11] Hiroto Sugahara, Hiroki Kato, Takashi Inoue, Akihiro Maruta, and Yuji Kodama. Optimal dispersion management for a wavelength division multiplexed optical soliton transmission system. *Journal of lightwave technology*, 17(9):1547, 1999.

[12] Adel AM Saleh and Jane M Simmons. Evolution toward the next-generation core optical network. *Lightwave Technology, Journal of*, 24(9):3303–3321, 2006.

[13] Kazuro Kikuchi. Coherent optical communications: Historical perspectives and future directions. In *High Spectral Density Optical Communication Technologies*, pages 11–49. Springer, 2010.

[14] Henning Bülow, Fred Buchali, and Axel Klekamp. Electronic dispersion compensation. *Lightwave Technology, Journal of*, 26(1):158–167, 2008.

[15] Masahiko Jinno, Hidehiko Takara, Bartlomiej Kozicki, Yukio Tsukishima, Yoshiaki Sone, and Shinji Matsuoka. Spectrum-efficient and scalable elastic optical path network: architecture, benefits, and enabling technologies. *Communications Magazine, IEEE*, 47(11):66–73, 2009.

[16] Douglas L McGhan, Will Leckie, and Chen Chen. Reconfigurable coherent transceivers for optical transmission capacity and reach optimization. In *Optical Fiber Communication Conference*, pages OW4C–7. Optical Society of America, 2012.

[17] Gwang-Hyun Gho and Joseph M Kahn. Rate-adaptive modulation and low-density parity-check coding for optical fiber transmission systems. *Journal of Optical Communications and Networking*, 4(10):760–768, 2012.

[18] Jeremie Renaudier, Oriol Bertran-Pardo, Amirhossein Ghazisaeidi, Patrice Tran, Haik Mardoyan, Patrick Brindel, Adrian Voicila, Gabriel Charlet, and Sebastien Bigo. Experimental transmission of nyquist pulse shaped 4-d coded modulation using dual polarization 16qam set-partitioning schemes at 28 gbaud. In *Optical Fiber Communication Conference*, pages OTu3B–1. Optical Society of America, 2013.

[19] Johannes Karl Fischer, Saleem Alreesh, Robert Elschner, Felix Frey, Markus Nölle, Carsten Schmidt-Langhorst, and Colja Schubert. Bandwidth-variable transceivers based on four-dimensional modulation formats. *Journal of Lightwave Technology*, 32(16):2886–2895, 2014.

[20] Johannes Karl Fischer, Carsten Schmidt-Langhorst, Saleem Alreesh, Robert Elschner, Felix Frey, Pablo Wilke Berenguer, Lutz Molle, Markus Nölle, and Colja Schubert. Generation, transmission, and detection of 4-d set-partitioning qam signals. *Journal of Lightwave Technology*, 33(7):1445–1451, 2015.

[21] Vittorio Curri, Andrea Carena, Pierluigi Poggiolini, Roberto Cigliutti, Fabrizio Forghieri, Chris R Fludger, and Theo Kupfer. Time-division hybrid modulation formats: Tx operation strategies and countermeasures to nonlinear propagation. In *Optical Fiber Communication Conference*, pages Tu3A–2. Optical Society of America, 2014.

[22] R Li, P Cortada, V Curri, and A Carena. Flex-pam modulation formats for future optical transmission system. In *Fotonica AEIT Italian Conference on Photonics Technologies, 2015*, pages 1–3. IET, 2015.

[23] Ori Gerstel, Masahiko Jinno, Andrew Lord, and SJ Ben Yoo. Elastic optical

networking: A new dawn for the optical layer? *Communications Magazine, IEEE*, 50(2):s12–s20, 2012.

[24] Gabriella Bosco, Vittorio Curri, Andrea Carena, Pierluigi Poggiolini, and Fabrizio Forghieri. On the performance of nyquist-wdm terabit superchannels based on pm-bpsk, pm-qpsk, pm-8qam or pm-16qam subcarriers. *Lightwave Technology, Journal of*, 29(1):53–61, 2011.

[25] Xiaosong Yu, Massimo Tornatore, Yongli Zhao, Jiawei Zhang, Xinbo Wang, Shuqiang Zhang, Rui Wang, Jianping Wang, Jie Zhang, and Biswanath Mukherjee. When and how should the optical network be upgraded to flex grid? In *2014 The European Conference on Optical Communication (ECOC)*, 2014.

[26] Marc Ruiz, Luis Velasco, Andrew Lord, Daniel Fonseca, Michal Pioro, Roland Wessaly, and Juan Pedro Fernandez-Palacios. Planning fixed to flexgrid gradual migration: drivers and open issues. *Communications Magazine, IEEE*, 52(1):70–76, 2014.

[27] Arturo Mayoral, Victor López, O González de Dios, and Juan Pedro Fernandez-Palacios. Migration steps toward flexi-grid networks. *Journal of Optical Communications and Networking*, 6(11):988–996, 2014.

[28] P Papanikolaou, K Christodoulopoulos, and E Varvarigos. Multilayer flex-grid network planning. In *Optical Network Design and Modeling (ONDM), 2015 International Conference on*, pages 151–156. IEEE, 2015.

[29] Charles H Henry. Theory of the linewidth of semiconductor lasers. *Quantum Electronics, IEEE Journal of*, 18(2):259–264, 1982.

[30] Adrian W Bowman and Adelchi Azzalini. *Applied smoothing techniques for data analysis*. Clarendon Press, 2004.

[31] Dayou Qian, Ming-Fang Huang, Ezra Ip, Yue-Kai Huang, Yin Shao, Junqiang Hu, and Ting Wang. 101.7-tb/s (370× 294-gb/s) pdm-128qam-ofdm transmission over 3× 55-km ssmf using pilot-based phase noise mitigation. In *National Fiber Optic Engineers Conference*, page PDPB5. Optical Society of America, 2011.

[32] S Chandrasekhar, AH Gnauck, Xiang Liu, PJ Winzer, Yan Pan, Ells C Burrows, TF Taunay, B Zhu, Michael Fishteyn, MF Yan, et al. Wdm/sdm transmission of 10 x 128-gb/s pdm-qpsk over 2688-km 7-core fiber with a per-fiber net aggregate spectral-efficiency distance product of 40320 km b/s/hz. *Optics express*, 20(2):706–711, 2012.

[33] Hidehiko Takara, Akihide Sano, Takayuki Kobayashi, Hirokazu Kubota, Hiroto Kawakami, Akihiko Matsuura, Yutaka Miyamoto, Yoshiteru Abe, Hirotaka Ono, Kota Shikama, et al. 1.01-pb/s (12 sdm/222 wdm/456 gb/s) crosstalk-managed transmission with 91.4-b/s/hz aggregate spectral efficiency. In *European Conference and Exhibition on Optical Communication*, pages Th–3. Optical Society of America, 2012.

[34] Dayou Qian, Ezra Ip, Ming-Fang Huang, Ming-jun Li, Arthur Dogariu, Shaoliang Zhang, Yin Shao, Yue-Kai Huang, Yequn Zhang, Xilin Cheng, et al. 1.05 pb/s

transmission with 109b/s/hz spectral efficiency using hybrid single-and few-mode cores. In *Frontiers in Optics*, pages FW6C–3. Optical Society of America, 2012.

[35] Masahiko Jinno, Takuya Ohara, Yoshiaki Sone, Akira Hirano, Osamu Ishida, and Masahito Tomizawa. Elastic and adaptive optical networks: possible adoption scenarios and future standardization aspects. *Communications Magazine, IEEE*, 49(10):164–172, 2011.

[36] C Laperle and K Roberts. Flexible transceivers. In *Eur. Conf. Opt. Commun., Amsterdam, The Netherlands*, 2012.

[37] Dirk van den Borne and Sander Lars Jansen. Dynamic capacity optimization using flexi-rate transceiver technology. In *2012 17th Opto-Electronics and Communications Conference*, 2012.

[38] Wei-Ren Peng, Itsuro Morita, and Hideaki Tanaka. Hybrid qam transmission techniques for single-carrier ultra-dense wdm systems. In *16th Opto-Electronics and Communications Conference*, 2011.

[39] Xiang Zhou and Lynn E Nelson. 400g wdm transmission on the 50 ghz grid for future optical networks. *Lightwave Technology, Journal of*, 30(24):3779–3792, 2012.

[40] Qunbi Zhuge, Xian Xu, Mohamed Morsy-Osman, Mathieu Chagnon, Meng Qiu, and David Plant. Time domain hybrid qam based rate-adaptive optical transmissions using high speed dacs. In *Optical Fiber Communication Conference*, pages OTh4E–6. Optical Society of America, 2013.

[41] Xiang Zhou, Lynn E Nelson, Pete Magill, Benyuan Zhu, Peter Borel, Dave Peckham, and K Carlson. 12,000 km transmission of 100ghz spaced, 8x495-gb/s pdm time-domain hybrid qpsk-8qam signals. In *Optical Fiber Communication Conference*, pages OTu2B–4. Optical Society of America, 2013.

[42] Xiang Zhou, Lynn E Nelson, Peter Magill, Rejoy Isaac, Benyuan Zhu, David W Peckham, Peter I Borel, and Kenneth Carlson. High spectral efficiency 400 gb/s transmission using pdm time-domain hybrid 32–64 qam and training-assisted carrier recovery. *Journal of Lightwave Technology*, 31(7):999–1005, 2013.

[43] Qunbi Zhuge, Mohamed Morsy-Osman, Xian Xu, Mathieu Chagnon, Meng Qiu, and David V Plant. Spectral efficiency-adaptive optical transmission using time domain hybrid qam for agile optical networks. *Lightwave Technology, Journal of*, 31(15):2621–2628, 2013.

[44] Han Sun, Roman Egorov, Bert E Basch, John McNicol, and Kuang-Tsan Wu. Comparison of two modulation formats at spectral efficiency of 5 bits/dual-pol symbol. In *39th European Conference and Exhibition on Optical Communication (ECOC 2013)*, 2013.

[45] IA Glover and PM Grant. Digital communications,prentice hall, 1998.

[46] Magnus Karlsson and Erik Agrell. Which is the most power-efficient modulation format in optical links? *Optics express*, 17(13):10814–10819, 2009.

[47] J-X Cai, Y Cai, Y Sun, CR Davidson, DG Foursa, A Lucero, O Sinkin, W Patterson, A Pilipetskii, G Mohs, et al. 112× 112 gb/s transmission over 9,360 km with channel spacing set to the baud rate (360% spectral efficiency). In *36th European Conference and Exhibition on Optical Communication*, 2010.

[48] Massimiliano Salsi, Clemens Koebele, Patrice Tran, Haik Mardoyan, Eric Dutisseuil, Jérémie Renaudier, Marianne Bigot-Astruc, Lionel Provost, Simon Richard, Pierre Sillard, et al. Transmission of 96× 100gb/s with 23% super-fec overhead over 11,680 km, using optical spectral engineering. In *Optical Fiber Communication Conference*, page OMR2. Optical Society of America, 2011.

[49] Shogo Yamanaka, Takayuki Kobayashi, Akihide Sano, Hiroji Masuda, Eiji Yoshida, Yutaka Miyamoto, Tadao Nakagawa, Munehiko Nagatani, and Hideyuki Nosaka. 11× 171 gb/s pdm 16-qam transmission over 1440 km with a spectral efficiency of 6.4 b/s/hz using high-speed dac. In *36th European Conference and Exhibition on Optical Communication*, 2010.

[50] Akihide Sano, Takayuki Kobayashi, Akihiko Matsuura, Shuto Yamamoto, Shogo Yamanaka, Eiji Yoshida, Yutaka Miyamoto, Munehiro Matsui, Masato Mizoguchi, and Takayuki Mizuno. 100× 120-gb/s pdm 64-qam transmission over 160 km using linewidth-tolerant pilotless digital coherent detection. In *36th European Conference and Exhibition on Optical Communication*, 2010.

[51] Vittorio Curri, Pierluigi Poggiolini, Andrea Carena, and F Forghieri. Dispersion compensation and mitigation of nonlinear effects in 111-gb/s wdm coherent pm-qpsk systems. *Photonics Technology Letters, IEEE*, 20(17):1473–1475, 2008.

[52] Dirk van den Borne, Vincent AJM Sleiffer, Mohammad S Alfiad, Sander L Jansen, and Torsten Wuth. Polmux-qpsk modulation and coherent detection: the challenge of long-haul 100g transmission. *ECOC 2009*, 2009.

[53] Giancarlo Gavioli, Enrico Torrengo, Gabriella Bosco, Andrea Carena, Vittorio Curri, Valerio Miot, Pierluigi Poggiolini, Fabrizio Forghieri, Sebastian J Savory, Lutz Molle, et al. Nrz-pm-qpsk 16 100 gb/s transmission over installed fiber with different dispersion maps. *Photonics Technology Letters, IEEE*, 22(6):371–373, 2010.

[54] Andrea Carena, Vittorio Curri, Gabriella Bosco, Pierluigi Poggiolini, and F Forghieri. Modeling of the impact of nonlinear propagation effects in uncompensated optical coherent transmission links. *Journal of Lightwave technology*, 30(10):1524–1539, 2012.

[55] Andrea Carena, Gabriella Bosco, Vittorio Curri, Pierluigi Poggiolini, M Tapia Taiba, and F Forghieri. Statistical characterization of pm-qpsk signals after propagation in uncompensated fiber links. In *Proc. ECOC*, volume 10, 2010.

[56] Francesco Vacondio, Olivier Rival, Christian Simonneau, Edouard Grellier, Alberto Bononi, Laurence Lorcy, Jean-Christophe Antona, and Sébastien Bigo. On nonlinear distortions of highly dispersive optical coherent systems. *Optics Express*, 20(2):1022–1032, 2012.

[57] Pierluigi Poggiolini, Gabriella Bosco, Andrea Carena, Vittorio Curri, Yanchao Jiang, and Fabrizio Forghieri. A detailed analytical derivation of the gn model of non-linear interference in coherent optical transmission systems. *arXiv preprint arXiv:1209.0394*, 2012.

[58] William Ryan and Shu Lin. *Channel codes: classical and modern.* Cambridge University Press, 2009.

[59] SJ Savory. Optimum electronic dispersion compensation strategies for nonlinear transmission. *Electronics Letters*, 42(7):1, 2006.

[60] Vittorio Curri, Pierluigi Poggiolini, Andrea Carena, and F Forghieri. Performance analysis of coherent 222-gb/s nrz pm-16qam wdm systems over long-haul links. *Photonics Technology Letters, IEEE*, 22(5):266–268, 2010.

[61] Mohammad S Alfiad, Dirk van den Borne, Sander Lars Jansen, Torsten Wuth, Maxim Kuschnerov, Guido Grosso, Antonio Napoli, and Huug De Waardt. A comparison of electrical and optical dispersion compensation for 111-gb/s polmux–rz–dqpsk. *Journal of Lightwave Technology*, 27(16):3590–3598, 2009.

[62] Xiang Liu, Sethumadhavan Chandrasekhar, Peter Winzer, Robert W Tkach, and Andrew R Chraplyvy. 406.6-gb/s pdm-bpsk superchannel transmission over 12,800-km twrs fiber via nonlinear noise squeezing. In *National Fiber Optic Engineers Conference*, pages PDP5B–10. Optical Society of America, 2013.

[63] Meng Qiu, Qunbi Zhuge, Xian Xu, Mathieu Chagnon, Mohamed Morsy-Osman, and David V Plant. Subcarrier multiplexing using dacs for fiber nonlinearity mitigation in coherent optical communication systems. *Proc. OFC, Tu3J*, 2, 2014.